CELLULAR MECHANISMS OF NEURONAL SWELLING UNDERLYING CYTOTOXIC EDEMA

by

Ravi Logan Rungta
B.Sc., McGill University, 2006

A THESIS SUBMITTED IN PARTIAL FULFILLMENT OF
THE REQUIREMENTS FOR THE DEGREE OF

DOCTOR OF PHILOSOPHY
in
The Faculty of Graduate and Postdoctoral Studies
(Neuroscience)

The University of British Columbia
(Vancouver)

July, 2014

Abstract

Cytotoxic brain edema is the principal cause of mortality following brain trauma and cerebral infarct yet the mechanisms underlying neuronal swelling are poorly understood. This thesis aims at identifying cellular mechanisms of neuronal swelling that cause cytotoxic edema (chapter 3) and describes a novel method for highly efficient neuronal transfection using lipid nanoparticle delivery of siRNA *in vitro* and *in vivo* (chapter 2).

In chapter 2, we demonstrate that neurons accumulate lipid nanoparticles in an apolipoprotein E dependent fashion, resulting in very efficient uptake in cell culture (100%) with little apparent toxicity. *In vivo*, lipid nanoparticle delivery of siRNA resulted in knockdown of target genes in either discrete regions around the injection site following intracortical injections or in more widespread areas following intracerebroventricular injections with no apparent toxicity or immune reactions from the lipid nanoparticles. Effective targeted knockdown was demonstrated by showing that lipid nanoparticle delivery of siRNA against GRIN1 (encoding GluN1 subunit of the NMDA receptor) selectively reduced synaptic NMDA receptor currents *in vivo* as compared to synaptic AMPA receptor currents. Therefore, lipid nanoparticle delivery of siRNA rapidly manipulates expression of proteins involved in neuronal processes *in vivo*, possibly enabling development of gene therapies for neurological disorders.

In chapter 3, we show that increasing intracellular sodium concentration ($[Na^+]_i$) by either activating voltage-gated sodium channels or NMDA receptors triggers a secondary Cl^- influx that leads to neuronal swelling and death. Cl^- but not Ca^{2+} entry was

required for neuronal swelling and cell death. Pharmacological analyses indicated that a DIDS-sensitive HCO_3^-/Cl^- exchanger was responsible for the majority of the Cl^- influx. We used lipid nanoparticle-siRNA mediated knockdown (described in chapter 2) to determine the molecular identity of the Cl^- influx pathway. Neuronal swelling was attenuated in brain slices by siRNA-mediated knockdown of the Cl^-, SO_4^{2-}, HCO_3^- exchanger, SLC26A11, but not by knockdown of other HCO_3^-/Cl^- exchangers examined. We conclude that cytotoxic brain edema can occur when sufficient Na^+ entry into neurons results in Cl^- entry via SLC26A11 to trigger subsequent neuronal swelling.

Preface

Chapter 2 is based on a published manuscript:

Rungta, R.L., Choi H.B., Lin, P.J.C., Ko, R, Ashby, D., Jay, N., Manoharan, M., Cullis, P.R., MacVicar, B.A. (2013) Lipid nanoparticle delivery of siRNA to silence neuronal gene expression in the brain. Molecular therapy Nucleic acids 2:e136. I designed the study with BAM and input from PRC, PJCL and HBC. I performed all live cell imaging, electrophysiology, injections and analyzed respective experiments. CHB performed cell culture experiments and biochemistry assays. PJCL encapsulated siRNA in lipid nanoparticles, RK performed PTEN immunostaining, DA performed ICV injections, NJ and MM designed and synthesized lipid. I wrote the manuscript with BAM. All coauthors edited the manuscript.

Chapter 3 is based on a manuscript under review:

Rungta, R.L., Choi H.B., Tyson, J.R., Lin, P.J.C., Cullis, P.R., Snutch, T.P., MacVicar, B.A., The cellular mechanisms of neuronal swelling underlying cytotoxic edema. I designed the study with BAM and input from HBC, JRT and TPS. I performed and analyzed all experiments except for cell death assays and qPCR analysis. HBC performed cell death assays. JRT performed qPCR analyses. JRT and TPS designed and tested siRNAs. PJCL performed siRNA-LNP encapsulations under supervision of PRC. I wrote the manuscript with BAM. All coauthors edited the manuscript.

All experimental protocols were approved by the Committee on Animal Care, University of British Columbia and conducted in compliance with guidelines provided by the Canadian Council of Animal Care.

Certificate numbers: A11-0031, A11-0088, A09-0933

Table of Contents

List of Tables

List of Figures

List of Abbreviations

AE	Anion exchanger
ACSF	Artificial cerebrospinal fluid
AMPA	α-Amino-3-hydroxy-5-methyl-4-isoxazolepropionic acid
ANOVA	Analysis of variance
ApoE	Apolipoprotein E
AQP	Aquaporin
ASO	Antisense oligonucleotide
ATP	Adenosine triphosphate
AVD	Apoptotic volume decrease
BBB	Blood brain barrier
BCECF	2',7'-bis(2-carboxymethyl),5(and-6)carboxyfluorescein
BDNF	Brain-derived neurotrophic factor
CaCC	Calcium-activated chloride channels
CNS	Central nervous system
CSF	Cerebrospinal fluid
DiI	1,1'-dioctadecyl-3,3,3',3'-tetramethylindocarbocyanine perchlorate
DIDS	4,4'-Diisothiocyano-2,2'-stilbenedisulfonic acid
dsRNA	Double-stranded RNA
EAAT	Excitatory amino acid transporter
EGTA	Ethylene glycol tetraacetic acid
EPSC	Excitatory postsynaptic current
E_m	Resting membrane potential
E_{Cl^-}	Chloride equilibrium potential
FLIM	Fluorescence lifetime imaging
GABA	Gamma-aminobutyric acid
GAT	GABA transporter
HEK	Human embryonic kidney
ICP	Intracranial pressure
ICV	Intracerebroventricular
IRF	Instrument response function
I-V	Current-voltage
KBAT	Kidney brain anion transporter
KO	Knock out
LDH	Lactate dehydrogenase
LNP	Lipid nanoparticle
Luc	Luciferase
MCAO	Middle cerebral artery occlusion
MMP	Matrix metalloproteinase
MQAE	*N*-(Ethoxycarbonylmethyl)-6-methoxyquinolinium bromide
NDCBE	Na^+ driven Cl^-/HCO_3^- exchanger
NMDA	N-methyl-D-aspartate
NMDG	N-methyl-D-glucamine
NPPB	5-Nitro-2-(3-phenylpropylamino)benzoic acid

OGD	Oxygen glucose deprivation
PEG	Polyethylene glycol
PTEN	Phosphatase and tensin homolog 1
R	Receptor
RNAi	RNA interference
RVD	Regulatory volume decrease
SBFI	Sodium-binding benzofuran isophthalate
SD	Spreading depression
siRNA	Small interfering RNA
shRNA	Short hairpin RNA
TBI	Traumatic brain injury
TNF-α	Tumor necrosis factor-α
TPSLM	Two photon scanning laser microscopy
TRP	Transient receptor potential
VAAC	Volume-activated anion channel
VGCC	Voltage-gated calcium channel
VGSC	Voltage-gated sodium channel
VRAC	Volume-regulated anion channel
VSOR	Volume-sensitive outward rectifying Cl^- channel

Chapter 1: General introduction

1.1 Research Hypotheses and Objectives

Hypotheses:

1) Lipid nanoparticle (LNP) delivery of siRNA is a highly efficient and non-toxic method to attenuate neuronal gene expression *in vitro* and *in vivo*.

2) Prolonged increases in intracellular sodium ($[Na^+]_i$) cause a secondary influx of Cl^- via an unknown pathway that is required for neuronal swelling underlying cytotoxic brain edema.

Aim 1: Develop new methodology for rapid transfection of neurons in vitro and in vivo.

Aim 2: Examine the interrelationship between neuronal $[Na^+]_i$, $[Cl^-]_i$ and volume in order to investigate roles for Cl^- entry pathways that contribute to neuronal swelling.

Aim 3: Use newly developed LNP transfection method to screen candidate proteins, and identify the predominant neuronal chloride entry pathway(s) underlying cytotoxic neuronal edema.

1.2 Cerebral Edema

1.2.1 Introduction to Cerebral Edema

Cerebral Edema is the process by which excess water accumulates in the brain and causes an increase in intracranial pressure (ICP). Cerebral edema is potentially lethal and can be caused by a variety of intracranial insults such as hemorrhage, ischemic stroke, infection, neoplasm, tumor, traumatic brain injury (TBI) or hypoxia (Klatzo, 1987; Quagliarello and Scheld, 1992; Kimelberg, 1995; Marmarou et al., 2000; Wick and Kuker, 2004; Marmarou et al., 2006; Raslan and Bhardwaj, 2007; Simard et al., 2007). Brain edema was first classified as either vasogenic or cytotoxic by Igor Katzo in 1967 (Klatzo, 1967) and was later expanded to include interstitial and osmotic edema (Fishman, 1975). Whereas vasogenic edema is characterized by water entry into the brain from the blood, due to breakdown of the blood brain barrier (BBB), cytotoxic edema is caused by water entry from the extracellular to intracellular space of neurons or astrocytes (Klatzo, 1987; Donkin and Vink, 2010) (**Figure 1.1**). Interstitial edema occurs in hydrocephalus and refers to the abnormal movement of cerebrospinal fluid (CSF) from the ventricles into the interstitial space, and differs from vasogenic edema in that CSF contains relatively low levels of proteins compared to the blood (Redzic, 2011). Osmotic edema is driven by an osmotic imbalance between the plasma and CSF and differs from vasogenic edema in that water flux into the brain occurs across an intact BBB.

The total brain volume is made up of 3 compartments; the parenchyma, the blood, and the CSF. Therefore, total brain volume can be calculated by the following equation: $(\text{Brain Volume})_{total}$= (Cellular volume) + (Blood volume) + (CSF volume) (Kimelberg, 2004; Wakeland and Goldstein, 2005). Brain edema therefore occurs if any of these components increase in volume without an equal volume decrease within another component. The skull, a rigid encasement, imposes a fixed boundary beyond which the brain is not able to swell and there is very little room for expansion of tissue volume without causing significant brain damage (Simard et al., 2007). Cerebral edema can be fatal if herniation of the brain towards the brain stem occurs, resulting in loss of the respiratory centers and death. Although vasogenic and cytotoxic edema can theoretically occur in isolation, cerebral edema is most often composed of both cytotoxic and vasogenic components occurring at different time points. The initial disturbance that triggers the edema is often complex, sometimes generating both types of edema in parallel and even when edema originates as either purely cytotoxic or vasogenic, one type of edema will ultimately drive the other (Kimelberg, 1995; Marmarou et al., 2006; Papadopoulos and Verkman, 2007; Simard et al., 2007; Donkin and Vink, 2010).

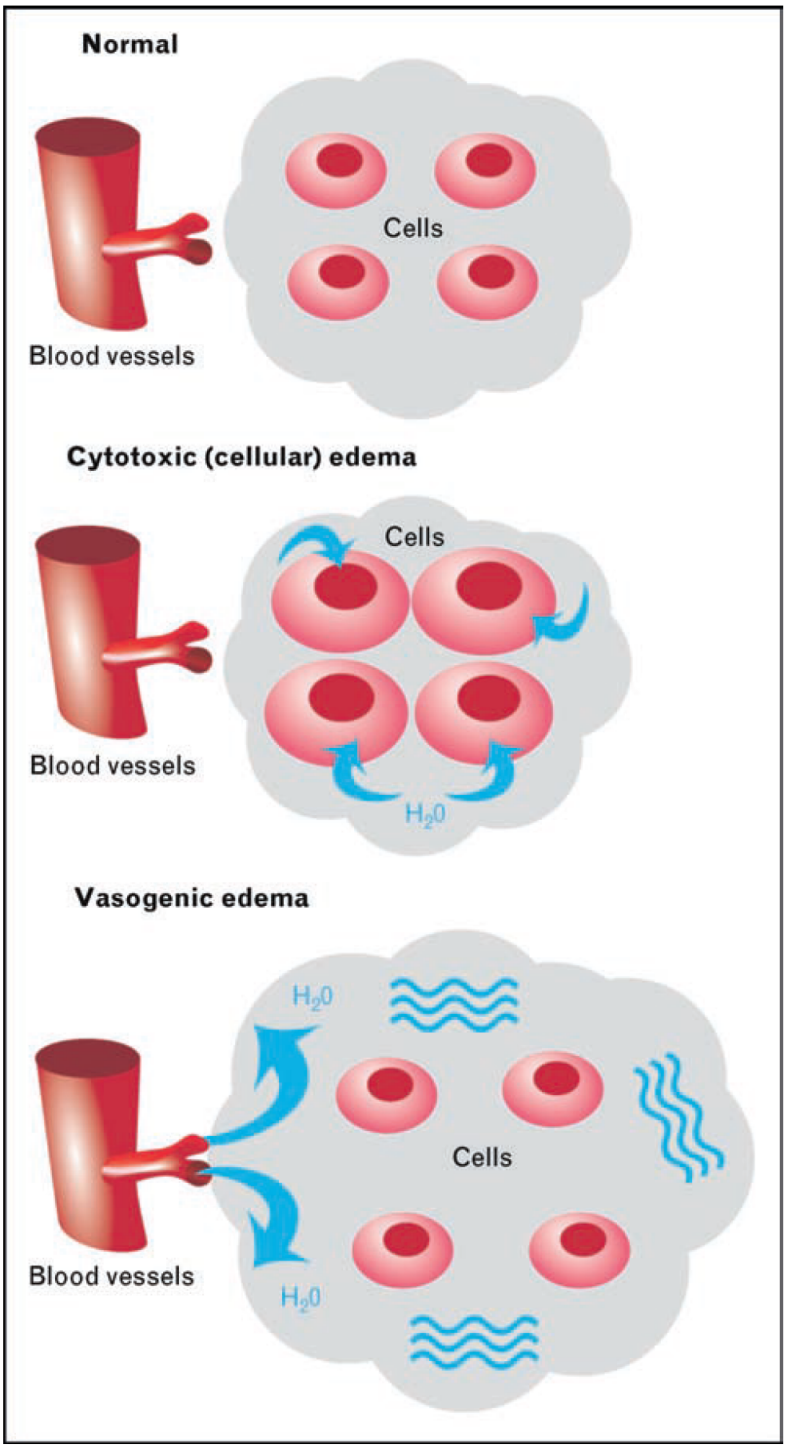

Figure 1.1: Schematic demonstrating cytotoxic and vasogenic cerebral edema. Cytotoxic edema is essentially a water compartment shift with no change in tissue water content or volume. In contrast, vasogenic edema increases tissue water content, leading to swelling. Tissue swelling thus requires a vascular contribution if it is to occur. From (Donkin and Vink, 2010), reprinted with permission from Wolters Kluwer Health.

1.2.2 Vasogenic Brain Edema

Vasogenic brain edema is caused by breakdown of the BBB that occurs following either physical disruption or the release of vasogenic compounds (Donkin and Vink, 2010). The BBB is made up of intercellular tight junctions between endothelial cells that line the blood vessels and capillaries of the central nervous system. Specialized transport systems therefore must exist on the membrane of the endothelial cell to move polar substances such as glucose from the blood to the brain and vice versa. In the healthy brain, water is efficiently kept out of the brain by the osmotic force imposed from retained ions and plasma proteins in the blood (Kimelberg, 1995). When BBB breakdown occurs, solutes are no longer retained in the vessel; the blood filtrate, including plasma proteins are driven into the brain by hydrostatic pressure and water is no longer retained in the vessel (Nagashima et al., 1990). In humans vasogenic edema primarily affects white matter due to higher compliance associated with the multiple unconnected parallel axonal tracts (Marmarou, 2007). Several inflammatory and vasoactive factors have been reported to cause breakdown of the BBB (Abbott, 2000). Neurogenic inflammation that occurs following cytotoxic edema has been shown to result in the release of vasoactive agents that can increase vascular permeability such as such as bradykinins and substance P (Donkin and Vink, 2010). The release of such factors is exacerbated if necrotic cell death occurs. **Matrix metalloproteinases** (MMPs) represent another interesting group of proteins that may contribute to vasogenic edema (Candelario-Jalil et al., 2009). MMPs can degrade extracellular matrix

proteins including tight junctions of the BBB. MMP inhibitors have been reported to reduce BBB injury, cerebral edema and cell death in animal models of TBI and ischemia (Candelario-Jalil et al., 2009; Homsi et al., 2009; Tejima et al., 2009), and transgenic mice lacking MMP-9 have been shown to be protected from ischemia and traumatic brain injury with reduced edema and improved functional outcome (Wang et al., 2000; Asahi et al., 2001).

1.2.3 Cytotoxic Brian Edema

Cytotoxic brain edema is the principal cause of mortality from stroke and traumatic brain injury (TBI) although the cellular mechanisms remain largely unknown (Klatzo, 1987; Marmarou et al., 2000; Rosenblum, 2007; Donkin and Vink, 2010). The cellular process of cell swelling termed, cytotoxic brain edema begins with the extracellular to intracellular movement of Na^+ and other cations into neurons and/or astrocytes (Liang et al., 2007). This occurs via transmembrane cation channels and transporters in combination with the failure of energy dependent extrusion mechanisms. The influx of cations then leads to a secondary influx of anions (most likely Cl^-) and osmotically obliged water thereby causing cell swelling. Although it is possible in principle for cytotoxic brain edema to occur without a change in brain volume, and solely a decrease in extracellular volume this is not the case *in vivo*. The depletion of extracellular ions will form new concentration gradients across the BBB and thereby trigger the transport of ions from the blood into the brain in order to replace them along with water that causes

an increase in brain volume (Liang et al., 2007; Simard et al., 2007). In addition, regulatory volume decrease (RVD) mechanisms are often activated in neurons and astrocytes in an attempt to compensate for and counteract cell volume increases. RVD in astrocytes is associated with the swelling-induced activation of channels such as the volume regulated anion channel (VRAC) that can release osmolytes such as taurine into the extracellular space (Phillis et al., 1997; Choe et al., 2012). As these osmolytes are not normally present in the extracellular space, they may contribute to new osmotic gradients across the BBB that will thereby draw water into the brain from the blood.

Regardless of whether brain edema originates from cytotoxic or vasogenic mechanisms, the increased intracranial pressure often leads to constriction of the cerebral vasculature and a resultant decrease in blood flow causing local ischemia. The decrease in energy supply to neurons and astrocytes results in failure to maintain their cationic gradients via adenosine triphosphate (ATP) driven pumps such as the Na^+/K^+ ATPase and generation or exacerbation of cytotoxic edema (Kimelberg, 1995).

1.2.4 Medical Management and Treatment of Cerebral Edema

As of today the treatment of cytotoxic edema is mainly symptomatic, with the major focus being on decreasing intracranial pressure (ICP) (Unterberg et al., 2004). **Osmotherapy**, defined as the elevation of plasma osmolarity, is undertaken to draw water from the extracellular CSF of brain back across the BBB into the blood in a

process called brain dehydration. The first attempts at manipulating brain volume by osmotic manipulations were done almost 100 years ago (Weed and McKibbens, 1919). However, initial clinical attempts were largely unsuccessful due to the adverse effects of the concentrated urea or human plasma proteins that were used as an osmolyte (Paczynski, 1997; Raslan and Bhardwaj, 2007). In 1960 the use of mannitol was introduced and remains the osmolyte of choice today (Shenkin et al., 1962; Fink, 2012). Although osmotherapy has been used in the clinical setting as an effective method for decreasing brain volume and ICP (Shenkin et al., 1962; Diringer and Zazulia, 2004), it's usefulness remains controversial and poorly understood for the several reasons. First, in cases of vasogenic edema with severe BBB disruption mannitol can accumulate in the injured brain and thereby worsen the edema, as previously reported (Kaufmann and Cardoso, 1992; Bereczki et al., 2000), which may contribute to a rebound effect (Palma et al., 2006). Second, mannitol administration in certain cases has been reported to shrink only the non-swollen regions of the brain (Hartwell and Sutton, 1993; Diringer and Zazulia, 2004). Although, this will still reduce ICP it offers limited therapeutic benefit to the damaged tissue. Third, healthy cells individually compensate for the decrease in volume by triggering unknown regulatory volume increase (RVI) mechanisms, and this may contribute to a rebound effect when mannitol is withdrawn (McManus and Soriano, 1998). It is interesting to note that mannitol also exerts biological effects, and it is possible that some of the reported positive actions could be a result of off target effects such as free radical scavenging (Shen et al., 1997).

Controlled **hyperventilation** can be used to decrease ICP by causing cerebral vasoconstriction and thereby a reduction the blood volume. However, hyperventilation can only be used acutely as it reduces brain tissue PO_2 (Rabinstein, 2006) and may cause secondary ischemic damage (Muizelaar et al., 1991), limiting it's usability. **Barbiturates** also act to decrease ICP by decreasing the cerebral blood volume as a result of lowering the metabolic demands of the brain. Barbituates are used in cases where the increases in ICP are life threatening and uncontrollable (Eisenberg et al., 1988; Raslan and Bhardwaj, 2007), however, whether they improve functional outcome remains controversial (Ward et al., 1985; Schwab et al., 1997; Rabinstein, 2006).

Glucocorticoids are used primarily in the treatment of vasogenic edema that accompanies tumors, and preceding neurosurgical manipulation (French and Galicich, 1964; Rabinstein, 2006). Glucocorticoids decrease tight-juntion permeability, thereby increasing vascular water retention across the BBB, however the precise mechanisms of action are unknown (Raslan and Bhardwaj, 2007). Unfortunately in clinical trials for ischemic stroke, hemorrhage and head injury, corticosteroids had no beneficial effect in treating edema, and may have even been harmful in some cases (Dearden et al., 1986; Qizilbash et al., 2002; Roberts et al., 2004; Gomes et al., 2005). Steroids have no beneficial effect in the treatment of cytotoxic brain edema.

Hypothermia lowers the metabolic demand of the brain and has been proven to reduce ICP in animal models and human patients (Choi et al., 2012a; Yenari and Han, 2012). The reduction in ICP is in part due to a reduction in cerebral

blood volume, but may also involve other mechanisms such as a reduction in the release of inflammatory factors that increase BBB permeability and by decreasing the rate of cellular energy consumption. Despite promising results of many observational studies and phase II clinical trials (Polderman, 2008), several phase III trials failed to demonstrate any benefit of hypothermia following TBI (Clifton et al., 2001; Hutchison et al., 2008). In addition to the potential systemic complications a major concern of these studies was that rewarming occurred after 24 to 48 hours, the time when brain edema is maximal (Choi et al., 2012a). Currently, cooling is generally only used to treat brain edema when other methods to reduce ICP are unsuccessful. Further studies to identify the optimal conditions and timing of hypothermia in the treatment of brain edema are needed to validate widespread clinical use. Hypothermia may be further beneficial when combined with other neuroprotective strategies.

Decompressive craniectomy, the removal of a portion of the skull, is a controversial surgery used to reduce ICP in life threatening cases of cerebral edema. Although it is clear that craniectomies reduce ICP and can be life saving, a beneficial functional outcome on survivors remains unproven, which may partly be explained by age of the patient and the time of surgery (Taylor et al., 2001; Rabinstein et al., 2006; Plesnila, 2007). Decompressive craniectomy is usually reserved for patients who fail to respond to all other therapeutic measures, a time delay which unfortunately may decrease the efficacy of the operation (Rabinstein, 2006; Plesnila, 2007).

Although treatments (outlined above) exist to reduce the ICP elevations associated with cytotoxic edema, they remain largely empirical, and **a better understanding of the underlying cellular and molecular mechanisms is needed to identify new and more effective forms of treatment** (Rabinstein, 2006; Marmarou, 2007; Raslan and Bhardwaj, 2007).

1.3 Volume Regulation in the Central Nervous System (CNS)

1.3.1 Water Transport in the Brain

Aquaporins (AQPs), discovered in 1992 (Preston et al., 1992), are transmembrane proteins that function as water channels. AQP1, AQP4 and AQP9 isoforms are expressed in the brain, with AQP4 showing the highest levels of expression (Amiry-Moghaddam and Ottersen, 2003). AQP4 expression is highly polarized and is found to be enriched on astrocyte endfeet that are in direct contact with blood vessels (Nielsen et al., 1997; Rash et al., 1998), suggesting involvement in cerebral water and volume homeostasis. AQP4 expression has been shown to be colocalized with Kir4.1 (Nagelhus et al., 1999), and deletion of AQP4 in mice results in increased seizure duration (Binder et al., 2006a; Binder et al., 2006b), suggesting a possible role for AQP4 water influx coupled to local K^+ buffering following neuronal activation. AQP4 KO mice have recently been shown to reduce the rate at which interstitial solutes are cleared from the brain (Iliff et al., 2012; Rangroo Thrane et al., 2013), and AQP4 may therefore be important for the clearance of

metabolites from the brain during sleep (Xie et al., 2013). However, AQPs are not the only transmembrane proteins capable of water transport but rather increase the energetic efficiency and rate of water transport (Zeuthen, 2010). This may explain the lack of an observable phenotype first described in AQP4 KO mice (Manley et al., 2000). In line with this, a quadruple knockout of all AQPs found present in the osmoregulatory tissues of caenorhabditis elegans had no effect on survival, development, growth, fertility or movement in normal or hypertonic media (Huang et al., 2007). The role of AQPs seems to generally become more clear under conditions of stress, for example the inability of AQP1 KO mice to concentrate urine only becomes apparent after 36 hours of water deprivation (Ma et al., 1998). Due to the high expression of AQP4 in astrocyte endfeet at the interface of astrocytes with endothelial cells forming the blood brain barrier, it seems likely that AQP4 may regulate the rate of water entry into the brain. This was confirmed in AQP4 KO mice following intraperitoneal (IP) distilled water infusions equal to 20% of the mouse body weight. Whereas only 8% of wild type mice survived, 60% of the AQP4 KO mice survived the insult (Manley et al., 2000). The same study also showed decreased hemispheric brain enlargement (a marker of cerebral edema) in AQP4 KO mice 24 hours after permanent middle cerebral artery occlusion (MCAO). However, targeting aquaporins for the treatment of cerebral edema remains controversial since aquaporins are also a pathway for water efflux from the brain (Iliff et al., 2012). In fact deletion of AQP4 severely worsens edema and outcome in models of vasogenic brain edema (Papadopoulos et al., 2004a; Papadopoulos et al., 2004b). Additionally, the initial analysis on hemispheric volume and neurologic scores by

Manley et al. was only done 24 hours following MCAO (Manley et al., 2004), whereas maximal edema may have yet to occur (Simard et al., 2007). In a more recent analysis of AQP4 KO mice following a transient MCAO (40min) model, AQP4 KO mice showed more severe neurological deficits and a striking mortality rate of 88% compared to 24% for WT mice (Zeng et al., 2012). Although, APQ4 inhibition may decrease the rate of water entry across an intact BBB following cytotoxic edema, due to their dual role in water extrusion, it is doubtful that that the generation AQP antagonists will serve much use in the treatment of brain edema. This is because the primary goal of edema treatment is to decrease ICP which is not realized by AQP4 deletion that exacerbates vasogenic edema that often succeeds the initial cytotoxic edema. Additionally, as the driving force for the generation of cytotoxic edema is imbalanced ionic concentrations, AQP4 inhibition will likely only reduce the speed of edema generation, but not the final extent of the volume increase.

Unlike astrocytes, neurons do not express aquaporin water channels (Amiry-Moghaddam and Ottersen, 2003). However, this does not mean that they do not transport water. **Water transport is a general feature of many co-transporters** (Zeuthen and Zeuthen, 2007; Zeuthen, 2010; Zeuthen and Macaulay, 2012) many of which are expressed on the neuronal plasma membrane such as cation-chloride cotransporters, glutamate transporters, gamma-aminobutyric acid (GABA) transporters and monocarboxylate transporters. There are two distinct modes of water transport that have been reported by transporters; secondary active cotransport and passive water transport (**Figure 1.2**). Secondary co-transport is water transport that occurs along with the transporter's substrate. The amount of

transported water can be quite significant, for example NKCC1 transports 590 water molecules per transport cycle (Hamann et al., 2005), and the lactate-H^+ transporter, MCT1, transports 500 water molecules per transport cycle (Hamann et al., 2003) . An important characteristic of secondary co-transport is that it does not require an osmotic driving force, and can actually transport water "uphill" against the osmotic gradient; water is always transported in the direction of substrates. Some transporters also display passive transport, which is defined by water transport through the pore of the protein analogous to AQP mediated transport (Zeuthen, 2010). This mode of transport does not apply to all co-transporters capable of water transport, and has been most thoroughly described in Na^+ coupled neurotransmitter transporters such as excitatory amino acid transporters (EAATs) and GABA transporters (GATs) (Loo et al., 1999; MacAulay et al., 2001; Loo et al., 2002; MacAulay et al., 2002). The osmotic water permeability per transporter for EAAT1 and GAT1 are $0.2*10^{-14}$ cm^3s^{-1} and $0.7*10^{-14}$ cm^3s^{-1} respectively versus $4*10^{-14}$ cm^3s^{-1} for AQP1 (Zeuthen, 2010). Given, the aforementioned studies on passive water transport, the observation that in contrast to astrocytes, neurons do not swell following a small (~13%) hyposomotic stimulation remains mysterious (Andrew et al., 2007). This result was attributed to the fact, that neurons do not express functional water channels. Another possibility in line with this hypothesis could be that as the water permeability of neurons is much lower than that of the aquaporin expressing astrocytes, volume regulatory mechanism are able to compensate for the water entry triggered by osmotic insults on a similar or more rapid time course.

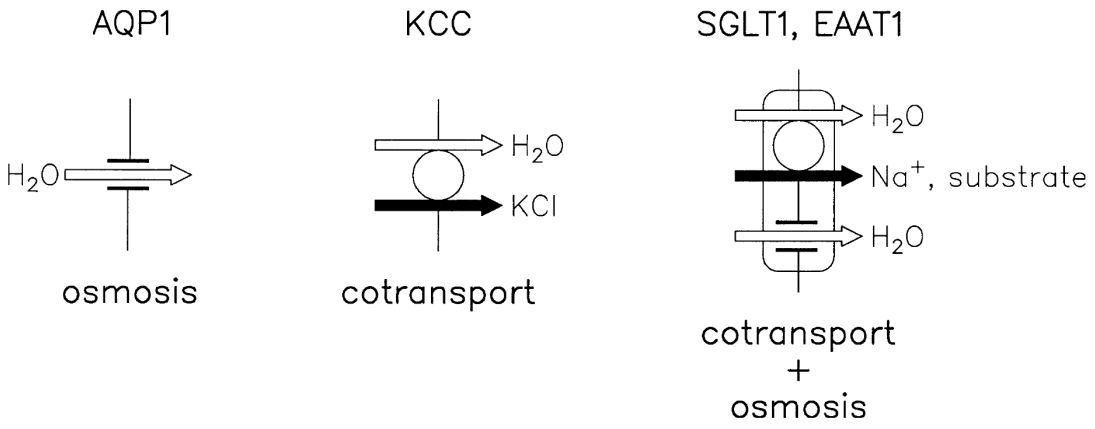

Figure 1.2: Molecular mechanism of water transport across cell membranes. Water crosses membranes by diffusion in the lipid bilayer, by osmosis in channels and by cotransport in cotransporters and uniporters. Diffusion and osmosis are driven by the water chemical potential difference. The cotransporters and the uniporters function as molecular water pumps in which free energy contained in the substrate gradient can be transferred to the transport of water; i.e., a downhill transport of substrate can energize an uphill transport of water. Some cotransporters, such as the KCC, employ only cotransport; others, such as the SGLT1 and the EAAT1, employ both cotransport and osmosis. From (Zeuthen, 2010), reprinted with permission from Springer.

1.3.2 Volume Regulation During Apoptosis and Necrosis

The morphological changes that occur during apoptosis and necrosis are drastically different. Whereas necrosis is characterized by karyolysis (dissolution of the nucleus), cell swelling and membrane blebbing, apoptosis is accompanied by cell shrinkage, pyknosis (chromatin condensation) and karyorrhexis (fragmentation of the nucleus) (**Figure 1.3**). Necrosis ultimately results in the loss of cell membrane integrity and the release of cytoplasmic contents triggering an inflammatory response, whereas during apoptosis cellular contents are contained in apoptotic bodies and rapidly phagocytosed (Elmore, 2007). Originally, necrosis was thought to be an uncontrollable passive process that did not require energy and was referred to as "accidental cell death" whereas apoptosis, an energy dependent process triggered by precise cellular mechanisms was referred to as "programmed cell death". However, recent research has suggested that some forms of necrotic cell death may also be governed by a set of distinct molecular mechanisms, and classified as necroptosis (described bellow).

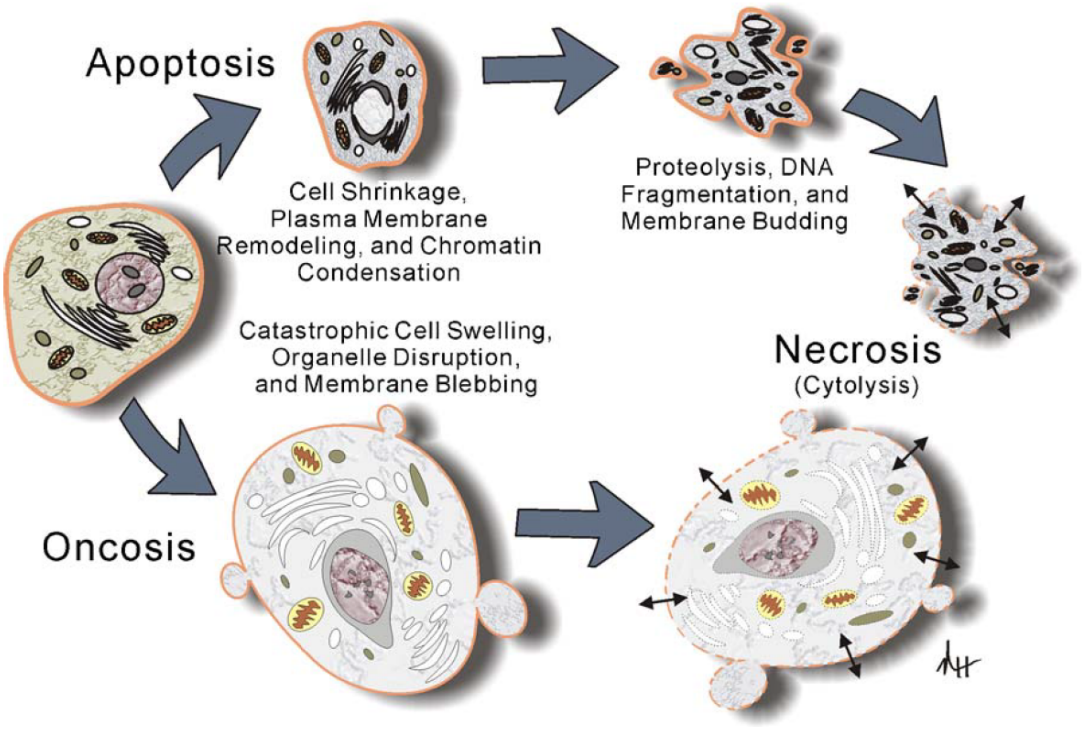

Figure 1.3: The morphological features of apoptosis, oncosis and necrosis. From (Hail et al., 2006), reprinted with permission from Springer.

Morphologically, apoptosis is characterized by cell rounding, pyknosis (chromatin condensation), nuclear fragmentation, the formation of apoptotic bodies and **cell shrinkage** and was originally termed "shrinkage necrosis" (Kerr, 1971; Kerr et al., 1972). The process of isotonic cell shrinkage that occurs during apoptosis is called **apoptotic volume decrease** (AVD). AVD is triggered by the efflux of potassium and chloride along with osmotically obliged water (Heimlich et al., 2004). The role for K^+ efflux in the generation of apoptosis is well established. Accumulating evidence suggests rather than playing a secondary passive role associated with cell death, AVD may actually play a key role in driving apoptosis. Blocking neuronal K^+ channels with TEA can inhibit apoptosis in neurons, even when increases in $[Ca^{2+}]_i$ persist (Yu et al., 1997) and the K^+ ionophore, valinomycin can trigger apoptosis (Allbritton et al., 1988; Ojcius et al., 1991; Yu et al., 1997). However, the effects of potassium on apoptosis are complex, although K^+ efflux is a requirement for AVD, K^+ also inhibits some of the apoptotic machinery (K_i of caspase-3 and endonucleases for K^+ are around 40mM and 65mM $[K^+]$ respectively) (Hughes et al., 1997; Yu and Choi, 2000). The ability to trigger apoptosis by inducing sustained shrinkage with hyperotonic solutions, led to the hypothesis that AVD may actually be an active process necessary for apoptosis (Bortner and Cidlowski, 1996, 1998). In support of this hypothesis AVD has been reported to occur early in the apoptotic cascade before DNA fragmentation, cytochrome c release and caspase-3 activation (Maeno et al., 2000; Okada et al., 2006) and pharmacological inhibition of K^+ or Cl^- channels can block both the AVD and the subsequent cell death triggered by apoptotic stimuli (Maeno et al., 2000; Porcelli et al., 2004; Okada et al., 2006). As

different cell types are endowed with different ion channels, the identity of the K^+ and Cl^- channels responsible for AVD most likely differ in different cell types. The most commonly reported Cl^- channel underlying AVD displays properties of the volume-sensitive outward rectifying Cl^- channel (VSOR) also named the volume-regulated anion channel (VRAC), which until very recently had no known molecular identity (Okada et al., 2006). Proposed candidates for the molecular identity of the Cl^- channel were CLC-3 (Duan et al., 1997) or the plasmalemmal voltage-dependent anion channel (pl-VDAC) (Elinder et al., 2005), however, these results remain controversial as apoptotic stimuli still trigger VSOR-like currents in the absence of either channel (Wang et al., 2005; Sabirov et al., 2006). Two recent and independent studies have claimed to have identified a key component of the classically described VRAC channel as LRRC8A (Qiu et al., 2014; Voss et al., 2014), a gene that shares a common ancestor with pannexins (Abascal and Zardoya, 2012). However, a potential role for LRRC8 proteins in AVD and apoptosis has yet to be investigated. TMEM16A and B were recently identified as molecular candidates for calcium activated chloride channels (Schroeder et al., 2008), that can be activated by cell swelling and contribute to regulatory volume decrease (Almaca et al., 2009). Interestingly, TMEM16B was recently shown to be functionally expressed in pyramidal neurons of the hippocampus as an outwardly rectifying calcium activated Cl^- channel (Huang et al., 2012). Given TMEM16B's ability to be activated by Ca^{2+} entry through N-methyl-D-aspartate (NMDA) receptors it would be interesting to test whether TMEM16B is activated during apoptosis and if it contributes to the AVD and resultant apoptotic cell death in neurons.

Necrosis is characterized morphologically by **cell swelling** and membrane blebbing. Necrosis refers to the degradative process that occurs after the cell has died and is therefore argued to be inappropriate. The term **Oncosis** (from onkos, meaning swelling) was coined by von Recklinghausen in 1910 to describe cell death by swelling, and is a more suitable term to describe the cellular processes leading to necrosis (Majno and Joris, 1995). Contrary to cell shrinkage in apoptosis the mechanisms underlying cell swelling are less well described, which may be attributable to the fact that oncosis/necrosis has long been thought of as an irreversible process. The increase in cell volume that causes necrosis is thought to arise mainly from increases in intracellular Na^+, due to defective outward pumping caused by ATP depletion or by influx via membrane transporters and channels (Barros et al., 2001). In hepatocytes for example, inhibition of intracellular Na^+ accumulation has shown to be protective against cellular swelling and the development of necrosis induced by inhibition of mitochondrial oxidative phosphorylation (Carini et al., 1995; Carini et al., 1999). However, few reports have investigated the underlying mechanisms that cause oncosis leading to necrosis.

Although necrosis was originally described as passive cell death, recent advances have in part challenged this view, suggesting that at least some forms of necrosis may be executed via precise mechanisms; a programed cell death process leading to necrosis termed **necroptosis** (Zhang et al., 2009; Vandenabeele et al., 2010; Wu et al., 2012; Re et al., 2014). Morphologically necroptosis exhibits features of necrosis such as cell swelling and disruption of the plasma membrane. Necroptosis involves a unique molecular signaling cascade involving specific

proteins RIP1 and RIP3 and can be inhibited by necrostatins (Zhang et al., 2009; Vandenabeele et al., 2010). These new findings suggest that the cellular process leading to necrosis may involve distinct steps that could be targeted therapeutically. Compared to apoptosis, however, the mechanisms underlying necroptosis are only starting to be uncovered and the role of cell swelling in this process remains unknown. It would be interesting to test the following questions: 1) Can cell swelling trigger necroptosis? and 2) Can necroptosis be blocked by blocking cell swelling?

1.3.3 A Brief History of Excitotoxic Neuronal Swelling

Following the observation by Lucas and Newhouse in 1957 that glutamate caused damage to the inner retina (Lucas and Newhouse, 1957), John Olney showed that the food additive monosodium glutamate killed brain neurons in newborn mice and coined the term **excitotoxicity** (Olney, 1969). He noted that the excessive activation of neurons by glutamate led to acute swelling of both the neuronal soma and their dendrites that preceded necrosis (Olney, 1971). In 1985, Rothman discovered that by removing chloride from the extracellular solution of neurons exposed to glutamate he was able to inhibit glutamate toxicity and the associated swelling in cultured hippocampal neurons (Rothman, 1985). Rothman concluded that the pathophysiology of amino acid neurotoxicity was rather straightforward, in that substances that caused a steady depolarization led to passive chloride influx which along with cations resulted in water entry and cell lysis. However it is now

known that Cl^- is not passively distributed across the neuronal plasma membrane (Alvarez-Leefmans and Delpire, 2009), and therefore the Cl^- entry required for swelling must either involve active transport or activation of a Cl^- conductance pathway that is not open at rest. Within months of Rothman's discovery, Dennis Choi discovered another pathway by which neurons could die following excitotoxic insults that depended on the influx of calcium and not sodium (Choi, 1985). In a subsequent paper Choi elegantly demonstrated that there were in fact two separate and distinguishable cell death pathways following excitotoxic insults (Choi, 1987). The first component was marked by neuronal swelling, occurred early, and was dependent on extracellular Na^+ and Cl^-, but was independent of extracellular Ca^{2+}. The second component was marked by gradual neuronal disintegration, occurred late, was dependent on extracellular Ca^{2+}, and could be mimicked by a Ca^{2+} ionophore. The mechanisms governing the entry of chloride remain largely unknown, although a partial reduction in neuronal swelling was observed by blocking $GABA_A$ receptors in cell culture (Hasbani et al., 1998). The role of $GABA_A$Rs in excitotoxic neuronal swelling are discussed in section 1.5.2, however, reports in situ have shown that the majority of Cl^- influx occurs via other unidentified mechanisms (Allen et al., 2004; Pond et al., 2006)

1.2.4 Cortical Spreading Depression and the Anoxic Depolarization

Discovered by Leao in 1944, spreading depression (SD) is a wave of depolarization that propagates in all directions across the brain at a velocity of 2-5 mm/min (Leao, 1944). Spreading depression also called spreading depolarization

and the closely related anoxic depolarization are characterized by a rapid and nearly complete depolarization of a population of neurons that occurs with a massive redistribution of intracellular and extracellular ions coincident with neuronal volume changes and cytotoxic edema (Somjen, 2001; Dreier, 2011; Lauritzen et al., 2011). Simultaneous with the near complete breakdown of ionic gradients occurs the swelling of neurons and distortion of dendritic spines (Takano et al., 2007; Zhou et al., 2010; Zhou et al., 2013). The neuronal swelling that occurs is coincident with a sharp peak in the intrinsic optical signal (Zhou et al., 2010), that occurs at the onset of SD. Electrophysiological recording in humans have shown unequivocally that SD occurs during a variety of brain injuries such as, subarachnoid hemorrhage, ischemic stroke and traumatic brain injury and that the occurrence of SD is often associated with worsened outcomes (Dreier, 2011; Lauritzen et al., 2011). Although the cellular mechanisms triggering SD and the SD like wave during the anoxic depolarization may be caused by different mechanisms, the ionic changes and neuronal swelling that occur are similar (Somjen, 2001; Dreier, 2011). A key difference between the transient spreading depolarization and the prolonged anoxic depolarization is the availability of ATP that is required to restore ionic gradients and repolarize the neuron. During ischemic insults, ATP levels drop drastically in the ischemic core, which leads to failure of the Na^+/K^+ ATPase. Extracellular Na^+ decreases and extracellular K^+ increases, thereby decreasing and possibly even reversing the function of Na^+ and K^+ driven transporters such as those required for the uptake of glutamate (Rossi et al., 2000). The increases in extracellular glutamate activates ionotropic glutamate receptors, thereby further increasing intracellular

Na^+ and causing a viscous feed-forward cycle resulting in the resultant anoxic depolarization (Somjen, 2001, 2002), which also involves the activation of non-selective cation channels (Aarts et al., 2003; Thompson et al., 2006). The situation in the penumbra is different due to relatively preserved ATP compared to the penumbra region (Welsh et al., 1991; Hossmann, 1994). Transient depolarizations are still observed in the penumbra resembling more similarity to the SD than to the anoxic depolarization (Ginsberg and Pulsinelli, 1994; Dreier, 2011), possibly triggered by increases in extracellular K^+ or glutamate released closer to the core (Nedergaard and Hansen, 1993; Hossmann, 1996). Very short and transient SDs such as those correlated with migraine aura do not cause cell death, however if the duration of SD is prolonged, brain damage is often observed (Dreier, 2011). During ischemic events, the number and duration of SDs observed in the penumbra is positively correlated with cell death and infract volume (Mies G., 1993; Dijkhuizen et al., 1999; Hartings et al., 2003). Additionally, artificially triggered spreading depolarizations outside the penumbra but that propagated into the penumbra caused an enlargement of the necrotic core (Back et al., 1996; Busch et al., 1996; Takano et al., 1996).

1.4 Chloride homeostasis

1.4.1 Introduction to Chloride Homeostasis and Chloride Equilibrium

The initial concept that Cl^- was passively distributed across the plasma membrane came about because it was dominated by work done in skeletal muscle where Cl^- permeability is extremely high, in fact Cl^- permeability is more than twice the permeability of K^+ (Hodgkin and Horowicz, 1959; Alvarez-Leefmans and Delpire, 2009), therefore setting resting membrane potential (E_m) very close to the chloride equilibrium potential (E_{Cl^-}). The discovery that activation of $GABA_AR$ ligand gated Cl^- channels hyperpolarized neurons (Boistel and Fatt, 1958; Kuffler and Edwards, 1958) while depolarizing other types of neurons such as sensory neurons (De Groat et al., 1972) made it clear that E_{Cl^-} was not set at E_m and therefore that chloride must be actively transported across the plasma membrane. Perhaps the best example of this is demonstrated by the fact that immature pyramidal neurons show depolarizing GABAergic responses that then switch to hyperpolarizing responses later in development (Ben-Ari et al., 2007), although it should be pointed out that in addition to Cl^-, $GABA_ARs$ are also permeable to HCO_3^-, and therefore [HCO_3^-] can also affect E_{GABA} (Rivera et al., 2005). The predominant transporters known to govern Cl^- transport in neurons and set up E_{Cl^-} are the cation-chloride cotransporters, KCC2 and NKCC1 (Blaesse et al., 2009)(see section 1.4.5). There also may be a role for Na^+ dependent and Na^+ independent anion exchangers that exchange Cl^- for HCO_3^- (Grichtchenko et al., 2001; Payne et al., 2003; Gonzalez-Islas et al., 2009).

Additionally, a recently discovered Cl^-, HCO_3^-, SO_4^{2-} exchanger was shown to be highly expressed in neurons throughout the brain, although a functional role for this transporter in neurons has not yet been tested (Rahmati et al., 2013). In addition to $[Cl^-]_i$ regulation by transporters, a recent study has suggested that the large impermeable intracellular anions that make up the bulk of the anionic intracellular milieu play a significant role in setting E_{Cl^-} (Glykys et al., 2014). This may in part explain how neurons display subcellular differences in E_{GABA} despite a relatively uniform distribution of cation-chloride cotransporters (Doyon et al., 2011). Importantly, it is these same large anions that also explain why small changes in intracellular Cl^- are tightly linked to cell volume changes; unlike the entry of Na^+ cations that can be balanced by efflux of K^+, sustained increases in $[Cl^-]_i$ create a Gibbs-Donnan imbalance, and therefore either combined cation and water influx or anion efflux must occur.

1.4.2 Aberrant Chloride Regulation in CNS Disorders

In the adult brain, equilibrium between excitation and inhibition is an essential feature for proper function, and disequilibrium is often a central theme underlying brain disorders such as epilepsy, neuropathic pain, addiction as well as psychiatric illnesses.

$GABA_A$ mediated inhibition is of utmost importance in dampening excitation, and agents that block $GABA_A$ receptors generate seizures. In adult neurons of the cortex and hippocampus, if $[Cl^-]_i$ increases and causes the equilibrium potential for

chloride (E_{Cl^-}) to become more depolarized relative to E_m, activation of $GABA_A$ receptors will result in Cl^- efflux and depolarizing responses. Temporal lobe epilepsy is associated with perturbed chloride homeostasis (Cohen et al., 2002), possibly due to decreased KCC2 expression as observed in a minority of pyramidal neurons from human epileptic tissue showing depolarized $GABA_A$ receptor mediated post-synaptic events (Huberfeld et al., 2007). Insults such as ischemia and TBI that cause increases in Cl^- concentration and cytotoxic edema, often result in seizures with patients responding poorly to anticonvulsants that act on $GABA_A$ receptors (Young et al., 1990). In a neonate (p5-7) brain slice model of TBI, it was noted that the NKCC1 inhibitor bumetanide was capable of decreasing the post-traumatic levels of Cl^- (Dzhala et al., 2012), consistent with other studies implicating a role for NKCC1 Cl^- transport in neonatal seizures (Dzhala et al., 2005; Dzhala et al., 2010). Identifying other mechanisms that cause neuronal Cl^- increases in the adult brain with low levels of NKCC1 expression (Wang et al., 2002) may help in developing therapeutics to reduce the excitation/inhibition imbalance following trauma and ischemia.

Aberrant Cl^- homeostasis within the spinal dorsal horn results in neuropathic pain, underlying tactile allodynia (Coull et al., 2003). Excitatory output of the dorsal horn is normally suppressed by a large network of inhibitory connections, however, following peripheral nerve injury a depolarizing shift in E_{Cl^-} occurs leading to decreased and often reversal of $GABA_A$ and glycine receptor responses. Surprisingly it was found that the mechanism underlying this shift in E_{Cl^-} was in fact caused by release of brain-derived neurotrophic factor (BDNF) from ATP stimulated microglia

acting on TrkB receptors in spinal lamina I neurons (Coull et al., 2005). The ATP-microglia-BDNF-TrkB signal causes down-regulation of KCC2, the major Cl^- extrusion mechanism in adult neurons, thereby reducing inhibition via Cl^- accumulation and a depolarizing shift in E_{Cl^-}. It was also found that this same mechanism was implicated in morphine hyperalgesia, caused by μ opioid receptor driven expression of P2X4Rs in microglia (Ferrini et al., 2013). Whether this microglia-BDNF-TrkB-KCC2 signaling pathway contributes to Cl^- homeostasis in other brain regions and other neurological disorders remains to be tested.

Similarly, opiate activation of the mesolimbic dopamine system causes the switching of $GABA_AR$ responses on ventral tegmental area GABAergic neurons from hyperpolarizing to depolarizing (Laviolette et al., 2004), underling the switch from an opiate-nondependent to an opiate-dependent state, likely via increases in BDNF (Vargas-Perez et al., 2009). However, the source of BDNF in this circuit has not yet been described.

1.5 Chloride Channels and Transporters in the CNS

1.5.1 CLC family of Chloride Channels and Transporters

The CLC family represents a highly conserved family of chloride transporters with 9 members found in the mammalian genome (Stauber et al., 2012). CLC proteins most commonly form homodiemers, however heterodimerization has been observed (Lorenz et al., 1996; Weinreich and Jentsch, 2001). CLCs are classified as

double barrel channels and transporters in that each subunit encloses it's own permeation pathway, with several members exhibiting electrogenic ($1Cl^-/2H^+$) exchange rather than being Cl^- selective channels (Accardi and Miller, 2004). CLC-1, -2, -Ka, and -Kb reside in the plasma membrane, whereas all other CLCs are predominantly found in intracellular organelles and vesicles. Of the CLCs shown to regulate Cl^- across the plasma membrane, only CLC-2 shows expression in the brain and has been detected in both neurons and glia (Sik et al., 2000). Interestingly, CLC-2 is activated by osmotically induced cell swelling (Grunder et al., 1992). However, CLC-2 is activated by hyperpolarization and CLC-2 currents display strong inward rectification, making it an unlikely Cl^- loader in neurons as hyperpolarization would lead to Cl^- efflux. In fact, CLC-2 has been shown to mediate exclusively Cl^- efflux from neurons (Staley et al., 1996; Rinke et al., 2010), and may aid in rapidly re-setting E_{Cl^-} after Cl^- influx. Surprisingly input resistance was increased by over 75% in CA1 pyramidal neurons of CLC-2 KO mice, suggesting a large role for CLC-2 in modulating neuronal excitability (Rinke et al., 2010). CLC-2 is strongly inhibited by Zn^{2+}, and poorly inhibited by nonspecific Cl^- channel inhibitors such as 4,4'-diisothiocyano-2,2'-stilbenedisulfonic acid (DIDS) and 5-Nitro-2-(3-phenylpropylamino)benzoic acid (NPPB) (Clark et al., 1998; Stauber et al., 2012).

1.5.2 $GABA_A$ Receptor Channels

Gamma-aminobutyric acid (GABA) and glycine are the major inhibitory neurotransmitters of the CNS. In pyramidal neurons of the hippocampus and cortex,

however, fast inhibitory transmission is mediated by $GABA_A$Rs, in contrast to the co-transmission by GABA and glycine that occurs in other systems such as the spinal cord (Jonas et al., 1998). $GABA_A$Rs are heteropentameric ion channels assembled from a large family of subunits, there exist 8 identified subunit families each with multiple subtypes and splice variants resulting in multiple different possible channel configurations with different properties. $GABA_A$Rs are permeable to both Cl^- and HCO_3^- with a ratio of around 4:1 (Kaila and Voipio, 1987; Staley et al., 1995). Therefore, the direction of net current depends on the intracellular and extracellular concentrations of Cl^- and HCO_3^- as well as the membrane potential of the cell. In most mature CNS neurons GABA receptor activation leads to Cl^- influx and therefore hyperpolarization, although in immature neurons and peripheral neurons $GABA_A$R activation can be depolarizing as intracellular Cl^- concentration is maintained above electrochemical equilibrium (Ben-Ari et al., 2007). For this reason changes in intracellular Cl^- can profoundly affect inhibitory transmission and is implicated in many CNS disorders (see section 1.4.2). $GABA_A$ receptors are the target of many drugs with clinical importance, including barbituates, benzodiazepines, steroids, anesthetics and alcohol. Following excitotoxic insults such as ischemia, the extracellular GABA concentration increases due to a combination of vesicular release and reversal of GABA transporters (GATs) (Allen et al., 2004), possibly causing Cl^- influx. Indeed, $GABA_A$Rs have been shown to mediate a portion of excitotoxic neuronal swelling in cell culture (Hasbani et al., 1998). In brain slices it was also shown that blocking $GABA_A$Rs led to a small reduction in the initial rapid increase (<1 min) of the intrinsic optical signal (a marker of cell swelling) following

oxygen glucose deprivation (OGD), however, blocking $GABA_A$Rs had no effect on final intrinsic optical signal increase (>2 min)(Allen et al., 2004). Additionally it was observed that calcium influx caused $GABA_A$Rs to become completely inactivated within 2 minutes of the anoxic depolarization. These results suggest that although $GABA_A$Rs can contribute to neuronal swelling via a transient increase in Cl^-, the majority of the Cl^- influx that occurs during ischemia and other excitotoxic insults occurs via another mechanism. Consistent with these results, Cl^- imaging in pyramidal neurons with the genetically encoded Cl^- indicator Clomeleon showed no effect of blocking $GABA_A$Rs on the magnitude of the chloride increase during *in vitro* ischemia (Pond et al., 2006).

1.5.3 Volume-Activated Anion Channels

Volume-activated anion channels (VAACs) represent the group of anion channels that are activated by increases in cell volume, originally identified based on patch clamp recordings of currents activated following hyposmotic stress. These can be separated into 2 main groups based on their electrophysiological properties; the **maxi-anion channel** and the **volume-sensitive outwardly rectifying anion channel** (VSOR). It is also plausible that various calcium-activated anion channels may function as VAACs. The molecular identities of these channels are just starting to be identified, and are still a large topic of controversy (Alvarez-Leefmans and Delpire, 2009). The maxi-anion channel is present in a variety of cell types and can be activated by swelling, or ATP depletion (Strange et al., 1996). The maxi anion

channel is characterized by a large (300-400pS) single-channel conductance (Sabirov and Okada, 2009), however, it has been observed that the channel may also function in many sub-conductance states. The fully open channel exhibits a linear I-V curve with no rectification. The maxi-anion channel is potently inhibited by Gd^{3+}, but only partially suppressed by non-selective anion channel blockers such as DIDS and NPPB (Sabirov et al., 2001; Alvarez-Leefmans and Delpire, 2009). The channel is also inhibited by arachidonic acid at the micromolar level (Liu et al., 2008a). Due to the large pore of the maxi-anion channel, it is a candidate protein for regulating ATP release, as has been shown in cultured astrocytes (Liu et al., 2008b). In dorsal root ganglion neurons a channel with maxi-anion like pharmacological properties was shown to mediate non-vesicular ATP release following action potential mediated minute swelling of axons (Fields and Ni, 2010), possibly involved in neuron-glia signaling. The most commonly reported VAAC is the volume-sensitive outwardly rectifying anion channel (VSOR), also referred to as the volume-regulated anion channel (VRAC) and $I_{Cl,swell}$ (Alvarez-Leefmans and Delpire, 2009). VSOR displays moderate outward rectification. In contrast to the maxi-anion channel, VSOR has a strict requirement for cytosolic ATP and is inhibited by intracellular Mg^{2+} (Oiki et al., 1994), possibly due to it's ATP binding properties. VSOR is also inhibited by intracellular acidification (Sabirov et al., 2000). VSOR can be inhibited by a wide spectrum of non-specific anion channel blockers, such as DIDS, NPPB and niflumic acid (Strange et al., 1996; Jentsch et al., 2002; Alvarez-Leefmans and Delpire, 2009). VSOR currents were reported to underlie the Cl^- influx required for excitotoxic neuronal necrosis in cell culture (Inoue and Okada,

2007), however these results contrast with a report from the same group suggesting that VSOR is required for neuronal volume recovery following swelling (Inoue et al., 2005). Additionally, it was observed by others that blocking VRAC with NPPB, inhibited neuronal volume recovery following excitotoxic insults such as veratridine exposure (Churchwell et al., 1996). These results, suggest that pyramidal neurons are endowed with volume regulatory machinery displaying pharmacological properties of VRAC. VRAC like currents have also been recorded from cultured astrocytes (Crepel et al., 1998) and may release excitatory amino acids when activated (Kimelberg et al., 2006). In vivo block of astrocyte but not neuronal VRACs with DCPIB (Zhang et al., 2011), resulted in decreased glutamate release and neuroprotection in a rat model of MCAO (Zhang et al., 2008). It is also possible that blocking VRACs could conceivably reduce cerebral edema, not solely by reducing neurotransmitter release or by blocking cell swelling (VRAC activation reduces cell volume), but by blocking the release of large osmolytes such as taurine, which may draw water into the brain across an intact BBB. The molecular identity of the classically described VRAC or VSOR channel, was recently proposed by two independent groups to be encoded by heteromers of the LRRC8 gene family, and to be comprised of LRRC8A (Qiu et al., 2014; Voss et al., 2014) and at least one of several other LRRC8 members (B-D) (Voss et al., 2014). The identification of LRRC8A as a key component of the VRAC was based on pharmacological and electrophysiological properties and that the hypoosmotic activated current in human embryonic kidney (HEK)-293 cells was blocked by siRNA against LRRC8A, however, it is still possible that VRAC may be encoded by different genes in different

cell types. CLC channels (see section 1.4.1) represent another possible VAAC, however, it is clear that these are distinct from VRAC due to smaller single channel conductance and strong inward rectification. CLC-2 is found on the plasma membrane, is osmosensitive (Grunder et al., 1992) and is expressed in both neurons and astrocytes.

1.5.4 Calcium-Activated Anion Channels

Calcium-activated chloride channels (CaCCs) or $I_{Cl(Ca)}$ were first identified in 1982 (Miledi, 1982). Although several candidates exist for CaCCs, their molecular identity has not been conclusive, however, this may be due to different genes encoding different CaCCs in different cell types. CaCCs are described by a single channel conductance ~5ps, that is either directly activated by Ca^{2+} or by Ca^{2+}/calmodulin-dependent kinase II (CaMKII) (Hartzell et al., 2005). A common protocol used to activate CaCCs is to trigger Ca^{2+} entry via voltage gated calcium channels (VGCCs) with a depolarizing step, CaCCs are slowly inactivating and generally give rise to a prolonged tail current. CaCCs can also be activated by other sources of Ca^{2+} entry such as TRP channels, cyclic nucleotide gated channels, and release of Ca^{2+} from intracellular stores. It can additionally not be ruled out that the VSOR may in fact be a CaCC in some cell types. CaCCs often show similar conductance, outward rectifying I-V (current-voltage) curves and pharmacology to VSOR. This is in line with work in cultured astrocytes showing that hyposmotic activation of VRAC was secondary to ATP release, and that ATP itself could trigger

activation of VRAC like currents (Darby et al., 2003). TMEM16A, a recently identified CaCC can also be activated by cell swelling via secondary ATP release and contribute to regulatory volume decrease (Almaca et al., 2009). Of the molecular candidates for CaCC, TMEM16A most closely resembles the properties of the initially described $I_{Cl(Ca)}$ (Schroeder et al., 2008). TMEM16B, also operates as an outwardly rectifying CaCC and was recently shown to be functionally expressed in pyramidal neurons of the hippocampus (Huang et al., 2012). Bestrophins represent another newly discovered family of proteins that exhibit Cl^- channel activity and also function as modulators of voltage gated calcium channels. Bestrophin-1, a calcium and volume sensitive channel (Fischmeister and Hartzell, 2005) was recently suggested as a pathway for non-vesicular glutamate and GABA release from astrocytes (Park et al., 2009; Lee et al., 2010), and possibly underlies the molecular identity of the astrocyte VRAC. The tweety family of anion channels represent yet another possible candidate for a CaCC in neurons (Suzuki, 2006). Tweety proteins show linear I-V curves with large single channel conductance (260pS), and are osmosensitive, similar to maxi-anion channels (Suzuki and Mizuno, 2004). Given the diversity of proteins that function as CaCCs, it is most likely that different genes encode for different CaCCs in different cell types and tissues.

1.5.5 Cation-Chloride Cotransporters

The mammalian cation-chloride cotransporters are encoded by the SLC12A gene family and consist of 9 distinct members, seven of which are known to be

expressed at the plasma membrane (Blaesse et al., 2009). Of the cation-chloride cotransporters, the Na^+, K^+, $2Cl^-$ transporter isoform 1 (NKCC1) and all four K^+, Cl^- cotransporters (KCC1-4) are expressed in the brain at some point in CNS development. KCC1 is not expressed in neurons whereas KCC2 shows exclusive expression in neurons, and has therefore been the most extensively studied KCC in the brain. Although KCC3 has been detected in all adult CNS regions, not much is known in regards to its functional contribution towards neuronal Cl^- regulation. NKCC1 and KCC2 are commonly studied by antagonism with loop diuretics, such as furosemide and bumetanide, however these results are not always conclusive as they inhibit both NKCC1 and KCC2 in a concentration dependent manner (Blaesse et al., 2009). Expression of NKCC1 and KCC2 are thought to be the main transporters responsible for the switch in the polarity of $GABA_AR$ currents that occurs in development. Whereas immature neurons express NKCC1 and low levels of KCC2, mature neurons are reported to express higher levels of KCC2, whereas NKCC1 expression drops substantially (Ben-Ari et al., 2007; Blaesse et al., 2009). As NKCC1 and KCC2 are electroneutral transporters equilibrium is defined solely by the concentration gradients of the transported ions. NKCC1 polarity is defined by $[Na^+]_o[K^+]_o[Cl^-]^2_o=[Na^+]_i[K^+]_i[Cl-]^2_i$. Given this stoichiometry one would expect that by increasing intracellular Na^+ and Cl^- the driving force for Cl^- entry by NKCC1 would be reduced. As KCC2 is the major neuronal chloride extrusion mechanism, KCC2 may be important for the recovery of E_{Cl^-} following excitotoxic Cl^- increases. However, $[K^+]_{ext}$ increases that occur will decrease and could possibly even reverse KCC2 polarity, as KCC2 functions close to equilibrium in mature pyramidal neurons.

In addition, it's been reported that glutamate activation of NMDARs leads to phosphorylation and decreased expression of KCC2, leading to decreased recovery from excitotoxic Cl^- loads (Lee et al., 2011). However, the authors of this study were unable to conclude the entry pathway of Cl^-, but noted that it was independent of NKCC1. Consistent with these results, another study examining mechanisms for Cl^- influx during OGD in hippocampal brain slices saw no reduction in Cl^- increases by blocking cation-chloride cotransporters with bumetanide/furosemide, or by blocking $GABA_A$Rs with picrotoxin (Pond et al., 2006). Interestingly, the authors were able to block a secondary increase in Cl^- that occurred (>1 hour) after re-oxygenation, although the significance of this late Cl^- influx in the brain slice remains uncertain.

1.5.6 SLC4 Family of Anion Exchangers and Transporters

The mammalian SLC4 family is made up of 10 functional members (SLC4A1 to -4A5 and SLC4A7 to -4A11). All members of the SLC4 family except for SLC4A11 mediate the transport of HCO_3^-. Of the SLC4 family, -A1, -A2, -A3, -A8 and -A10 have been reported to also transport Cl^- in exchange for HCO_3^- (Pushkin and Kurtz, 2006; Alper, 2009; Romero et al., 2013). Another common feature to all SLC4 family members is the reported inhibition by disulfonic stillbenes, DIDS and SITS (Alper, 2009; Romero et al., 2013). The anion exchangers that mediate the electroneutral, sodium independent exchange of Cl^- for HCO_3^- are the anion exchangers - AE1, AE2 and AE3 encoded by the genes SLC4A1, SLC4A2 and SLC4A3 respectively (Alper,

2009). AE1 to -3 prefer Cl^- and HCO_3^- as substrates, however they can also transport OH^-, and AE1 has been reported to cotransport SO_4^{2-} and H^+ in exchange for Cl^-, although at a very low transport rate compared to Cl^-/HCO_3^- exchange (Jennings, 1976). AE3 is predominantly expressed in the brain and in the heart and is highly expressed in hippocampal and cortical pyramidal neurons (Hentschke et al., 2006; Svichar et al., 2009). AE1 and AE2 are also expressed in the brain, however, AE1 was shown to be absent from pyramidal neurons and AE3 mRNA expression has been reported to be 5 fold higher than AE2 (Svichar et al., 2009). Additionally, the generation of SLC4A3 knockout mice has revealed that AE3 is the dominant sodium-independent anion exchanger in the hippocampus, mediating acid loads in response to alkalosis (Hentschke et al., 2006; Svichar et al., 2009). Interestingly, AE3 KO mice show reduced seizure threshold possibly due to impaired pH regulation (Hentschke et al., 2006), however it is also possible that the Cl^- transport by AE3 may influence the reversal potential for $GABA_AR$ mediated inhibitory transmission, as previously reported in embryonic motorneurons (Gonzalez-Islas et al., 2009). In addition to the sodium-independent Cl^-/HCO_3^- exchangers, the brain also shows expression of two distinct Na^+ coupled Cl^-/HCO_3^- exchangers, encoded by the genes SLC4A8 and SLC4A10. The Na^+ driven Cl^-/HCO_3^- exchanger (NDCBE), SLC4A8, is expressed in both hippocampal and cortical neurons of rodent and human brain (Damkier et al., 2007; Chen et al., 2008; Sinning et al., 2011). Under resting conditions, SLC4A8 mitigates against acid loads by exchanging extracellular HCO_3^- for intracellular Cl^- driven by the large inward Na^+ gradient. However, it is possible for NDBCE to reverse depending on the intracellular and extracellular concentrations of Na^+, Cl^-

and HCO_3^- (Grichtchenko et al., 2001). Since NDCBE is an electroneutral exchanger transporting one Na^+ and two HCO_3^- ions in exchange for one Cl^- ion, equilibrium for NDCBE can be described by $[Na^+]_o[HCO_3^-]_o^2[Cl^-]_i=[Na^+]_i[HCO_3^-]_i^2[Cl^-]_o$. Knockout mice for the SLC4A8 gene were recently shown to exhibit diminished acid extrusion and decreased spontaneous glutamate release in vitro and increased seizure threshold in vivo (Sinning et al., 2011). Although SLC4A8 was recently shown to be localized preferentially to presynaptic terminals (Sinning et al., 2011; Burette et al., 2012), the antibodies used in these studies were made against a site located at the C-terminus of the full length protein, and which is spliced out in 2 of the 4 splice variants identified in human brain (Parker et al., 2008a). Other studies using an antibody targeting the N-terminus of SLC4A8 show a soma/dendritic staining pattern in pyramidal neurons (Damkier et al., 2007; Chen et al., 2008). SLC4A10 represents another electroneutral Na^+, HCO_3^- cotransporter that has been reported to exhibit Cl^- exchange activity, although this remains controversial (Parker et al., 2008b; Damkier et al., 2010; Romero et al., 2013). Whereas rat and mouse expression of SLC4A10 products have been shown to function as Na^+ driven HCO_3^-/Cl^- exchangers similar to SLC4A8 (Damkier et al., 2010), human SLC4A10 expressed in *Xenopus* Oocytes showed no functional requirement for the presence of Cl^-, and no net change in Cl^- concentration when Cl^- was present (Parker et al., 2008b). These results suggest the difference in reported Cl^- exchange activity may be simply due to differences in rodent vs. human SLC4A10 gene products, however, functional differences due to different expression systems cannot be ruled out. SLC4A10 is expressed in the brain (Damkier et al., 2007), with high expression of SLC4A10 in

CA3 neurons of the hippocampus (Jacobs et al., 2008). Genetic deletion of SLC4A10 has been shown to result in decreased recovery from acid loads in the CA3 region of the hippocampus, increased seizure threshold and decreased brain ventricle size (Jacobs et al., 2008).

1.5.7 SLC26 Family of Anion Exchangers and Transporters

The solute linked carrier 26 isoforms, originally described as sulfate transporters, are made up of a family of anion transporters with 10 distinct members. The isoforms are made up of SLC26A1-A11, with SLC26A10 being a pseudo-gene. It is now clear that most SLC26 isoforms are actually quite versatile capable transporting a variety of different anions such as chloride, bicarbonate, sulfate, formate, iodide, oxalate and hydroxyl (Mount and Romero, 2004; Romero et al., 2004; Alper and Sharma, 2013). Various SLC26 members have been shown to be highly expressed in the kidney and play critical roles in kidney salt adsorption, acid-base balance, vascular volume homeostasis and blood pressure regulation (Mount and Romero, 2004; Romero et al., 2004; Alper and Sharma, 2013). SLC26A3, A4, A6, A9 and A11 have all been shown to mediate Cl^-/HCO_3^- exchange (Soleimani, 2013). Several SLC26 members have also been shown to be expressed in brain tissue, including SLC26A11 which was recently shown to be highly expressed in pyramidal neurons of the cortex and hippocampus (Rahmati et al., 2013), and named Kidney Brain Anion Transporter (KBAT). Of note, SLC26A11 is the most divergent member of the SLC26 family, more closely related to sulfate transporters

from yeast and plants than to other members of the mammalian SLC26 family (Vincourt et al., 2003; Soleimani, 2013). SLC26A11 has been shown to be a DIDS sensitive transporter capable of functioning in several different modes; a sulfate transporter, an exchanger for Cl^-, SO_4^{2-}, HCO_3^- or H^+-Cl^- or as a Cl^- channel, depending on the tissue type or the expression system (Vincourt et al., 2003; Xu et al., 2011; Lee et al., 2012a; Rahmati et al., 2013). The explanation for these differences in the reported properties of SLC26A11 are unclear but may represent variations in the recombinant protein that was expressed, differences in the expression systems or physiological changes in the functional states of SLC26A11. The degree of DIDS sensitivity of SLC26A11 has also been reported to vary depending on the expression system used to analyze the properties of recombinant SLC26A11. Recently SLC26A11 was shown to be able to function as an electrogenic Cl^- transporter by measurements of ^{36}Cl flux and also as a Cl^-/HCO_3^- exchanger by measurements of pH with the pH indicator 2',7'-bis(2-carboxymethyl),5(and-6)carboxyfluorescein (BCECF) (Xu et al., 2011). SLC26A11 has also been proposed to function as a constitutively active plasma membrane Cl^- channel independent of intracellular Ca^{2+} or cAMP, based on voltage clamp recordings in HEK-293 cells overexpressing SLC26A11 (Rahmati et al., 2013). SLC26A11 was reported to be co-localized with the vacuolar H^+-ATPase in the plasma membrane of Purkinje neurons and of intercalated kidney cells (Xu et al., 2011; Rahmati et al., 2013), where they may functionally cooperate. SLC26A11 is trafficked to the plasma membrane in expression systems with the N-terminus of the protein directed towards the extracellular side (Vincourt et al., 2003). Although the abundant expression of

SLC26A11 protein has been reported in neurons, the function of endogenous SLC26A11 expressed in neurons remains untested.

Chapter 2: Lipid Nanoparticle Delivery of siRNA to Silence Neuronal Gene Expression in the Brain.

2.1 Introduction

Since the discovery that RNA interference (RNAi) is mediated by double-stranded RNA (dsRNA) (Fire et al., 1998), the use of small interfering RNA (siRNA) to silence specific genes has become a powerful method for manipulating gene expression *in vitro* and, increasingly, *in vivo*. However, issues concerning the delivery of siRNA into neurons both *in vitro* and *in vivo* limit the widespread use of siRNA in neuroscience research in mammals. Viral delivery of short hairpin RNA (shRNA) has been used successfully *in vivo* (e.g. (Sun et al., 2009)) to knock down selected targets, but the time and expense of packaging shRNA into high titre viruses, as well as the toxicological and immunological problems associated with viral vectors, must be considered. In cell culture the utility of siRNA approaches for silencing genes in neurons remains limited due to low transfection levels and toxicity with techniques such as lipofectamine. Transgenic approaches to modulate CNS gene expression are time consuming and costly. Antisense oligonucleotides (ASOs) can be effective when stabilized forms are injected into the brain but they require large quantities of ASOs to be injected for effective uptake. The development of alternative delivery methods to facilitate the use of siRNA to manipulate gene expression in the mammalian CNS would be of great value to

neuroscientists, and would accelerate progress in our understanding of brain function.

Lipid nanoparticles (LNPs) are currently the leading delivery systems for enabling the therapeutic potential of siRNA in peripheral cells (Zimmermann et al., 2006; Davidson and McCray, 2011). LNP siRNA systems containing optimized cationic lipids can silence therapeutically relevant genes in a variety of tissues (particularly liver) (Semple et al., 2010; Basha et al., 2011; Lee et al., 2012b) following intravenous injection in animal models. Positive clinical trial results using these LNPs have been reported for treatment of cardiovascular disease, certain forms of amyloidosis and other disorders (http://www.alnylam.com/Programs-and-Pipeline/Alnylam-5x15/index.php). However the efficacy of LNP approaches for delivering siRNA to neurons in the CNS is unknown. Due to the inability of LNP systems to cross the blood-brain barrier the potency of these systems for silencing genes in brain tissue has not been investigated. Here we report the conditions under which LNP delivery of siRNA is a remarkably efficient method for silencing neuronal gene expression in both primary neuronal culture and following intracranial injection *in vivo*.

2.2 Materials and Methods

2.2.1 Synthesis of the Lipid, 3-(dimethylamino)propyl 3,3-bis(linoleyl) propionate, DMAP-BLP, Compound 8

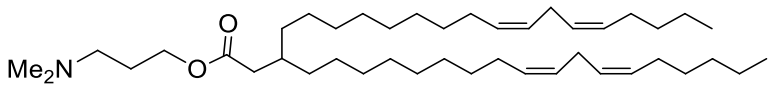

(12*Z*,15*Z*) 3-(dimethylamino)propyl 3-((9*Z*,12*Z*)-heptadeca-9,12-dien-1-yl)icosa-12,15-dienoate

The pKa of the amine headgroup is 6.64 and the ED_{50} is 0.009 mg/kg for FVII knockdown.

Scheme 1

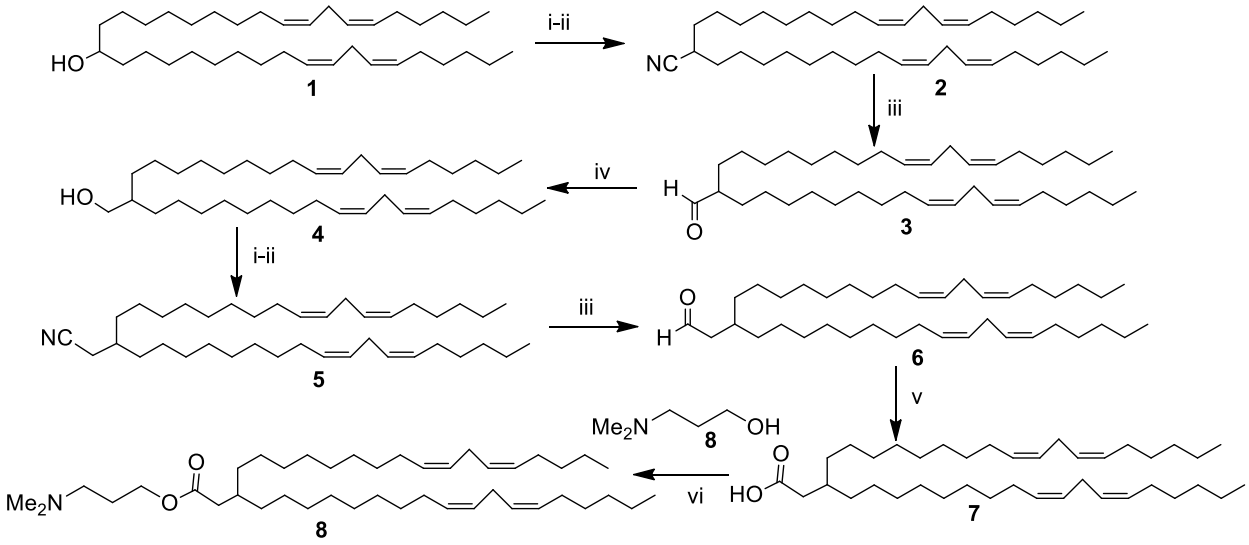

i) Ms-Cl, TEA, DMAP, DCM; ii) NaCN, DMF, 53-72%; iii) DIBAL-H, toluene, 68-69 %; iv) $NaBH_4$, THF/methanol, 86%; v) oxone, DMF, 69%; vi) EDAC, DMAP, DIEA, DCM, 81%.

Synthesis of compound 2

To a solution of compound 1 (50 g, 94.45 mmol) in DCM (400 mL) under argon atmosphere was added TEA (53 mL, 378 mmol) and DMAP (1.2 g, 9.5 mmol), and the solution was stirred at room temperature for 5 minutes. The reaction mass was cooled to -5 °C, and a solution of methyl sulfonyl chloride (15 mL, 190 mmol) in DCM (100 mL) was added slowly at temperature below -5°C and then allowed to warm to room temperature. After 30 minutes, the reaction was quenched with ice cold water (20 ml). The organic layer was separated, washed with 1 N HCl (30 mL), water, and brine, dried over sodium sulfate, and evaporated at reduced pressure to obtain the mesylate as a pale yellow liquid (55 g, 95%). ^{1}H NMR (400 MHz, CDCl3): d 0.89 (t, 6H, J = 6.8), 1.2-1.5 (m, 36H), 1.67 (m, 4H), 2.05 (q, 8H, J1 = 6.8, J2 = 6.8), 2.77 (t, 4H, J = 6.4), 2.99 (s, 3H), 4.71(m, 1H) and 5.36 (m, 8H). This product was used for the next step without any further purification. To a solution of the mesylate (55 g, 90.6 mmol) in dimethylformamide (400 mL) was added sodium cyanide at room temperature. Reaction mixture was heated to 65 °C for 16 hrs. The reaction was monitored by TLC (10% ether-hexane). It was then cooled to room temperature and diluted with 7 volumes of water and extracted with ether (three times 5 volumes). The combined ether layers were washed with water (two times 3 volumes) and brine (two times 3 volumes), dried over sodium sulfate, and

evaporated at reduced pressure to obtain the crude product, which was purified by silica gel chromatography using a hexane as eluent yield compound 2 (26.1 g, 53%) as a pale yellow liquid. ^{1}H NMR (400 MHz, $CDCl_3$): d 0.89 (t, 6 H, J_1 = 6 Hz, J_2 = 6.8 Hz), 1.29-1.37 (m, 36 H), 1.41-1.49 (m, 2 H), 1.60-1.63 (m, 2 H), 2.05 (q, 8 H, J_1 = 6.8 Hz, J_2 = 13.6 Hz), 2.78 (t, 4 H, J_1 = 6.4 Hz, J_2 = 6 Hz), 5.32-5.41 (m, 8 H).

Synthesis of compound 3

To a solution of compound 2 (29 g, 54 mmol) in toluene (300 mL) at -60 °C under argon atmosphere was added diisobutylaluminium hydride (108 mL, 108 mmol, 1 M solution in toluene) gradually through a cannula. The solution was stirred for 1 hr at -60 °C. The reaction mixture was then quenched at -60 °C with saturated solution of sodium potassium tartrate, warmed to room temperature, and filtered through a celite bed. The filtrate was washed twice with 500 mL brine, dried over sodium sulfate, and evaporated at reduced pressure to obtain the crude product, which was purified by silica gel chromatography using 3% ether/97% hexane to afford pure product 3 (19.8 g, 68%) as a pale yellow liquid. ^{1}H NMR (400 MHz, $CDCl_3$): d 0.89 (t, 6 H, J_1 = 6.4 Hz, J_2 = 7.2 Hz), 1.25-1.42 (m, 38 H), 1.56-1.63 (m, 2 H), 2.02 to 2.06 (m, 8 H), 2.17 to 2.26 (m, 1 H), 2.78 (t, 5 H, J = 6.4 Hz), 5.30-5.42 (m, 8 H), 9.54 (d, 1 H, J = 2.8 Hz). ^{13}C NMR (100 MHz, $CDCl_3$): d 14.0, 22.6, 25.6, 27.1, 27.2, 28.9, 29.2, 29.3, 29.4, 29.43, 29.6, 29.7, 31.5, 52.0, 127.9, 128.0, 130.1, 128.0, 130.2, 205.6. MS calculated for $C_{38}H_{68}O$ 540.52, found 541.54 (M+H).

Synthesis of compound 4

To a solution of compound 3 (10 g, 18.4 mmol) in THF/methanol (1:1, 100 mL) at 0 °C was added sodium borohydride (1.4 g, 37 mmol). The solution was gradually warmed to room temperature and stirred for 1 hr. The reaction was quenched with ice-cold water and extracted with three times with ether (100 ml). The organic layer was washed once with brine (100 mL), dried over sodium sulfate, and evaporated at reduced pressure to obtain the crude product, which was purified by silica gel chromatography using 3% ether/97% hexane to afford pure product 4 (8.7 g, 86%) as pale yellow liquid. ^{1}H NMR (400 MHz, $CDCl_3$): d 0.87 (t, 6 H, J_1 = 6.8 Hz), 1.25-1.33 (m, 40 H), 1.4-1.5 (m, 1 H), 2.05 (m, 8 H), 2.78 (t, 5 H, J = 6.4 Hz), 3.53 (d, 2 H, J = 5.2 Hz), 5.30-5.42 (m, 8 H). ^{13}C NMR (100 MHz, $CDCl_3$): d 14.1, 22.6, 25.6, 26.9, 27.2, 29.3 29.6, 29.6, 29.7, 30.1 30.9, 31.5, 40.5, 127.9, 130.1. MS calculated for $C_{38}H_{70}O$ 542.54, found 542.90 (M+).

Synthesis of compound 5

To a solution of compound 4 (215 g, 390 mmol) in DCM (2 L) under nitrogen atmosphere was added TEA (220 mL, 1.58 mol) and DMAP (4.83 g, 39 mmol). The solution was stirred at room temperature. The reaction mass was cooled to -5 °C and a solution of mesyl chloride in DCM was slowly added ensuring that the temperature remained below -5 °C. The solution was allowed to warm to room temperature and stirred for 1 hr. The reaction was then quenched with ice cold water. The organic layer was separated, washed successively with 1 N HCl, water, and brine, dried over sodium sulfate, and evaporated at reduced pressure to obtain the pure product as a yellow liquid (250 g, 96%).^{1}HNMR (400 MHz, $CDCl_3$): d 0.89 (t,

6 H, J = 6.8 Hz), 1.2 – 1.4 (m, 40 H), 1.65 – 1.72 (m, 1 H), 2.05 (dd, 8 H, J = 6.8 Hz, J = 13.6Hz), 2.78 (t, 4 H, J = 6.4 Hz), 3.00 (s, 3 H), 4.12 (d, 2 H, J = 5.6 Hz), 5.29 – 5.43 (m, 8 H). ^{13}C NMR (100 MHz, $CDCl_3$): d 14.0, 22.5, 25.6, 26.5, 27.1, 27.2, 29.2, 29.3, 29.5, 29.6, 29.8, 30.6, 31.5, 37.1, 37.7, 72.4, 127.85, 127.9, 130.0, 130.1. To a solution of the mesylate in dimethylformamide (1.75 L) was added sodium cyanide (59 g, 1.20 mol) at room temperature under argon. The solution was heated to 65 °C for 16 hrs. The reaction was cooled to 0 °C and added to cold water (6L) with stirring, and the temperature was maintained below 10 °C. The mixture was extracted with diethylether (five times 2 L), and the combined organic layers were washed successively with water and brine, dried over sodium sulfate, and evaporated at reduced pressure to obtain the crude product, which was purified by silica gel chromatography using 1% ether/99% hexane as eluent to yield product 5 (160 g, 72%) as a pale yellow liquid. ^{1}H NMR (400 MHz, $CDCl_3$): d 0.89 (t, 6 H, J = 6.8 Hz), 1.2 – 1.46 (m, 40 H), 1.64 – 1.71 (m, 1 H), 2.05 (dd, 8 H, J = 6.8 Hz, 13.6 Hz), 2.32 (d, 2 H, J = 6 Hz), 2.78 (t, 4 H, J = 6.4 Hz), 5.29 – 5.43 (m, 8 H).

Synthesis of compound 6

To a solution of compound 5 (55 g, 100 mmol) in toluene (500 mL) at -70 °C under argon atmosphere was added diisobutylaluminium hydride (200 mL, 200 mmol, 1 M solution in toluene) gradually through a cannula. The solution was stirred for 1 hr at -70 °C. The reaction mixture was then quenched at -70 °C with a saturated solution of sodium potassium tartrate, warmed to room temperature, and filtered through a celite bed. The filtrate was evaporated at reduced pressure to obtain the crude

product. The crude product was dissolved in THF (6 volumes), and 1 N HCl (10 volumes) was added. The solution was stirred for 1 hr at room temperature. Ether was added, and the mixture was transferred to a separatory funnel. The ether layer was washed four times with water (400 mL), then with saturated $NaHCO_3$ solution (200 ml), and finally with brine (200 ml), dried over sodium sulfate, and evaporated at reduced pressure to obtain the crude product, which was purified using 230 x 400 mesh silica gel chromatography with 2% ether/98% hexane as eluent to afford pure product 6 (38 g, 69%) as a pale yellow liquid. ^{1}H NMR (400 MHz, $CDCl_3$): d 0.89 (t, 6 H, J = 6.8 Hz), 1.2 – 1.41 (m, 40 H), 1.89 – 1.99 (m, 1 H), 2.05 (dd, 8 H, J = 6.8 Hz, J = 13.6 Hz), 2.32 (dd, 2 H, J = 2.4 Hz, J = 6.4 Hz), 2.77 (t, 4 H, J = 6.4 Hz), 5.28 – 5.42 (m, 8 H), 9.76 (t, 1 H, J = 2.4 Hz).

Synthesis of compound 7

To a solution of compound 6 (21 g, 38 mmol) in diethylether (85 mL) and dimethylformamide (125 mL) was added oxone (23.2 g, 38 mmol) at room temperature. The solution was stirred at room temperature for 5 hrs. The reaction was quenched with cold water (500 mL) and extracted five times with ether (150 ml). The combined organic layer was washed successively with water and brine, dried over sodium sulfate, and evaporated at reduced pressure to obtain the crude product, which was purified by silica gel chromatography using 5% ether/95% hexane as eluent to yield the product 7 as a pale yellow liquid (15 g, 69%). ^{1}H NMR (400 MHz, $CDCl_3$): δ 0.89 (t, 6 H, J = 6.8 Hz), 1.27-1.42 (m, 40 H), 1.8 – 1.9 (m, 1 H), 2.05 (dd, 8 H, J = 6.8, J = 13.6 Hz), 2.27 (d, 2 H, J = 6.4 Hz), 2.77 (t, 4 H, J = 6.4 Hz),

5.29-5.42 (m, 8 H). ^{13}C NMR (100 MHz, $CDCl_3$): d 14.0, 22.6, 25.6, 26.5, 27.2, 27.2, 29.3, 29.4, 29.5, 29.6, 29.7, 29.9, 31.5, 33.8, 34.8, 39.0, 76.7, 77.0, 77.3, 127.9, 130.0, 180.3. MS calculated for $C_{39}H_{70}O_2$ Cal 570.54, found 570.97 (M+).

Synthesis of compound 8

Carboxylic acid 7 (20.00 g, 35.02 mmol) and the alcohol 8 (5.78 g, 56 mmol) were dissolved in dichloromethane (100 mL) under argon. To this mixture EDCI (10.02 g, 1.5 eq.), DMAP (500 mg, 10 mol%), and DIEA (18.25 ml, 3 eq.) were added, and the mixture was stirred overnight. The reaction progress was monitored by TLC (5% methanol in dichloromethane). The reaction mixture was transferred to a separatory funnel, diluted with DCM, and washed with twice water (200 mL). The organic layer was dried over sodium sulfate. Solvent was removed, and the crude product was purified by silica gel chromatography using hexane/EtOAc (30-50%) containing triethylamine as eluent to isolate the product as a colorless, viscous liquid (18.36 g, 81%). ^{1}H NMR (400 MHz, CDCl3) δ 5.48 – 5.24 (m, 8 H), 4.11 (t, J = 6.5 Hz, 2H), 2.77 (t, J = 6.4 Hz, 4 H), 2.32 (t, J = 6.5 Hz, 2 H), 2.26 – 2.17 (m, 8 H), 2.04 (q, J = 6.8 Hz, 8 H), 1.82-1.77 (m 4 H), 1.37-1.36 (m, 39 H), 0.89 (t, J = 6.9 Hz, 6 H). ^{13}C NMR (101 MHz, CDCl3) δ 173.84, 130.38, 130.35, 128.15, 128.14, 62.74, 56.54, 45.70, 39.49, 35.32, 34.11, 31.74, 30.15, 29.89, 29.83, 29.77, 29.56, 29.54, 27.45, 27.41, 27.27, 26.94, 26.78, 25.84, 22.78, 14.28. MS calculated for $C_{44}H_{82}NO_2$ 656.6346 (M+H); found 656.6329 (M+H).

2.2.2 Lipid Nanoparticle Formulation and siRNA Encapsulation

The ionizable cationic lipid DMAP-BLP and polyethylene glycol (PEG) lipid PEG-DMG were synthesized as described above. 1,2-distearoyl-sn-glycero-3-phosphocholine (DSPC) and cholesterol were obtained from Avanti (Alabaster, AL) and Sigma-Aldrich Co. (St. Louis, MO) respectively. Lipophilic carbocyanine dyes to monitor LNP siRNA uptake 3,3′-dioctadecyloxacarbocyanine perchlorate ($DiOC_{18}$) and 1,1'-dioctadecyl-3,3,3',3'-tetramethylindocarbocyanine perchlorate ($DiIC_{18}$) were obtained from Invitrogen (Carlsbad, CA). All lipid stocks were dissolved and maintained in 100% ethanol. Lipids were mixed together at a molar % ratio of 50% cationic lipid, 1.5% PEG-DMG, 37.5% cholesterol, 10% DSPC and 1% $DiOC_{18}$ or $DiIC_{18}$. LNP were prepared by mixing appropriate volumes of lipid stock solutions in ethanol with an aqueous phase containing siRNA duplexes employing a microfluidic micro-mixer (Lee et al., 2012b) provided by Precision NanoSystems (Vancouver, BC). For the encapsulation of siRNA, the desired amount of siRNA (0.056mg siRNA: μmole of lipid) was dissolved in formulation buffer (25mM sodium acetate, pH 4.0). 1 X volume of the lipid in ethanol and 3 X volumes of the siRNA in formulation buffer were combined in the microfluidic micro-mixer using a dual-syringe pump (Model S200, KD Scientific, Holliston, MA) to drive the solutions through the micro-mixer at a combined flow rate of 2ml/min (0.5mL/minute for syringe with lipid mixture and 1.5mL/minute for syringe with siRNA in formulation buffer). The LNP-siRNA systems formed were then dialyzed for 4 hrs against 50mM MES/50mM sodium citrate buffer pH 6.7 followed by an overnight dialysis against 1 X phosphate

buffered saline, pH 7.4 (GIBCO, Carlsbad, CA) using Spectro/Por dialysis membranes (molecular weight cutoff 12000 – 14000Da, Spectrum Laboratories, Rancho Dominguez, CA). The mean diameter and polydispersity of the LNP are listed in **Table 2.1**. LNP size was determined by dynamic light scattering (number mode; NICOMP 370 Submicron Particle Sizer, Santa Barbara, CA). Encapsulation efficiency was determined by quantifying siRNA by measuring absorbance at 260nm in samples collected before and after dialysis following removal of free siRNA using VivaPureD MiniH columns (Sartorius Stedim Biotech, Aubagne, France). Lipid concentration was determined by measurement of cholesterol content by using a Cholesterol E enzymatic assay (Wako Chemicals USA, Richmond, VA). The final siRNA:lipid ratios (mg/μmol) are listed in **Table 2.1**.

Table 2.1: LNP-siRNA properties

siRNA	Size (nm)	PDI	Measured siRNA/Lipid (mg/μmol)
PTEN	55.4	0.041	0.053
Luc	62.5	0.034	0.057
GluN1-1	62.0	0.045	0.056
GluN1-2	40.8	0.108	0.058
GluN1-3	55.9	0.058	0.059

2.2.3 Hippocampal Neuronal Cultures and Lipid Nanoparticle Treatments.

Hippocampal cultures were prepared as described previously with a slight modification from (Craig et al., 1996). In brief, hippocampi were dissociated from 18-d-old rat embryos by treating with trypsin then triturated with a constricted Pasteur pipette. Subsequently, the dissociated cells were plated on poly-l-lysine coated glass coverslip using minimum essential medium (MEM) supplemented with 10% horse serum. Then the coverslips were inverted over a feeder layer of astroglia cells to facilitate communication between neurons and feeder layer cells. Neurons were maintained in Neurobasal medium with B-27 and L-glutamine (Invitrogen). Cytosine arabinoside (5μM; Calbiochem, Darmstudt, Germany) was added after 2 days *in vitro* to inhibit the proliferation of glia. Neuronal cultures were used for the experiment between 12 and 14 DIV. Cells were treated with either LNP-phosphatase and tensin homolog 1 (PTEN) siRNA, LNP-luciferase (luc) siRNA or with non-encapsulated PTEN-siRNA as a control.

2.2.4 Intracranial and Intracerebroventricular Injections

All experimental protocols were approved by the Committee on Animal Care, University of British Columbia, and conducted in compliance with guidelines provided by the Canadian Council of Animal Care. Sprague-Dawley rats (P22-P26) were anaesthetized with isofluorane before and throughout the surgery. A small hole (diameter ~1mm) was drilled in the skull to allow access to the brain (-2.0mm AP and ±3.0mm ML from bregma, 0.8mm DV). A glass micropipette (tip diameter

~40μm) was connected to a Hamilton syringe and LNP-siRNAs were injected using an infusion pump (Harvard Apparatus) at a rate of 50nL/min. The total volume injected was 500nL of LNP siRNA (5mg siRNA/mL in sterile PBS). For intracerebroventricular (ICV) injections holes were drilled -0.8mm AP and ±1.4mm ML from bregma and -3.1mm DV and microdialysis silicon tubing was used to inject LNPs. The total volume injected was 2 μL bilaterally at a rate of 200nL/min.

2.2.5 Brain Slice Preparation

Five days after LNP siRNAs (GluN1, PTEN, Luciferase) were injected into the cortex, Sprague-Dawley rats (postnatal day 26-30) were anaesthetized with halothane and decapitated according to protocols approved by the University of British Columbia Committee on Animal Care. Brains were rapidly extracted and placed into ice-cold slicing solution containing (in mM): N-methyl-D-glucamine (NMDG), 120; KCl, 2.5; $NaHCO_3$, 25; $CaCl_2$, 1; $MgCl_2$, 7; NaH_2PO_4, 1.25; glucose, 20; Na-pyruvate, 2.4; Na-ascorbate, 1.3; saturated with 95% O_2/5% CO_2. Coronal hemi-sections, 300μm thick, were sliced using a vibrating tissue slicer (VT1200, Leica, Nussloch, Germany). For Western blot preparation tissue within 1mm but not including the injection sites (needle tracts) was collected. For electrophysiology experiments slices were incubated at 32°C in artificial cerebral spinal fluid (ACSF) containing (in mM): NaCl, 126; KCl, 2.5; $NaHCO_3$, 26; $CaCl_2$, 2.0; $MgCl_2$, 1.5; NaH_2PO_4, 1.25; glucose, 10; saturated with 95% O_2/5% CO_2 for 45min. For experiments slices were at 22–24°C and perfused at ~2ml/min.

2.2.6 Electrophysiology

Whole-cell patch clamp recordings were made using electrodes (4–6 MΩ resistance) filled with a pipette solution containing (in mM): Cs-methanesulfonate ,108; Na-Gluconate, 8; Cs-EGTA, 1; TEA-Cl, 8; $MgCl_2$, 2; HEPES, 10; K_2ATP, 4; Na_3GTP, 3; at pH 7.2. Whole-cell voltage-clamp recordings were obtained from neurons of the somatosensory cortex (layer 5) under microscope guidance using differential interference contrast. All recordings were filtered at 2 kHz, digitized at 10 kHz and acquired with Clampex (Axon Instruments, Foser City, CA). Membrane potential was clamped at −70mV. A monopolar stimulation electrode was positioned ~100μm from the soma of the recorded neuron. The extracellular solutions were supplemented with 50μM picrotoxin (Sigma) and 8mM of each $MgCl_2$ and $CaCl_2$ to block $GABA_A$ synaptic potentials, block epileptiform activity and minimize polysynaptic responses. Synaptic responses were evoked with monophasic voltage pulses every 10 s. Cells were allowed to dialyze for at least 15 min before starting recordings. Access resistance was continuously monitored during the experiments. The AMPAR excitatory postsynaptic current (EPSC) was recorded at V_{hold}=-70mV followed by the NMDAR + AMPAR EPSC at V_{hold}=+40mV. V_{hold} was then returned to -70mV at the end of the experiment to verify there was no change in the baseline. 20-50 traces were averaged per recording. 25μM D-APV (Abcam Biochemichals, Cambridge, MA) was applied to some experiments to illustrate outward NMDAR and AMPA currents. Signals were amplified with the Multiclamp 700B amplifier (Axon Instruments, Foser City, CA), low-pass filtered at 2kHz, and digitized at 10kHz using the Digidata 1322 (Axon Instruments). Data were collected (pClamp, version 9.2;

Axon Instruments) and stored on computer for offline analysis using clampfit software (Axon Instruments).

2.2.7 Imaging

Live cell imaging (brain slice) was performed with a two-photon laser-scanning microscope (Zeiss LSM510-Axioskop-2; Zeiss, Oberkochen, Germany) with a 40X-W/1.0 numerical aperture objective lens directly coupled to a Chameleon ultra2 laser (Coherent, Santa Clara, CA). DiI and CoroNa were excited at 760nm and the fluorescence from each fluorophore was split using a dichroic mirror at 560nm, and the signals were each detected with a dedicated photo multiplier tube (PMT) after passing through an appropriate emission filter (DiI: 605nm, 55nm band-pass; CoroNa: 525nm, 50nm band-pass) Transmitted light was simultaneously collected using understage IR-DIC optics and an additional PMT. For AM-dye loading slices were incubated at 32°C for 45 min at 16.7μg/mL. Cell density was measured in 10μm z-stacks of 200μm x 200μm, and all cells including partial cells were counted, therefore resulting in an overestimate of cell density/mm^3.

2.2.8 Immunohistochemistry

Free-floating sections (40μm transverse sections) were processed for immunostaining as described previously (Choi et al., 2012b). The primary antibodies used for immunostaining were as follows: Rabbit anti-PTEN (Santa Cruz, 1:300), mouse anti-microtubule associated protein-2 (MAP-2, Chemicon, 1:2000).

Alexa Fluor 633 anti-mouse or Alexa Fluor 488 anti-rabbit IgG (1:1000) secondary antibodies (Invitrogen, Carlsbad, CA) were used for immunofluorescent staining. As a negative control experiment, the primary antibody was omitted during the immunostaining.

2.2.9 Immunocytochemistry

Rat hippocampal neurons (DIV 12-14 days) grown on poly-L-lysine-coated glass coverslips were incubated in neurobasal media with LNP siRNAs (Luciferase siRNA or GluN1 siRNA) for 48 hrs and then processed with immunostaining. In brief, cells were fixed in 2% paraformaldehyde in 0.1M PBS for 10 min, washed with PBS, and then permeabilized in 0.05% Tween20 in 0.1M PBS for 20 min. Cells were then incubated in mouse anti-GluN1 (1:300 dilution; Invitrogen) or rabbit anti-MAP-2 at 4°C for 24 hrs and followed by Alexa Fluor 488 anti-mouse IgG secondary antibody (1:1000; Molecular Probes, Eugene, OR) or Alexa Fluor 633 anti-rabbit IgG (1:1000) incubation at room temperature for 1 hr in the dark. After PBS washes, coverslips were then immersed in 4′,6-diamidino-2-phenylindole (DAPI; Molecular Probes) at 1μg/ml in water to visualize cell nuclei. The coverslips were mounted onto glass slides using FluoroSave (Calbiochem) and examined under an Olympus confocal microscope (FluoView 1000, Olympus, Center Valley, PA).

2.2.10 Western Blotting

Cultured rat hippocampal neurons and rat cortical brain slices were used for Western blotting. At 5 days post-injection with LNP-siRNAs (GluN1, PTEN, Luciferase) into the cortex, cortical brain slices were prepared as previously described (Choi et al., 2012b). Cells and brain slices were homogenized using lysis buffer containing (in mM): Tris pH 7.0 (100), EGTA (2), EDTA (5), NaF (30), sodium pyrophosphate (20), 0.5% NP40 with phosphatase and protease inhibitor cocktail (Roche, Basel, Switzerland). The homogenates were then centrifuged at 13,000 × *g* (20 min, 4°C) to remove cellular debris, then protein concentrations of the crude lysates were determined by performing a Bradford assay with the DC Protein Assay dye (Bio-Rad, Mississauga, ON, Canada). The protein samples were diluted with 2 X Laemmli sample buffer and boiled for 5 minutes. Following SDS/PAGE, proteins were transferred to PVDF membranes, blocked in 5% milk overnight at 4°C, rinsed with Tris buffered saline with 0.1% Tween 20 (TBST) and incubated with mouse anti-GluN1 monoclonal antibody (1:300) or rabbit anti-PTEN polyclonal antibody (1:300) overnight at 4°C. Following four washes with TBST, the membranes were incubated with the anti-mouse or anti-rabbit secondary antibody conjugated to horseradish peroxidase (1:500) for 1 hr at room temperature. The membranes were then washed 3-4 times (15 min) with TBST, and bands were visualized using enhanced chemiluminescence (GE HealthCare, Cleveland, OH).

Tissue analyzed from ICV injections was sampled as follows; entire dorsal hippocampal slices were dissected from -2.0mm to -4.2mm AP from bregma;

striatal slices were taken +1.0mm to -0.5mm AP from bregma within 1.5mm from the ventricle border.

2.2.11 Lactate dehydrogenase (LDH) Assay

LDH assay kits (Biomedical Research Service Center, State Univerisity of New York at Buffalo) were used to examine cell death using cultures of hippocampal neurons with astrocytes on a separate feeder layer. Cells were treated with LNP siRNA (Luciferase siRNA) for 72 hrs then assessed for cell death using LDH assay. Media containing Triton X-100 (1%) was used as a positive control for cell death. Supernatants were collected at 72 hours after the treatment then cells on the coverslips were lysed using lysis buffer. The LDH level in the supernatant represents the cell death while the LDH level in lysed cells represents the viable cells. In brief, supernatants and cell lysates were centrifuged for 3 min at maximal speed (16,000g) at 4^{o}C. All samples were added into a 96-well plate with LDH assay solution and incubated for 30 min at 37^{o}C. The reaction was stopped with 3% acetic acid. LDH reduces tetrazolium salt INT to formazan, which is water-soluble and exhibits an absorption maximum at 492nm. Absorbance at 492nm was measured using a microplate reader. Cell death was calculated as percentage of released LDH compared to the sum of superfusate LDH and cell lysate LDH.

2.2.12 DiI Uptake Assay

Cortical neuronal cultures (3 x 10^4 cell in 12 well plate) were treated with Luc siRNA-LNP (at 1.6mg/ml) conjugated with DiI for 2 hr in the absence and presence of recombinant apolipoprotein E (ApoE) 4 (Peprotech, Rocky Hill, NJ) at different concentrations (0.1, 1, 5, 10 mg/ml). Then cultures were washed with PBS 5 times to wash out unbound Luc siRNA-LNP. Subsequently, 400 µl of filtered dH_20 was added to the wells to rupture cells. DiI fluorescence was measured (excitation at 520nm, emission at 578nm) using Gemini fluorescence microplate reader systems (Molecular Devices Corporation, Union city, CA). Fluorescence reading from the untreated group was subtracted from other groups.

2.2.13 Tumor necrosis factor-α (TNF-α) ELISA

Enzyme-linked immunosorbent assays (ELISA) were performed according to the manufacturer instructions (eBioscience, San Diego, CA). In brief, hippocampal brain slices (400µm) were incubated and treated in a homemade chamber (using 6 multi-well plates) equipped with continuous aeration with 95% O_2/5% CO_2. Slices were treated with Luc siRNA-LNPs (3.3µg/ml) for 5 hrs. As a positive control, LPS (40µg/ml) was applied to the slices. Then the hippocampal brain slices were harvested and homogenized. Cell lysates were centrifuged for 20 minutes at 4˚C and subsequent supernatants were used for protein assay and tumor necrosis factor-α (TNF-α) measurement.

2.2.14 siRNA Sequences and Chemistry

PTEN siRNA: The PTEN siRNA strands had the following sequence and chemistry: sense strand, 5'-GAuGAuGuuuGAAAcuAuudTsdT-3' and antisense strand 5'-AAuAGUUUcAAAcAUcAUCdTsdT-3' where the uppercase letters represent unmodified ribonucleotides, lowercase letters represent 2'-OMe modified nucleotides and "s" represents a phosphorothioate (P=S) linkage between the two dT at the 3'-end. The P=S linkage provided protection from exonuclease degradation and the 2'-OMe modifications reduced potential for immunostimulatory activity and provided stability towards endonucleolytic degradation.

Luciferase siRNA had the following sequence as previously described (Addepalli et al., 2010): sense strand, 5'- cuuAcGcuGAGuAcuucGAdTsdT-3' and antisense strand, 5'-UCGAAGuACUcAGCGuAAGdTsdT-3' with the modification designation as listed above.

GRIN1 siRNA: The sequences of "stealth siRNA" (Invitrogen Life Technologies, Gaithesburg, MD) had the following sequences:

GRIN1-#1, sense strand, 5'-UGCAUGUCCCAUCACUCAUUGUGGG-3'

and antisense strand, 5'-CCCACAAUGAGUGAUGGGACAUGCA-3';

GRIN1-#2, sense strand, 5'-CUUCUGUGAAGCCUCAAACUCCAGC-3'

and antisense strand, 5'-GCUGGAGUUUGAGGCUUCACAGAAG-3';

GRIN1-#3, sense strand, 5'-UUGACGUACACGAAGGGCUCUUGGU-3'

and antisense strand, 5'-ACCAAGAGCCCUUCGUGUACGUCAA-3'.

The reason for variations in the siRNA constructs is due to production from different suppliers.

2.2.15 Statistical Analysis

Experimental values are presented as the mean ± SEM, expressed in percent from 100% baseline. The "n" value represents the number of experiments conducted for analysis. Statistical analyses were performed using a two-tailed Student's t test or analysis of varience (ANOVA) followed by Newman-Keuls Multiple Comparison Test. $p < 0.05$ was accepted as statistically significant (*$p < 0.05$, **$p < 0.01$, ***$p<0.001$).

2.3 Results

2.3.1 Encapsulation of siRNA in Lipid Nanoparticles

LNPs were prepared by mixing appropriate volumes of lipid mixture in ethanol with an aqueous phase containing siRNA duplexes employing a microfluidic micro-mixer (**Figure 2.1a**) as described elsewhere (Belliveau et al., 2012). The lipid composition used was DMAP-BLP (structure shown in **Figure 2.1b**) /distearoylphosphatidlycholine (DSPC)/cholesterol/PEG-DMG in the molar % ratios 50/10/37.5/1.5. The LNPs also contained 1 mol% of the fluorescently labeled lipids $DiOC_{18}$ or $DiIC_{18}$ to monitor LNP uptake. Previous work has shown that LNP systems

with this lipid composition can silence target genes in hepatocytes following intravenous injection at dose levels as low as 0.01mg siRNA/kg body weight (Belliveau et al., 2012; Jayaraman et al., 2012) in an ApoE dependent fashion (Akinc et al., 2010). The LNP PTEN-siRNA systems produced had a diameter 55±11nm (size distribution shown in **Figure 2.1c**). The sizes of the other LNP siRNA systems are listed in **Table 2.1**. No further optimization was done to increase the efficiency of LNP-siRNA systems in this study.

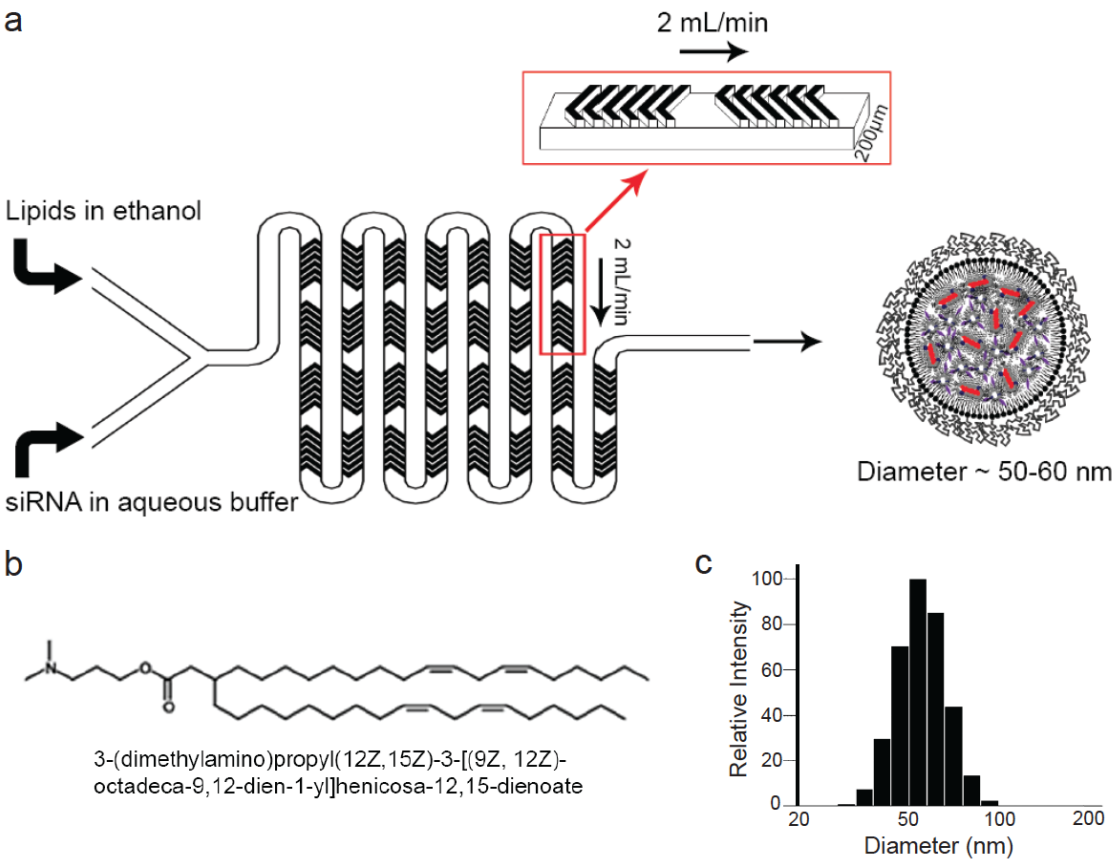

Figure 2.1: Schematic of LNP-siRNA formulation process employing the staggered herringbone micromixer.

a, The lipid mixture in ethanol and siRNA in aqueous solution are pumped separately into the two inlets of the microfluidic mixing device using a syringe pump with a total flow rate of 2mL/min. Herringbone structures induce chaotic advection of the laminar streams causing rapid mixing of the ethanol and aqueous phases and correspondingly rapid increases in the polarity experienced by the lipid solution. At a critical polarity precipitates form as LNPs. Dimensions of the mixing channel were 200µm x 79µm, and the herringbone structures were 31µm high and 50µm thick. (modified from (Belliveau et al., 2012)) **b,** Chemical structure of ionizable cationic lipid – 3-(dimethylamino)propyl (12Z,15Z)-3-[(9Z,12Z)-octadeca-9,12-dien-1-yl]henicosa-12,15-dienoate (DMAP-BLP). **c,** Representative size distribution of LNPs (LNP PTEN-siRNA) analyzed in number mode using the NICOMP 370 Submicron Particle Sizer.

2.3.2 Lipid Nanoparticle Mediated Neuronal Gene Silencing *in vitro*

To test whether LNPs are taken up by neurons, cultured neurons were incubated with siRNA-containing LNPs at a final concentration of 246nM (3.3μg siRNA/mL). For LNPs of 55 nm diameter at an siRNA-to-lipid ratio of 0.056 (mg/μmol) this represents approximately $5.6x10^{11}$ LNPs/mL. We used a culture system containing pure hippocampal neurons on a coverslip with astrocytes on a separate feeder layer (Craig et al., 1996) (**Figure 2.2a**). Surprisingly, we found that 100% of neurons in the culture dish had taken up LNPs following incubation for 24 hours, as indicated by discrete punctate DiI fluorescence within neurons (**Figure 2.2b**). DiI labeled intracellular puncta were observed in both live cultured neurons and in neurons after cultures were fixed. The punctate staining pattern of DiI indicates LNPs located in endosomes and lysosomes (Basha et al., 2011). LNPs were non-toxic at the concentrations used, with no observable differences in cell death relative to controls measured either by comparing nuclear morphology or by lactate dehydrogenase (LDH) release (**Figure 2.2c**). As a positive control cultures treated with 1% Triton X-100 showed a large increase in LDH release (90.21±0.62%).

We next tested whether the LNP mediated delivery of siRNA to neurons effectively silenced gene expression by using Western blots to examine changes in protein expression encoded by the corresponding target gene. We first tested LNP delivery of siRNA against PTEN, a protein highly expressed in pyramidal neurons (Kwon et al., 2006). Incubation of primary rat neuronal cultures with LNPs containing PTEN siRNA (246nM) for 48 hrs resulted in robust knockdown of PTEN

protein indicated by Western blot (PTEN/β-actin reduced by 80% compared to control, P<0.001, **Figure 2.2d**). Importantly, in control experiments, incubation of cultures with LNPs containing siRNA against luciferase (luc), which is not found in the mammalian genome, had no effect on levels of PTEN protein (**Figure 2.2d**). Additionally, neurons treated with non-encapsulated PTEN siRNA (246nM) showed no significant change in PTEN/β-actin compared to control (**Figure 2.2e**). To determine the efficiency of these LNP-siRNA systems we performed a dose response curve and found that even concentrations as low as 0.7nM resulted in robust protein knockdown (PTEN/β-actin reduced by 59% compared to control, P<0.001, **Figure 2.2e**). These results indicate that LNPs are much more efficient and less toxic than current methods used to deliver siRNA to cultured neurons such as electroporation, calcium phosphate or lipofection which usually result in transfection rates of 1-10% (Karra and Dahm, 2010). Higher transfection rates have been reported upon optimization, but generally at the expense of cell toxicity (Karra and Dahm, 2010).

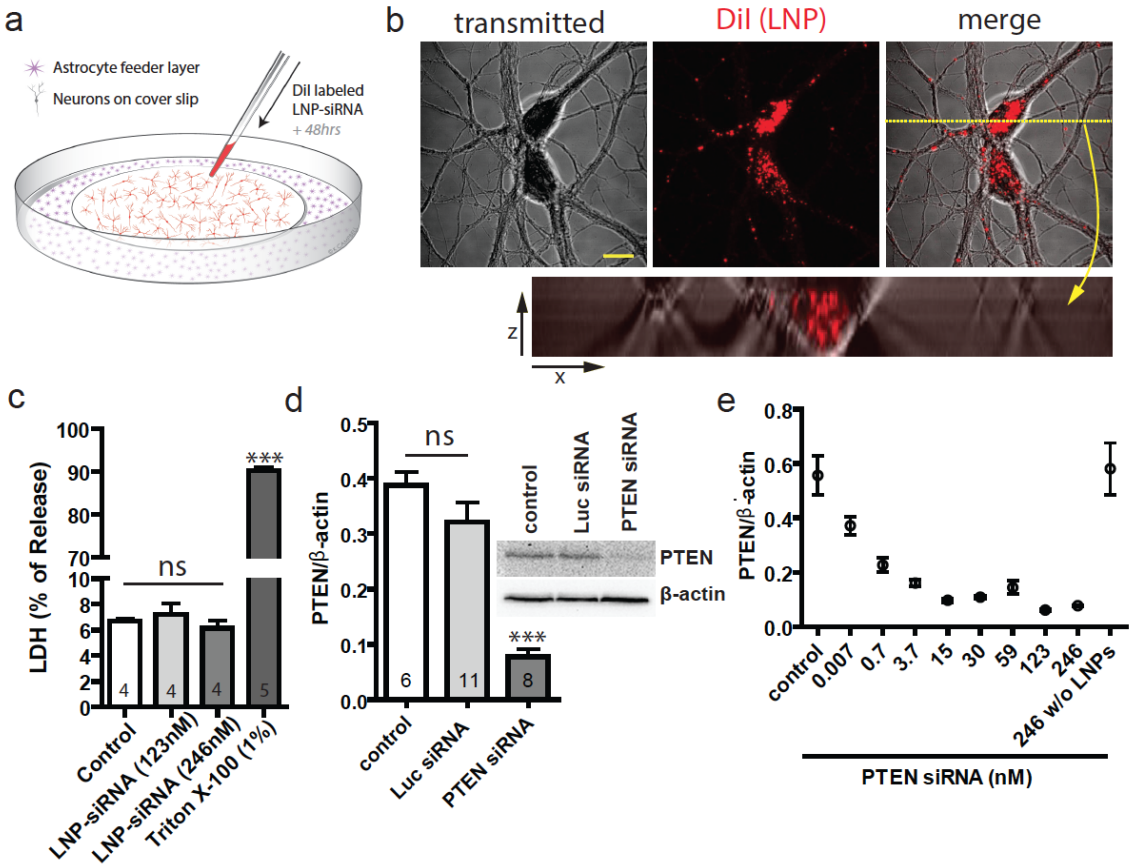

Figure 2.2: LNP-siRNA systems mediate knockdown of target gene in neuron cultures

a, Pure neuron cultures on a coverslip in a petri dish with a separate astrocyte feeder layer. LNP-siRNA was added directly to the media. **b,** DiI fluorescence (red) shows that LNPs are found in the cytoplasm of neurons. Bottom: Cross-sectional analysis of an image stack of fluorescence and transmitted IR images revealed that that DiI puncta were found within the boundaries of the cell membrane. scale: 15µm **c,** Quantification of LDH release revealed that LNP were not toxic at concentrations used. **d,** Western blots reveal LNP-PTEN siRNA resulted in knockdown of PTEN protein compared to Luc siRNA-LNP control and non-treated cultures. **e**, Dose response of LNP-siRNA concentration versus PTEN knockdown, last column shows that non encapsulated siRNA did not result in protein knockdown. In all figures, experimental values are the mean and SEM. LDH, lactate dehydrogenase; LNP, lipid nanoparticle; ns, not significant; siRNA, small interfering RNA.

2.3.3 Uptake of Lipid Nanoparticles by Neurons is Apolipoprotein E (ApoE)-Dependent.

In hepatocytes *in vivo*, LNP uptake is facilitated by adsorption of ApoE to the LNPs (Akinc et al., 2010), which can then be recognized by scavenging receptors and low density lipoprotein receptors (LDLR) on the hepatocyte surface. Because ApoE is the dominant lipoprotein in the brain we tested whether uptake of LNPs by neurons in cell culture was also ApoE dependent. ApoE is produced mainly by astrocytes and delivers cholesterol and other essential lipids to neurons via binding to members of the LDLR family followed by endocytosis (Pitas et al., 1987; Bu, 2009). To directly test the ApoE dependence we transferred the neurons to media that had not been in contact with astrocytes and applied LNPs (246nM) with or without exogenous ApoE4 (10μg/mL) (**Figure 2.3a**). After 1 hour, we noticed rapid uptake of DiI labeled LNPs in the presence of exogenous ApoE, compared to neurons incubated without ApoE4 (**Figure 2.3a, b**). Furthermore, we tested the dose dependence of ApoE vs. LNP uptake by measuring the total DiI fluorescence from ruptured cells 1 hour after treatment. We found that LNP uptake reached saturation at around 5μg ApoE/mL (**Figure 2.3c**), in line with measurements from human cerebrospinal fluid (CSF) *in vivo* of 9.09μg/mL (Wahrle et al., 2007). These results suggest that the efficient LNP uptake by neurons is facilitated by association with ApoE and subsequent endocytosis into neurons via an ApoE receptor.

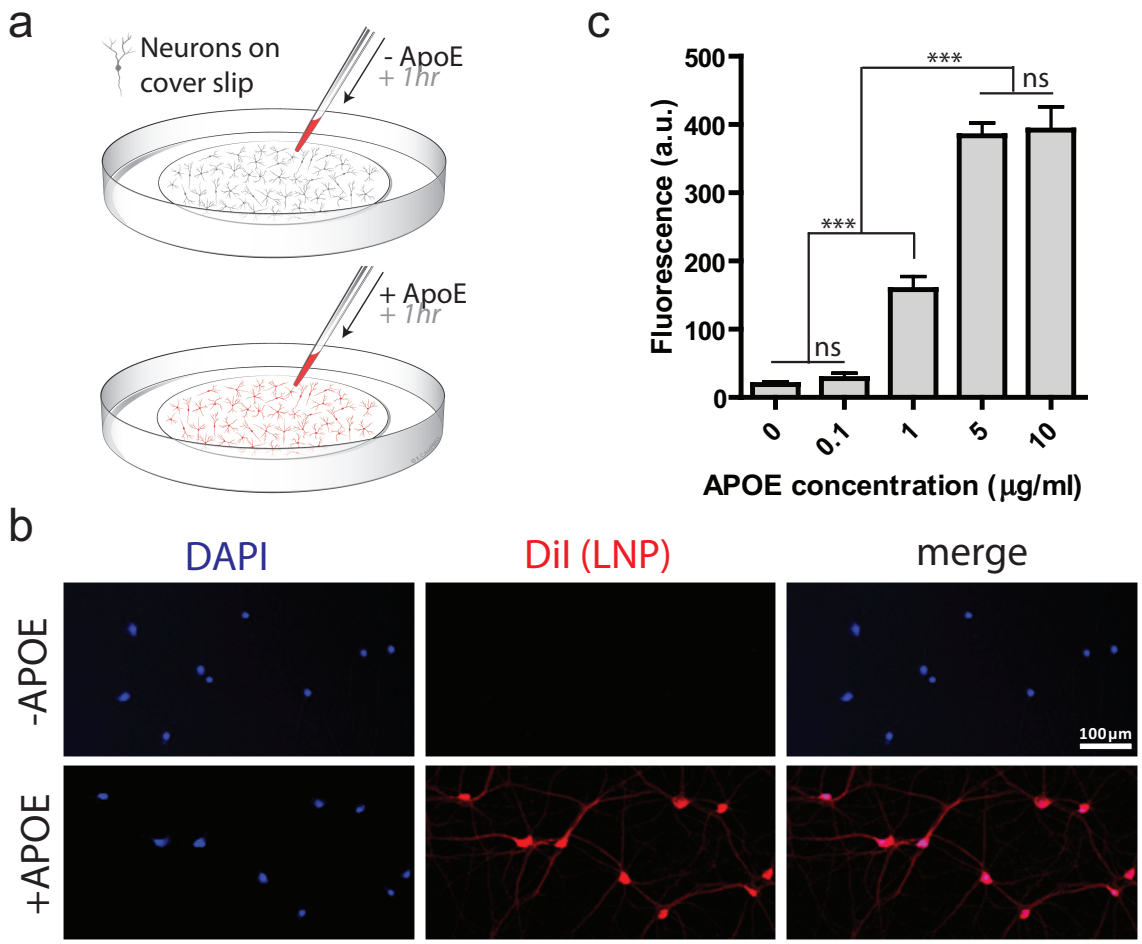

Figure 2.3: LNPs are taken up by neurons in an ApoE dependent manner.

a,b, In the absence of astrocytes, addition of ApoE facilitated the uptake of LNPs by neurons shown by an increase in DiI fluorescence. Treatment: 1 hour LNP-siRNA ± ApoE. **c,** Dose dependence of LNP uptake vs. ApoE concentration measured as DiI fluorescence. In all figures, experimental values are the mean and SEM. ***P<0.001; DAPI, 4′,6-diamidino-2-phenylindole; ns, not significant; siRNA, small interfering RNA.

2.3.4 Lipid Nanoparticle Mediated Neuronal Gene Silencing *in vivo*

The gene silencing potency of LNP siRNA formulations was tested *in vivo* by direct injection into the cortex. In these experiments a single injection of LNPs (500nL at 5mg/mL siRNA/10mins) was administered directly into the somatosensory cortex (**Figure 2.4a**) and the distribution of DiI labeled LNPs and the impact on gene expression monitored subsequently. These LNPs had an average diameter of 50-60nm (**Figure 2.1c**), small enough to diffuse through the extracellular space of the brain (Thorne and Nicholson, 2006). To first test whether neurons *in vivo* accumulated LNPs, acute cortical slices were made from injected rats 5 days following injection, and monitored for DiI positive neurons. Astrocytes *in vivo* produce and secrete ApoE (Bu, 2009); therefore no additional ApoE was added to injected LNPs. We consistently found robust DiI staining localized to neurons within a radius of ~800μm from the injection site (**Figure 2.4b**). The neurons were visualized using a live cell fluorescent assay by loading the cells with an –AM form of a fluorescent Na^+ dye, CoroNa-AM that is only retained in live cells (Tsien, 1981). Consistent with the *in vitro* cell culture results, a single injection of LNP PTEN siRNA resulted in knockdown of PTEN protein measured using Western blots (PTEN to β-actin ratios reduced by 72% and 69% compared to non-injected or luc siRNA injected controls respectively, $P<0.001$, **Figure 2.4 c,d**). Luc siRNA injected tissue was not significantly different from non-injected controls (**Figure 2.4c, d**). Additionally, to test for toxicity of LNPs *in vivo*, we loaded cells with the vital dye calcein-AM, which is only fluorescent when cleaved by endogenous

esterases present in live cells, and compared cell density in LNP injected rats and non injected rats. In Luc siRNA-LNP injected rats we observed no significant difference in cell density 200mm-500mm from the injection tract compared to control (**Figure 4e**). This is a region with robust LNP uptake and gene knockdown but not damaged from the injection needle itself, suggesting that LNPs themselves are non-toxic *in vivo*. These results demonstrate that when administered directly into the brain, LNPs are capable of diffusing through the extracellular milieu to deliver siRNA to neurons and induce gene silencing at sites distant from the site of injection.

Although clinical studies suggest that intravenous delivery of LNP-siRNAs are rarely immunogenic, the immunostimulatory effects of LNPs on brain tissue has not yet been examined. To test whether LNP-siRNAs caused any immunostimulatory effects in the brain, we directly incubated acute cortical/hippocampal brain slices in LNP-siRNA and measured immune responses using tumor necrosis factor-α (TNF-α) ELISA. TNF-α is a pro-inflammatory cytokine that is released when immune responses occur in the brain. The results suggest that there was no immunostimulatory effect when Luc siRNA-LNPs (246nM) were applied to brain slices. TNF- α levels in the Luc siRNA-LNP-treated group were not significantly different from the control group (**Figure 4f**, $P>0.05$). As a positive control, LPS (40mg/ml) was applied to the slices and induced a significant increase of TNF-a compared to control and Luc siRNA-LNPs groups (**Figure 4f**, $P<0.05$). In Addition, TNF-a levels were not significantly increased in siRNA-LNP positive tissue following

direct injection *in vivo* (**Figure 4g**, P>0.05). These data suggest that LNPs themselves do not cause immunostimulatory responses in the brain.

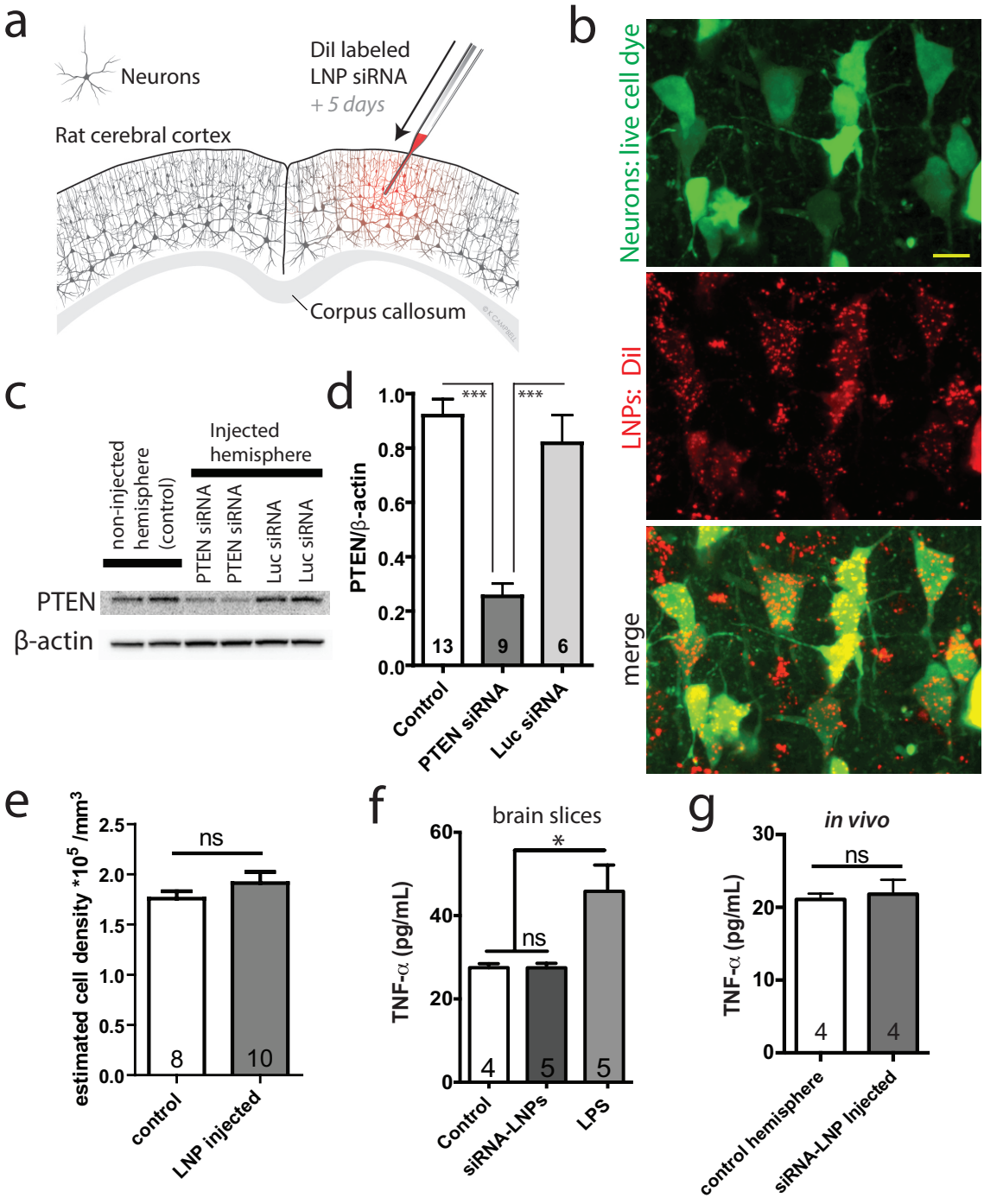
a
Neurons
DiI labeled
LNP siRNA
+ 5 days
Rat cerebral cortex
Corpus callosum
b
Neurons: live cell dye
LNPs: DiI
merge
c
non-injected hemisphere (control)
Injected hemisphere
PTEN siRNA
PTEN siRNA
Luc siRNA
Luc siRNA
PTEN
β-actin
d
PTEN/β-actin
***
***
13
9
6
Control
PTEN siRNA
Luc siRNA
e
estimated cell density *10^5 /mm^3
ns
8
10
control
LNP injected
f
brain slices
TNF-α (pg/mL)
*
ns
4
5
5
Control
siRNA-LNPs
LPS
g
in vivo
TNF-α (pg/mL)
ns
4
4
control hemisphere
siRNA-LNP Injected

Figure 2.4: LNP-siRNA systems mediate knockdown of target gene *in vivo*.

a, LNP-siRNA was injected directly into the somatosensory cortex using a glass micropipette. **b,** Imaging of acute brain slices 5 days following a single injection of LNP-siRNA revealed that live neurons (AM-dye) had taken up fluorescent LNPs (DiI). Scale: 10 μm. **c, d,** Western blots revealed that injection of LNP-PTEN siRNA resulted in knockdown of PTEN protein compared to tissue from the non-injected hemisphere and Luc siRNA-LNP injected rats. Tissue was dissected within 1mm from the site of injection after 5 days. **e,** Analysis of the density of live cells stained with the vital dye calcein-AM showed there was no indication of toxicity or cell loss with LNP uptake *in vivo* (200-500μm from injection). **f,** TNF-α ELISA measurements from acute brain slices treated with Luc siRNA-LNPs shows lack of an immunostimulatory response to LNPs in brain tissue. g, TNF-α ELISA measurements taken from LNP positive tissue (~100-500um from injection), were not significantly different from the LNP negative non-injected hemisphere. Measurements were normalized to 0.5mg of protein. *$P < 0.05$; ***$P < 0.001$. ELISA, enzyme-linked immunosorbent assay; LNP, lipid nanoparticle; LPS, lipopolysaccharide; NS, not significant; siRNA, small interfering RNA; TNF-α, tumor necrosis factor-α.

2.3.5 Time Course and Distance Analysis of PTEN Knockdown *in vivo*

We next determined how far from the injection site was gene silencing effectively induced, as well as the time course of the LNP mediated PTEN knockdown. To characterize the distance profile of the knockdown, we used a combination of immunohistochemistry as well as Western blot analysis on tissue taken at different distances away from the injection tract. Immunostaining of fixed tissue taken from rats 5 days following a single injection of PTEN siRNA LNPs revealed clear loss of PTEN staining in neurons less than 1mm from the injection site, compared to higher levels of PTEN staining at distances further away (**Figure 2.5a**). The montage in **Figure 2.5a** shows a sectioning plane where the asterisk indicates the region 400μm from the injection tract. The pattern of decreased immunofluorescence showed a good correlation with the Western blot analysis, which revealed that PTEN protein levels were significantly reduced at distances within 1mm of the injection tract but not 1-3mm away (**Figure 2.5b**). To test the time course of PTEN knockdown following single injections of LNP siRNA, the amount of PTEN protein expressed within 0.5mm of the injection sites was measured using Western blots in a series of animals at different time points following injection. PTEN suppression following a single injection was sustained for at least 15 days (PTEN/β-actin reduced by 91% compared to control, $P<0.001$, **Figure 2.5c**), the longest time point tested.

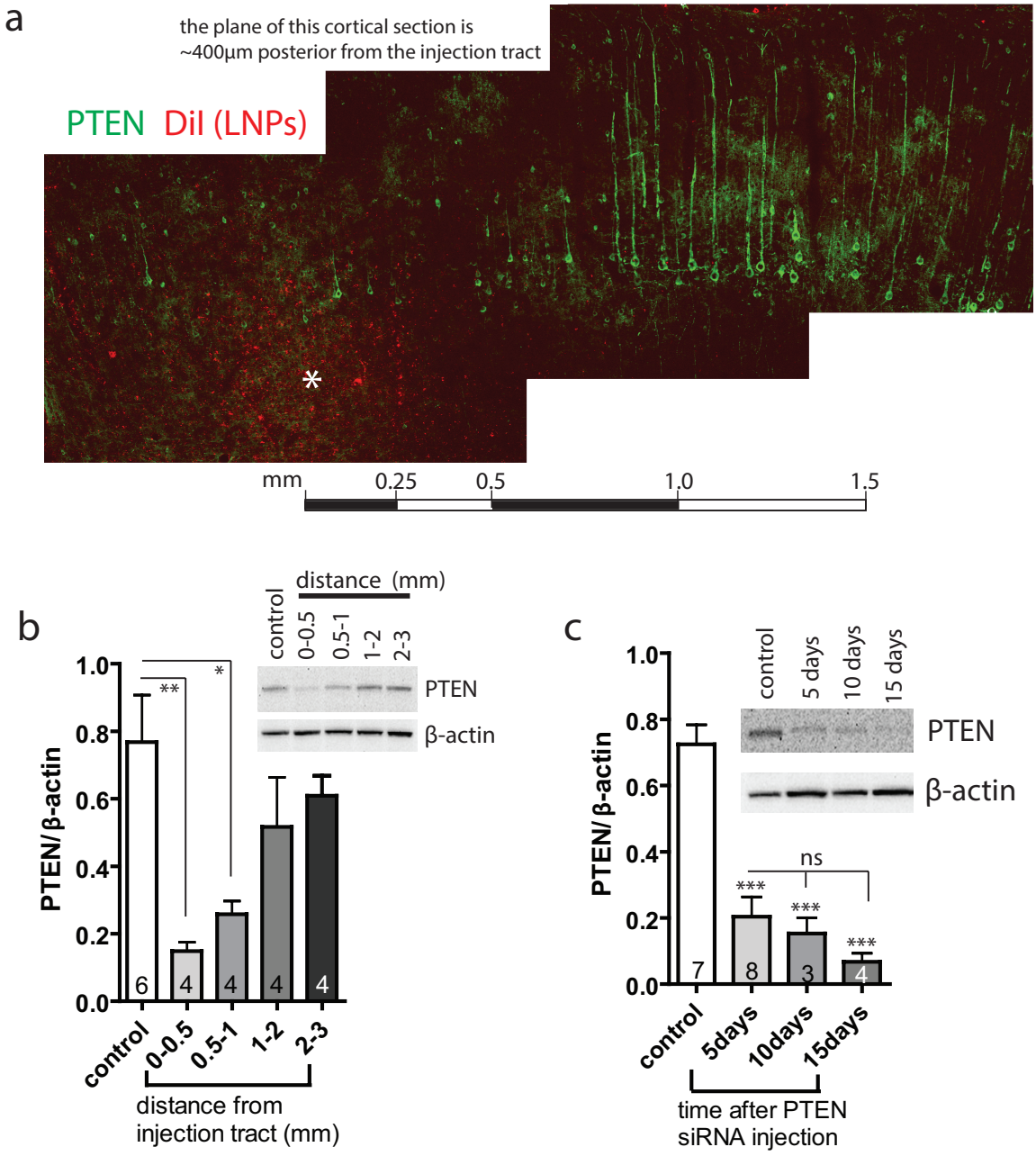
a
the plane of this cortical section is
~400μm posterior from the injection tract
PTEN DiI (LNPs)
mm
0.25
0.5
1.0
1.5
b
distance (mm)
control
0-0.5
0.5-1
1-2
2-3
PTEN
β-actin
PTEN/β-actin
1.0
0.8
0.6
0.4
0.2
0.0
**
*
6
4
4
4
4
control
0-0.5
0.5-1
1-2
2-3
distance from
injection tract (mm)
c
control
5 days
10 days
15 days
PTEN
β-actin
PTEN/β-actin
ns
***
***
***
7
8
3
4
control
5days
10days
15days
time after PTEN
siRNA injection

Figure 2.5: Distance profile and time course of protein knockdown *in vivo*.

(**a**) Immunofluorescence for PTEN protein is decreased in neurons less than 1 mm from the site of LNP-siRNA injection. The illustrated montage was obtained from a section plane posterior to the injection tract and the asterisk indicates the point that was 400 μm from the injection. (**b**) An example Western blot (inset) shows decreased PTEN protein in tissue obtained less than 1 mm from the injection tract. Bar graph showing the summarized data from Western blots on tissue dissected at different distances adjacent to LNP-siRNA injection. (**c**) Western blot revealed sustained knockdown of PTEN at 5, 10, and 15 days following a single intracranial injection of LNP-siRNA. **P* < 0.05; ***P* < 0.01; ****P* < 0.001. LNP, lipid nanoparticle; NS, not significant; siRNA, small interfering RNA.

2.3.6 Lipid Nanoparticles are Capable of Widespread Distribution and Knockdown After ICV Administration

Although local knockdown can be quite useful when attempting to target specific brain regions, sometimes more widespread knockdown is preferable. We therefore tested whether intracerebroventricular (ICV) injections could overcome the distance limitations imposed by small volume local injections. For the purpose of this study we focused on two brain regions close to the ventricular system, the dorsal hippocampus and the striatum. Following a single injection of 2μL PTEN siRNA-LNPs bilaterally into the lateral ventricles we observed robust LNP uptake in neurons as shown by DiI uptake in the CA1 cell body layer of the hippocampus (**Figure 2.6a**) at a distance over 4mm from the injection site itself. We verified that the siRNA-LNP was effective by measuring PTEN levels in both the striatum and the dorsal hippocampus of rats injected with PTEN siRNA-LNPs (PTEN/β-actin reduced 55.8% in hippocampus and 51.2% in striatum compared to control siRNA injected rats **Figure 2.6b-d**).

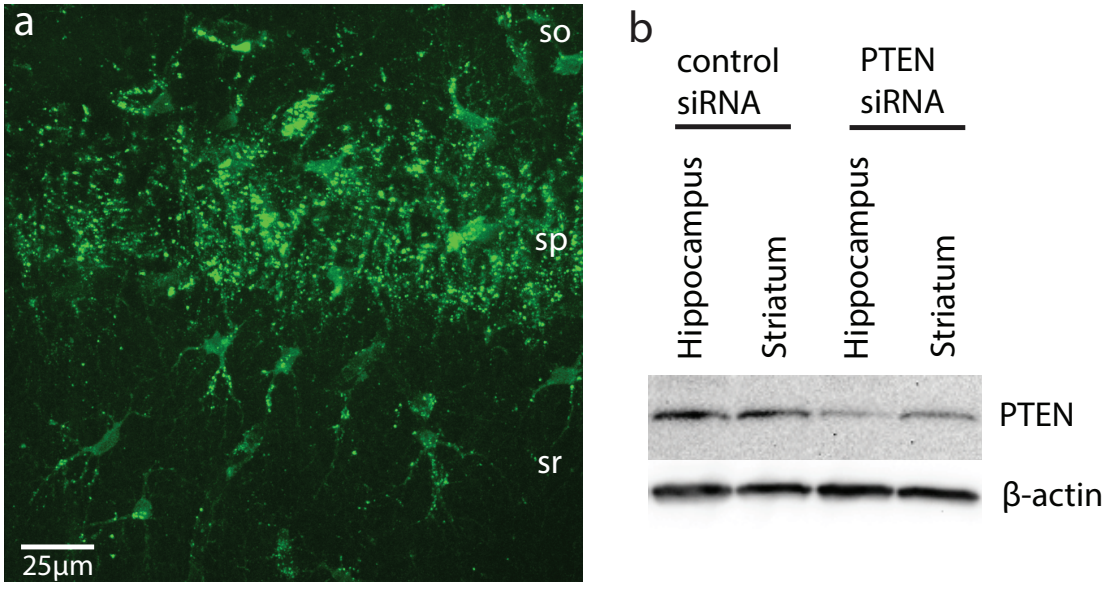
a
so
sp
sr
25μm
b
control siRNA
PTEN siRNA
Hippocampus
Striatum
Hippocampus
Striatum
PTEN
β-actin

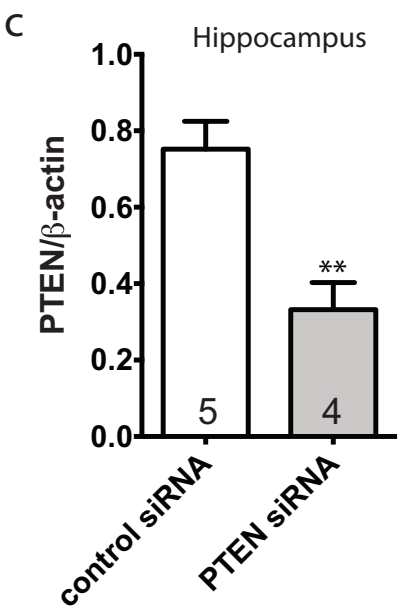
c
Hippocampus
PTEN/β-actin
1.0
0.8
0.6
0.4
0.2
0.0
**
5
4
control siRNA
PTEN siRNA

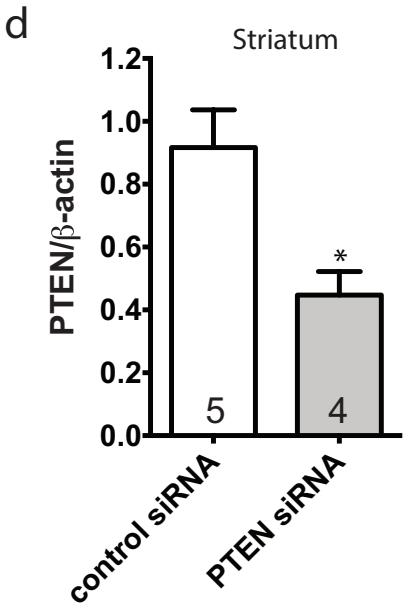
d
Striatum
PTEN/β-actin
1.2
1.0
0.8
0.6
0.4
0.2
0.0
*
5
4
control siRNA
PTEN siRNA

Figure 2.6: Lipid nanoparticles (LNPs) are capable of widespread distribution and knockdown after intracerebroventricular (ICV) administration.

(**a**) DiI fluorescence in CA1 region of the hippocampus shows robust uptake of LNPs by neurons in the cell body layer (sp). Scale: 25 μm. (**b**–**d**) Western blots show ICV-injected siRNA-LNPs results in knockdown of the target protein (PTEN) in different brain regions (dorsal hippocampus and striatum). **P* < 0.05; ***P* < 0.01. siRNA, small interfering RNA; so, stratum oriens; sp, stratum pyramidale (cell body layer); sr, stratum radiatum.

2.3.7 Lipid Nanoparticle Mediated Knockdown of GluN1 in Cell Culture

The ability of LNP-siRNA technology to modify the synaptic function of nerve cells was tested. siRNA against GRIN1, the gene encoding the GluN1 subunit of the NMDA receptor (NMDAR), was used to determine if a LNP siRNA delivery approach could effectively interfere with NMDAR function. The NMDAR ion channel is heteromeric, composed of two obligatory GluN1 subunits plus two GluN2 or GluN3 subunits. Expression of GluN1 is necessary for the formation of a functional NMDAR channel in the plasma membrane (Traynelis et al., 2010). Three different siRNAs directed against different regions of GRIN1 were tested using LNP delivery in cultured neurons to determine their efficacy. All three siRNA sequences resulted in significant knockdown of GluN1 expression (**Figure 2.7a,b**), however sequence #1 resulted in the most robust knockdown, and was therefore used for the subsequent experiments *in vivo*. Additionally, as a control for selectivity against the target gene, PTEN expression was not reduced by GluN1 siRNA (**Figure 2.7a,c**).

NMDARs are typically arranged in clusters at synaptic and extrasynaptic sites (Rao and Craig, 1997; Washbourne et al., 2002). To test the effect of GluN1 knockdown on the presence of GluN1 clusters, cultures of cortical neurons were treated with LNPs containing either GluN1 siRNA or a control luc siRNA. Neurons exposed to LNP GluN1 siRNA but not Luc siRNA-LNP resulted in a significant decrease in the density of GluN1 clusters (GluN1 clusters/μm reduced by 41% compared to control, $P<0.001$, **Figure 2.7d, e**).

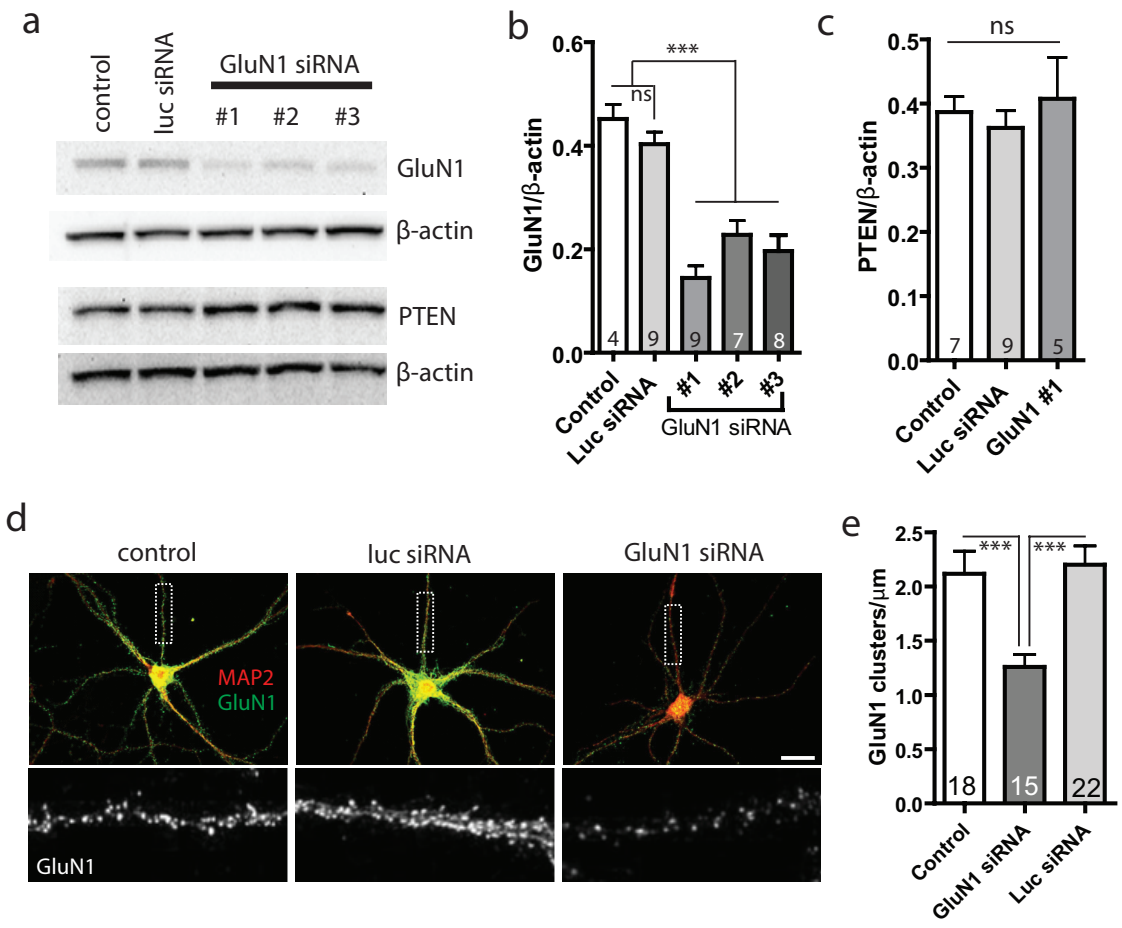

Figure 2.7: LNP-GluN1 siRNA results in knockdown of the NMDAR obligatory subunit GluN1.

(**a**,**b**) Western blots show that LNP encapsulation of siRNAs targeted against three distinct regions of GluN1 RNA all resulted in knockdown of GluN1 protein (compared with nontreated control and luc siRNA). Mean knockdown with GluN1 siRNA no. 1 was greatest and was used for subsequent experiments. (**c**) Control shows LNP-GluN1 no. 1 siRNA did not affect PTEN expression. (**d**) Decreased GluN1 immunofluorescence was observed in LNP-GluN1 siRNA–treated cultures (right panels) as compared with nontreated (controls) or cultures treated with LNP-luc siRNA. Bottom: shows higher magnification of dashed box indicating GluN1 clusters along dendrite. Scale: 20 µm. (**e**) Summary data of GluN1 clusters/µm of dendrite. ***P < 0.001. LNP, lipid nanoparticle; NS, not significant; siRNA, small interfering RNA.

2.3.8 Functional Knockdown of NMDAR Currents *in vivo*

After establishing that LNP encapsulated siRNA against GRIN1 can reduce GluN1 and therefore NMDAR expression *in vitro*, we proceeded to test the ability of this approach to knock down GluN1 expression and synaptic function *in vivo*. A single injection of LNPs containing GRIN1 siRNA resulted in a significant decrease in GluN1 protein expression compared to controls (no injection or rats injected with LNPs containing luc siRNA) when tested 5 days later (GluN1/β-actin reduced by 51%, and 54% compared to non-injected and Luc siRNA-LNP injected controls respectively, $P<0.01$ and $P<0.05$, **Figure 2.8a, b**). We then tested the functional impact of disrupting GluN1 expression by measuring the ratio of NMDAR/AMPAR excitatory postsynaptic currents (EPSCs) in voltage clamped neurons. Glutamate is the major excitatory neurotransmitter in the brain and acts on both AMPA and NMDA receptors at synapses. However, the NMDAR is normally blocked at resting membrane potential, and requires the simultaneous binding of glutamate plus depolarization to remove the voltage-dependent open channel block by extracellular Mg^{2+}. Therefore, a common protocol to test the NMDAR/AMPAR ratio in response to the synaptic release of glutamate is to measure the ratio of the evoked EPSC when the NMDAR is blocked by holding the cell at -70mV to obtain a pure AMPAR component versus when the cell is held at +40mV to get a mixed AMPAR plus NMDAR component (Sah and Nicoll, 1991; Mameli et al., 2011)(**Figure 2.8d**).

Rats were injected with LNPs containing GluN1 siRNA or luc siRNA and the NMDAR/AMPAR ratio was measured in cortical brain slices 4-6 days later, a time

that corresponded to decreased expression of GluN1 expression as shown in Western blots. Neurons that were chosen for experiments were within 500μm of the injection site, and were verified to have taken up LNPs based on punctate intracellular DiI fluorescence **(Figure 2.8c**), and the ratio of NMDAR/AMPAR was measured. To get the NMDA component we measured the amplitude of the outward current at V_h +40mV 50ms after the stimulation artifact, a time point when the AMPAR current had returned to baseline (This was verified by subtracting the trace in the presence of the NMDAR antagonist, APV to show the outward I_{NMDAR} (blue) and I_{AMPAR} (red) components separately). The AMPA component was measured as the inward current when the cell was held at -70mV (**Figure 2.8d**). Consistent with the observed decrease in GluN1 expression, we found that neurons treated with LNPs that contained GluN1 siRNA had significantly decreased NMDAR/AMPAR ratios compared to neurons with LNPs from luc siRNA injected rats (**Figure 2.8d-f**). Therefore the NMDAR component of the synaptic response was selectively reduced by LNP-delivered GluN1 siRNA. These results further validate the use of LNPs to manipulate gene expression in the brain, showing that both the total protein levels as well as the function of the target protein were successfully disrupted.

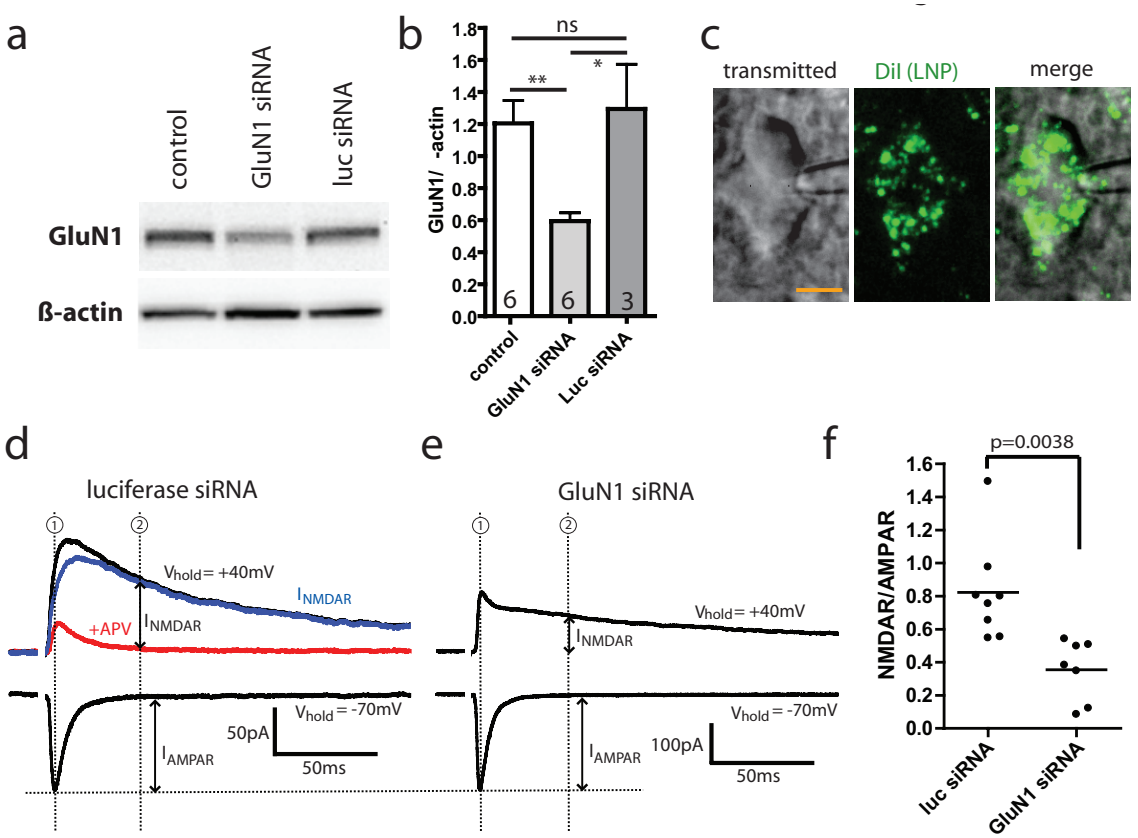

Figure 2.8: Selective knockdown of GluN1 protein *in vivo* results in functional disruption of NMDAR synaptic currents.

(**a**,**b**) Western blot shows intracranial injection of LNP-GluN1 siRNA resulted in knockdown of GluN1 protein. Luc siRNA-LNP control injection showed no effect. (**c**) DiI staining was observed in a voltage-clamped neuron in a brain slice obtained 5 days after *in vivo* LNP injection indicating LNP uptake in this cell. (**d**) NMDA receptor (NMDAR)/AMPA receptor (AMPAR) ratio was calculated using the ratio of the NMDAR current at V_{hold} = +40 mV (upper traces) at point 2 when the AMPAR component (in the lower trace) returned to baseline (50 ms) divided by the peak current at V_{hold} = −70 mV (lower traces) at point 1 which was the peak AMPAR current. Red trace: in the presence of the NMDAR antagonist, APV, the NMDAR-dependent current was blocked revealing the outward AMPAR current. Blue trace: total current−red (APV) current = NMDAR component. (**e**,**f**) Voltage clamp revealed a selective decrease in NMDAR/AMPAR currents in neurons from rats injected with LNP-GluN1 siRNA compared with a luc siRNA-LNP control. *P < 0.05; **P < 0.01. LNP, lipid nanoparticle; NS, not significant; siRNA, small interfering RNA.

2.4 Discussion

The results presented here show that LNP siRNA systems can exhibit efficient gene silencing properties in neurons both *in vitro* and *in vivo* that lead to functional consequences without inducing significant toxicity. In cell culture 100% of neurons were observed to have taken up the LNPs as indicated by the appearance of DiI within the cytoplasm with no apparent toxicity or indications of neuron loss over several days to a week. In addition the reduction of protein expression from siRNA was extensive enough to detect by Western blots using total protein from cultures or immunocytochemistry of individual neurons. In experiments *in vivo* localized injection of siRNA-LNPs within the cortex or ICV injections to cause more diffuse and widespread LNP uptake led to consistent decreases in both mRNA and protein expression again with no indication of cell loss or damage from the uptake of LNPs.

Here we discuss the mechanism of action of LNP siRNA delivery; the utility of these LNP siRNA systems for gene knockdown both *in vitro* and *in vivo* in the brain; and potential therapeutic applications with regard to neurological and psychiatric diseases. With respect to the mechanism of action, the LNP delivery systems employed here contain the ionizable cationic lipid DMAP-BLP, a lipid that exhibits optimized bilayer destabilizing and pKa properties leading to highly potent gene silencing in hepatocytes following intravenous administration (see Supplementary Information) that is similar to "gold standard" lipids such as DLinMC3-DMA[8]. Detailed studies have shown that the ability of LNP siRNA systems containing

related ionizable cationic lipids to induce hepatocyte gene knockdown *in vivo* is ApoE dependent (Akinc et al., 2010). In ApoE knockout mice LNP siRNA gene silencing activity is inhibited in hepatocytes and can be re-established by incubating the LNPs with ApoE prior to IV administration. In the brain and in neuronal cultures ApoE is synthesized in astrocytes(Pitas et al., 1987; Bu, 2009). The astrocytes in the neuronal culture system are separated into a feeder layer that allowed us to test the ApoE dependence of LNP uptake by removing the separate astrocyte feeder layer. With no added ApoE there was no evidence of neuronal LNP uptake whereas graded uptake was observed when ApoE concentrations were increased above 0.1μg/ml to 1 and 5μg/ml ApoE. The concentrations of ApoE found in the brain are similar to the concentrations we found to be effective in cell culture (Wahrle et al., 2007). This suggests that the natural affinity of these LNP systems for endogenous ApoE in the brain provides a highly efficient method for LNP delivery into neurons *in vivo*.

The utility of the LNP siRNA systems for silencing target genes in neurons in cell culture is indicated by our observations that transfection efficiencies approached 100%, without overt signs of toxicity. In contrast current non-viral vectors exhibit transfection efficiencies of 10% or less, and are often accompanied by cell damage (Karra and Dahm, 2010). LNPs appear to be a superior alternative to presently used techniques to transfect neurons in cell culture based not only on the high rate of uptake but also on the benign nature of the LNPs. Another key finding in our study is that the LNP-siRNA approach we describe here provides an effective alternative to other *in vivo* transfection vectors presently used. Viral delivery is the most effective available way to transfect neurons (Hommel et al.,

2003). The disadvantage of viral delivery is the requirement for constructing virus vectors that take added time, potentially cause immune responses and raise safety concerns. The use of LNPs can circumvent these issues, and provides a method to rapidly test various siRNA constructs against the expression of different target proteins, and then examine the protein's function. Injection of antisense oligonucleotides (ASOs) into the CSF represents another promising method to silence neuronal gene expression *in vivo* (Karra and Dahm, 2010; Kordasiewicz et al., 2012). However, two major problems associated with ASOs are the high doses required to achieve gene silencing effects and immunostimulatory effects (Zalachoras et al., 2011; Robinson, 2012). With regard to dose levels, ICV infusion of free antisense oligonucleotides against superoxide dismutase (SOD) by osmotic pump at 100μg/day per rat over 28 days (total of 2.8mg of antisense oligonucleotide) resulted in approximately 50% SOD mRNA silencing (Smith et al., 2006). Here we demonstrate that a single LNP siRNA injection of 2.5μg of siRNA per rat by intracortical administration results in pronounced (up to 91%) gene silencing that is sustained for at least 15 days post injection. Clinical studies suggest that the immunostimulatory effects of LNP siRNA injections are infrequent and readily managed, see http://www.alnylam.com/capella/wp-content/uploads/2012/07/Alnylam-ALN-TTR02-PhaseI-Results-120716.pdf. Consistently, we found no evidence that LNP-siRNAs caused immunostimulatory effects in brain tissue as we found no increased synthesis of TNF-α triggered by LNPs (**Figure 2.4f**). In addition there are now well-established methods to reduce

or eliminate siRNA immunogenicity by adjusting siRNA chemistry (Bramsen and Kjems, 2012).

The LNP formulation employed here used PEG-DMG which is a type of PEG-lipid with short acyl chains that allow it to dissociate rapidly (Holland et al., 1996) from LNPs upon dilution, allowing association of proteins such as ApoE. It would be expected that larger radii of distribution could be achieved for LNPs containing a PEG-lipid with longer acyl chains, which do not dissociate so rapidly. Enhanced tissue penetration would also be expected for smaller LNPs that can be achieved at higher PEG-lipid levels (Belliveau et al., 2012). The LNP platform is highly flexible, potentially allowing delivery of other materials to neurons such as drugs, fluorescent dyes and plasmids.

The results presented here demonstrate the utility of LNP siRNA systems for silencing target genes in neurons both *in vitro* and *in vivo*, with obvious utility for rapidly advancing functional genomics studies. The ability to silence multiple genes, even five or more genes at once (Love et al., 2010), may also prove useful. The therapeutic utility of direct intra-cranial administration of LNP siRNA for treatment of neurological disorders remains to be established, however there are now a number of clinically accepted therapies relying on direct pumping of therapeutics into the CSF (North, 1997; Dash and Cudworth, 1998). A lipid-based formulation of cytarabine has gained clinical acceptance for treatment of brain cancer following direct administration into CSF (Phuphanich et al., 2007). Further, a number of clinical trials are now in progress for treatments for serious neurological diseases

that rely on continuous infusion of ASOs into the CSF (Smith et al., 2006; Robinson, 2012).

Chapter 3: Mechanisms of neuronal chloride loading underlying cytotoxic edema.

3.1 Introduction

Brain edema, the pathological hallmark of excitotoxic injury and traumatic brain injury (Klatzo, 1987; Marmarou et al., 2006; Rosenblum, 2007; Donkin and Vink, 2010) was first characterized by Klatzo (1967) as either vasogenic or cytotoxic. Cytotoxic brain edema is caused by water movement into the intracellular compartment of neurons and/or astrocytes leading to brain swelling, while vasogenic edema is due to water entry into the brain from the vasculature (Klatzo, 1967). Excitotoxic swelling of cultured neurons is known to involve influx of both Na^+ and Cl^- although the influx pathway(s) for Cl^- remain obscure (Rothman, 1985; Choi, 1987; Hasbani et al., 1998). The low resting Cl^- permeability in neurons suggests that a Cl^- channel or exchange mechanism must be activated for Cl^- entry to occur at sufficient levels to increase cell volume and cause cytotoxic edema. In mature pyramidal neurons of the cortex and hippocampus, the equilibrium potential for Cl^- (E_{Cl^-}) is set more hyperpolarized to the resting membrane potential (E_m) by KCC2-mediated active transport of Cl^- out of the cell against it's electrochemical concentration gradient (Blaesse et al., 2009). As such, the Cl^- influx that is required for cytotoxic neuronal edema occurs as a result of either the activation of a Cl^- channel that is not open at rest, or activation of a Cl^- transporter. Putative candidates for Cl^- loading leading to swelling are the volume regulated anion

channel (VRAC), the Na^+-K^+-Cl^+ cotransporter 1 (NKCC1) and GABA activated Cl^- channels (Hasbani et al., 1998; Allen et al., 2004; Inoue et al., 2005; Pond et al., 2006). In addition, there are several newly described Cl^- channels and transporters that could also be important contributors to neuronal edema. Our experiments were designed to examine the interrelationship between neuronal volume, intracellular Na^+ ($[Na^+]_i$) and intracellular Cl^- ($[Cl^-]_i$) in order to investigate the roles for Cl^- entry pathways that contribute to neuronal swelling.

Neuronal swelling occurs as a result of multiple triggers that increase $[Na^+]_i$ including excessive glutamate receptor activation, intense neuronal spiking, activation of non-selective cation channels and inhibition of Na^+, K^+, ATPase (Liang et al., 2007). We tested the impact of increasing $[Na^+]_i$ via ligand- or voltage-gated ion channels on neuronal swelling to test the hypothesis that extensive Na^+ influx itself, independent of the route of entry, leads to swelling by triggering Cl^- influx. Two-photon imaging of cell morphology and fluorescence lifetime measurements (FLIM) of $[Na^+]_i$ and $[Cl^-]_i$ in hippocampal and cortical neurons in acutely prepared brain slices were combined to specifically examine the relationship between increased $[Na^+]_i$, subsequent $[Cl^-]_i$ changes and neuronal swelling. The cytotoxic nature of this swelling was measured by lactate dehydrogenase (LDH) efflux (e.g. (Kajta et al., 2005)). Pharmacological blockers of known Cl^- channels and exchangers were further examined in order to determine the relative contribution of different Cl^- loading pathways to neuronal swelling. Finally, a novel nanoparticle (LNP) strategy to introduce siRNA into neurons in vivo (described in chapter 2) (Rungta et al., 2013) was employed to determine the exact Cl^- pathway critical and

required for the majority of neuronal swelling. These results indicate that a large proportion of neuronal swelling and subsequent cell death requires SLC26A11; a Cl^-, HCO_3^-, SO_4^- exchanger recently reported to be highly expressed in cortical and hippocampal neurons (Rahmati et al., 2013). The identification of the principal pathway required for Cl^- entry could potentially lead to novel targets and therapies for treating cytotoxic brain edema.

3.2 Materials and Methods

3.2.1 Slice Preparation.

Rats were anesthetized with halothane and decapitated according to protocols approved by the University of British Columbia Committee on Animal Care. Brains were rapidly extracted and placed into ice-cold slicing solution containing (in mmol/l): NMDG, 120; KCl, 2.5; $NaHCO_3$, 25; $CaCl_2$, 1; $MgCl_2$, 7; NaH_2PO_4, 1.25; glucose, 20; Na-pyruvate, 2.4; and Na-ascorbate, 1.3; saturated with 95% O_2/5% CO_2. Coronal hemisections or transverse hippocampal slices, 400 μm thick, were sliced using a vibrating tissue slicer (VT1200, Leica, Nussloch, Germany). Slices were incubated at 32 °C in artificial CSF containing (in mmol/l): NaCl, 126; KCl, 2.5; $NaHCO_3$, 26; $CaCl_2$, 2.0; $MgCl_2$, 1.5; NaH_2PO_4, 1.25; and glucose, 10; saturated with 95% O_2/5% CO_2 for 30 minutes. For experiments, slices were at 22–24 °C and perfused at ~2 ml/minute.

3.2.2 Imaging

Live cell imaging (brain slice) was performed with a two-photon laser-scanning microscope (Zeiss LSM510-Axioskop-2; Zeiss, Oberkochen, Germany) with a 40X-W/1.0 numerical aperture objective lens directly coupled to a Chameleon ultra2 laser (Coherent, Santa Clara, CA). CoroNa, SR101 and DiI were excited at 770 nm, and *N*-(ethoxycarbonylmethyl)-6-methoxyquinolinium bromide (MQAE) was excited at 760 nm. The fluorescence from each fluorophore was split using a dichroic mirror at 560 nm, and the signals were each detected with a dedicated photo multiplier tube after passing through an appropriate emission filter (DiI, SR101: 605 nm, 55 nm band pass; CoroNa, MQAE: 525 nm, 50 nm band pass). Transmitted light was simultaneously collected using understage infrared differential interference contrast optics and an additional photo multiplier tube.

3.3.3 Fluorescence Lifetime Imaging (FLIM)

Fluorescence lifetime images were acquired using a Becker & Hickl SPC-150 module. Photon emission was detected using a high speed hybrid detector, HPM-100-40 (Hamamatsu). Images were acquired 128 by 128 pixels in fast xy raster scanning mode. Photons were collected over 20 seconds before calculating and extracting lifetimes at each pixel using SPCImage software (Becker & Hickl). Instrument response function (IRF) was calculated using a 10nm gold nanoparticle suspension (Sigma-Aldrich) to generate a second-harmonic signal. The IRF had a full width at half the maximum amplitude of 121ps. The lifetimes presented in the

figures were the average of all lifetimes within a region of interest from the cytoplasm of the soma. The mean lifetime from all cells in a given experiment were combined and represented as an n=1. MQAE: The Cl^- dependence of MQAE lifetime is described by the Stern-Volmer relation ($\tau_0/\tau = 1 + Ksv\ [Cl^-]_i$), where τ_0 is the fluorescence lifetime in 0 mM Cl^-, and Ksv (the Stern-Volmer constant) is a measure of the Cl^- sensitivity of MQAE. Ksv varies greatly between studies due to differences in cell types, preparation and calibration methods (Kaneko et al., 2001; Kaneko et al., 2004; Hille et al., 2009; Doyon et al., 2011), making it difficult to accurately estimate absolute $[Cl^-]_i$ in situ. CoroNa: A biexponential decay was used to fit CoroNa lifetimes due to poor fit with a single exponential decay, suggesting fluorescence from multiple components. For calibration, neurons were continually voltage-clamped at -70 mV and dialyzed for >10 min before image acquisition. The intracellular solution contained (in mM) potassium gluconate, 108; KCl, 8; sodium gluconate, 8; MgCl2, 2; HEPES, 10; potassium EGTA, 1; potassium, ATP, 4; and sodium GTP, 0.3; pH 7.2 with KOH. Sodium concentration was altered by replacement of potassium gluconate with sodium gluconate. A linear fit of τ_{fast} vs $[Na^+]$ was used to then estimate experimental values of $[Na^+]_i$.

3.2.4 Dye Loading Protocols

Slices were incubated in ACSF plus SR101 (1 μM) at room temperature for 30 minutes. For CoroNa and Calcein Red-AM loading, slices were preincubated in 3 mL aCSF and 8 μL Cremophor EL solution (0.5% in DMSO) at 32 °C for 5 min. AM dye

(50 μg) mixed with 8 μL DMSO and 2 μL pluronic F-127 solution (10% in DMSO) was then added, and slices were allowed to incubate for an additional 45 min. For MQAE loading, slices were bulk loaded with the dye MQAE (6 mM) for 15 minutes at 34 °C.

3.2.5 LDH Assay

LDH assay kits (Biomedical Research Service Center, State University of New York at Buffalo) were used to investigate cell death using rat hippocampal slices. Hippocampal brain slices were prepared as described in brain slice preparation section above. Hippocampal slices were pre-treated for 30 min. with a cocktail of ligand gated and voltage gated ion channel inhibitors (100 μM picrotoxin , 20 μM CNQX, 1 μM TTX) when 100 μM NMDA was applied or (100 μM picrotoxin , 20 μM CNQX, 30 μM Cadmium, 100 μM d-APV) when 50 μM veratridine was applied. NMDA experiments were done in 0 mM Ca^{2+}, 2 mM ethylene glycol tetraacetic acid (EGTA). NMDA or Veratridine was applied to slices for 15 min in a 6 well plate aerated with 95% O_2/5% CO_2 on an insert for organotypic culture (Millipore) for better aeration. Subsequently slices were transferred to incubation chamber and further incubated for 90 min. Supernatants were collected at 90 min and then slices were lysed using lysis buffer. The LDH level in the supernatant represents the cell death, whereas the LDH level in lysed cells represents the viable cells. In brief, supernatants and cell lysates were centrifuged for 3 min at maximal speed (16,000 *g*) at 4 °C. Samples were added into a 96-well plate with LDH assay solution and

incubated for 30 min at 37 °C. Acetic acid (3%) was added to stop the reaction. LDH reduces tetrazolium salt INT to formazan, which is water-soluble and exhibits an absorption maximum at 492 nm. Absorbance was measured at 492 nm using a microplate reader. Cell death is presented as the percentage of LDH released (LDH in supernatant/cell lysate LDH) *100.

3.2.6 Intracranial Injections

All experimental protocols were approved by the Committee on Animal Care, University of British Columbia and conducted in compliance with guidelines provided by the Canadian Council of Animal Care. Sprague–Dawley rats (P22-P26) were anesthetized with isofluorane before and throughout the surgery. A small hole (diameter ˜1 mm) was drilled in the skull to allow access to the brain (−2.0 mm anterior/posterior (AP) and ±3.0 mm medial/lateral (ML) from bregma and 0.8 mm dorsal/ventral (DV)). A glass micropipette (tip diameter ∼40 μm) was connected to a Hamilton syringe and LNP-siRNAs in sterile PBS were injected using an infusion pump (Harvard Apparatus, Holliston, MA) at a rate = ∼50 nl/minute. The total volume injected was 500 nl of LNP-siRNA (5 mg siRNA/ml in sterile PBS).

3.2.7 Lipid Nanoparticle Encapsulation of siRNA

The ionizable cationic lipid 3-(dimethylamino)propyl(12Z,15Z)-3-[(9Z,12Z)-octadeca-9,12-dien-1-yl]henicosa-12,15-dienoate (DMAP-BLP) and PEG lipid PEG-

DMG were provided by Alnylam Pharmaceuticals and have been previously described (Rungta et al., 2013). 1,2-distearoyl-sn-glycero-3-phosphocholine (DSPC) and cholesterol were obtained from Avanti (Alabaster, AL) and Sigma-Aldrich Co. (St. Louis, MO) respectively. The lipophilic carbocyanine dye to monitor LNP siRNA uptake, 1,1'-dioctadecyl-3,3,3',3'-tetramethylindocarbocyanine perchlorate ($DiIC_{18}$), was purchased from Invitrogen (Carlsbad, CA). The lipid composition of all lipid nanoparticles containing siRNA (LNP-siRNA) was DMAP-BLP/DSPC/cholesterol/PEG-DMG/DiIC18 (50/10/37.5/1.5/1; mol%) LNP-siRNA were prepared employing a microfluidic mixing apparatus as previously described (Rungta et al., 2013). Physical parameters characterizing the LNP siRNA systems and the siRNA;lipid ratio are listed in **Table 3.1**.

Table 3.1: Characterization of LNP-siRNA systems

siRNA	Size (nm)	PDI	siRNA/Lipid ratio (mg/μmol)
Luc	48.9	0.039	0.050
SLC4A3	50.6	0.134	0.064
SLC4A8	61.5	0.075	0.067
SLC4A10	59.3	0.080	0.062
SLC26A11-1	51.4	0.200	0.052
SLC26A11-2	49.3	0.048	0.051

PDI, polydispersity index; siRNA small interfering RNA.

3.2.8 Quantitative PCR (qPCR)

Total RNA was Purified using Life Technologies MagMax™-96 Microarray Total RNA Isolation Kit (AM1839), and cDNA created using the Applied Biosystems High Capacity cDNA Reverse Transcription Kit (4368814). Gene specific qPCR reactions were set up using the KAPA Probe Fast Universal qPCR Kit (KK4702) using TaqMan™ probes from Life Technologies and Integrated DNA Technologies (IDT). Specific TaqMan™ probes used in this study:- rSLC4A1 (Rn00561909_m1), rSLC4A2 (Rn00566910_m1), rSLC4A3 (Rn00436642_m1), rSLC4A4 (Rn00584747_m1), rSLC4A5 (Rn01420902_m1), rSLC4A7 (Rn00589539_m1), rSLC4A8 (Rn01532883_m1), rSLC4A9 (Rn00596175_m1), rSLC4A10 (Rn00710136_m1), rSLC4A11 (Rn01515154_m1), rACTB (4352340E), rGAPD (4352338E) from Life Technologies, and rSLC26A1 (Rn.PT.53a.10186844), SLC26A2 (Rn.PT.53a.38316256), rSLC26A3 (Rn.PT.53a.13331783), rSLC26A4 (Rn.PT.53a.37046344), rSLC26A5 (Rn.PT.53a.14115266), rSLC26A6 (Rn.PT.53a.12307129gs), rSLC26A7 (Rn.PT.53a.10816391), rSLC26A9 (Rn.PT.53a.6784539), rSLC26A10 (Rn.PT.53a.5866317), rSLC26A11-1 (Rn.PT.53a.36735939), rSLC26A11-2 (Rn.PT.53a.13211186), rGAPDH (Rn.PT.56a.35727291) all from IDT. Quantitative PCR reactions were performed on a Life Technologies 7500 Real-Time PCR system or Bio-Rad CFX Real-Time Systems, using cycling conditions of 95°C for 3 minutes then 95°C for 15 seconds followed by 60°C for 45 seconds for 40 cycles. The rGAPDH or rACTB probes were used for

normalization of controls in relative quantification of other gene expression measurements.

3.2.9 Gene Knock-Down Dicer-Substrate RNAs (DsiRNAs)

Chemically synthesized siRNA 27mer duplexes were obtained from IDT and screened for knockdown potency by qPCR in culture using plasmid expression knockdown of the cloned rSLC targets expressed in HEK293 cells and of cultured rat cortical neurons. The most potent duplexes were then re-synthesised with 2'-O-methyl (m) patterning for *in vivo* stabilization, packaged into LNPs and re-tested for potency of gene expression knockdown in cultured rat cortical neurons by qPCR.

rSLC4A3 (Sense- rGrGrArUrUrArCrUrCrUrArUrCrArCrArGrArCrArCrCrUAC, Antisense-rGrUrArGrGrUrGrUrCrUmGrUmGrArUrArGrArGrUmArAmUrCmCmAmC)

rSLC4A8 (Sense- rArCrArGrCrGrGrUrCrUrUrArArArGrUrUrUrArUrCrCrCAA, Antisense-rUrUrGrGrGrArUrArArArAmCrUmUrUrArArGrArCrCmGrCmUrGmUmCmA)

rSLC4A10 (Sense- rUrGrCrUrUrArUrArArArGrCrUrArArArGrArCrCrGrCrAAT, Antisense-rArUrUrGrCrGrGrUrCrUmUrUmArGrCrUrUrUrArUmArAmGrCmAmAmC)

rSLC26A11-1 (Sense- rGrCrArUrGrUrCrArGrCrArArUrArUrArGrArCrUrArCrACC, Antisense-rGrGrUrGrUrArGrUrCrUmArUmArUrUrGrCrUrGrAmCrAmUrGmCmGmU)

rSLC26A11-2

(Sense-mGmGrAmGrAmUrCrCrArArUmArCmGrGmCrAmUrCrCrUrGrGmCA,

Antisense-rUrGmCrCrArGrGrAmUrGmCrCmGrUrArUrUrGrGrArUrCmUrCmCmCmA)

3.2.10 Drugs

Drugs were purchased from the following suppliers; Veratridine, d-APV, TTX, CNQX (abcam); DIDS, picrotoxin, niflumic acid, carbenoxelone, acetazolamide, bumetinide (sigma); NPPB (tocris). Targets are as follows (Supplementary Table 1); NPPB (200 μM), volume regulated anion channel (VRAC, VSOR) (Inoue et al., 2005; Inoue and Okada, 2007); niflumic acid (NFA) (200 μM), Ca^{2+} activated Cl^- conductance (CaCC, TMEM16B) (White and Aylwin, 1990; Huang et al., 2012); Gd^{3+} (100 uM), Maxi-anion channel(Sabirov et al., 2001; Sabirov and Okada, 2009; Fields and Ni, 2010); Zinc (300 μM), CLC-2(Staley et al., 1996); carbenoxelone (CBX) (100 μM), pannexins/connexins(Bruzzone et al., 2005; Thompson et al., 2008); bumetanide (100 μM), cation chloride cotransporters (NKCC1 and KCC2) (Payne et al., 2003; Glykys et al., 2014); DIDS (250 μM), SLC4 and SLC26 family $Cl^-/HCO3^-$ exchangers (Grichtchenko et al., 2001; Vincourt et al., 2003; Parker et al., 2008b; Svichar et al., 2009; Xu et al., 2011; Romero et al., 2013). Veratridine and NMDA application; a glass micropette (tip diameter ~2 μm) was positioned 10 μm above the slice and 25 μm lateral to the centre of the imaging frame. The pipette was filled with the perfusion solution plus either veratridine or NMDA. A monometer was used to standardize the rate of drug application.

3.2.11 Data Collection, Analysis and Statistics

Translational movement was removed using Image J software. Fluorescence signals were defined as delta F/F (dF/F) = $[((F_1 - B_1)-(F_0 - B_0))/(F_0 - B_0)]$, where F_1 and F_0 are fluorescence at a given time and the control period mean, respectively. B_1 and B_0 are the corresponding background fluorescence signals. Swelling of individual neurons in cortical slices was analyzed as (%) increase in cross sectional area relative to a mean baseline period. The cross sectional area of the neuron was calculated using the fluorescence boundary of the neuron soma stained with CoroNa. To estimate the tissue volume from the 2 dimensional images of hippocampal slices a line was drawn to measure the diameter and the volume was estimated based on the equation for volume of sphere: $(4/3)\pi r^2$.

Experimental values are the mean ± SEM; baseline equals 100%; n is the number of experiments conducted, data from ≥3 cells/experiment was combined and averaged to make 1 n so that equal weight was given to each experiment and not affected by the number of cells imaged/experiment. Statistical tests were either a two-tailed Student's *t* test or an ANOVA with a Neumann-Keuls post-hoc test for comparison between multiple groups. $P < 0.05$ was accepted as statistically significant (*$P < 0.05$, **$P < 0.01$, ***$P < 0.001$)

3.3 Results

3.3.1 Neuronal Swelling is Caused by Prolonged Increases in Intracellular Na^+ and is Independent of Ca^{2+}.

Several pathways that increase intracellular Na^+, many of which occur in parallel, can trigger cytotoxic brain edema. However, it has been known for almost 30 years that in addition to Na^+ entry, excitotoxic neuronal swelling ultimately requires Cl^- entry (Rothman, 1985). We examined the basis for Cl^- entry following prolonged Na^+ influx via two different pathways to determine if Na^+ influx itself, independent of the route of entry would activate a common Cl^- entry pathway that could conceivably be targeted therapeutically.

We first investigated whether increasing $[Na^+]_i$ is itself capable of triggering a cascade leading to an increase in cell volume and secondly, whether this cascade also leads to rapid cell death. Two parallel and independent approaches were taken to increase $[Na^+]_i$ by either applying veratridine, which removes inactivation of voltage-gated sodium channels (VGSCs) (Strichartz et al., 1987) prolonging Na^+ entry, or by applying NMDA to activate NMDA receptors (NMDARs). NMDA activates a non-selective cation conductance leading to entry of Na^+ and also Ca^{2+}. Neuronal Na^+ entry was induced under conditions in which other voltage-gated ion channels and ligand-gated transmitter receptors were blocked by a combination of Cd^{2+} (30 μM), CNQX (20 μM) and picrotoxin (100 μM). Either veratridine or NMDA was rapidly applied by pressure ejection from a pipette positioned directly above the region of the brain slice that was imaged. To ensure the selectivity of either

approach veratridine was applied with d-APV (100 μM) to block NMDARs and NMDA was applied with TTX (1 μM) to block VGSCs. Changes in $[Na^+]_i$ were monitored using the fluorescent Na^+ indicator CoroNa-Green (Meier et al., 2006) which preferentially stains hippocampal and cortical neurons in brain slices (**Figure 3.1 a**). Astrocytes which did not show any obvious volume changes under these experimental manipulations were visualized using SR101 (Nimmerjahn et al., 2004) to provide landmarks to track during swelling of the tissue. Of note, the activation of either VGSCs by veratridine or NMDARs by NMDA consistently led to a significant increase in $[Na^+]_{i,}$ followed after a delay of seconds, by an increase in neuronal cell volume (**Figure 3.1 b-d, j, k**, **Figure 3.2a, b**). We further compared the impact of Ca^{2+} versus Na^+ entry through NMDARs on swelling by repeating experiments in Ca^{2+} or Na^+ free extracellular solutions. The increase in cell volume from NMDAR activation was still observed in extracellular Ca^{2+} free solution (cross sectional area increased to 161.60 ± 10.55 % of baseline). However, in the presence of low extracellular Na^+ $[Na^+]_{ext}$ and normal (2mM) $[Ca^{2+}]_{ext}$, swelling was completely absent and NMDAR activation actually resulted in a decrease in neuronal volume (**Figure 3.1j** and **Figures 3.2c and d**). Control experiments showed that neuronal $[Na^+]_i$ increases and swelling induced by veratridine were blocked by the VGSC antagonist, TTX (**Figure 3.1j, k**; $p< 0.001$, two-tailed student's *t* test) and those induced by NMDAR were blocked by the NMDAR antagonist, d-APV (**Figure 3.1j, k**; $p< 0.001$, analysis of variance (ANOVA)).

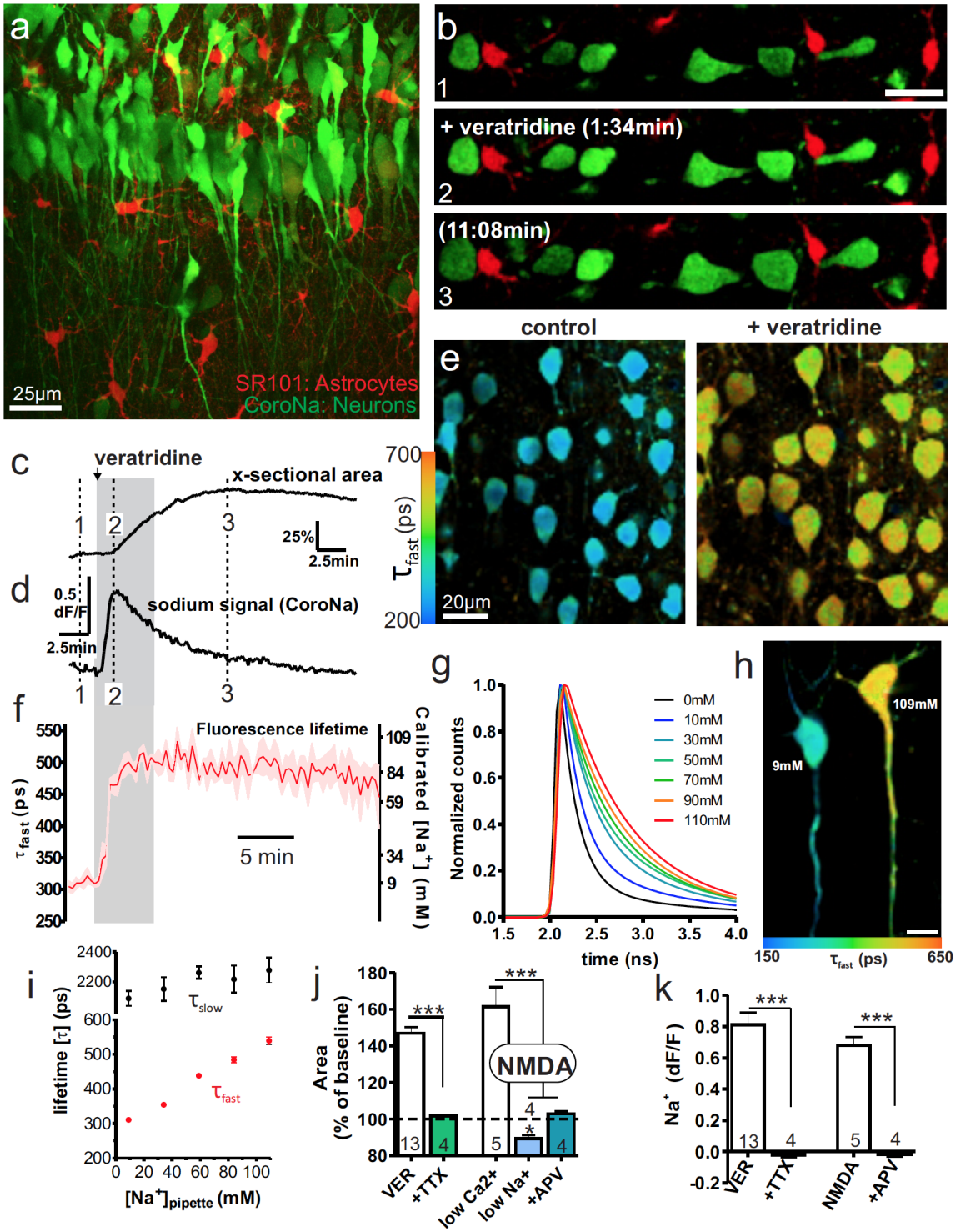
a
25µm
SR101: Astrocytes
CoroNa: Neurons
b
1
+ veratridine (1:34min)
2
(11:08min)
3
control
+ veratridine
e
20µm
700
200
τfast (ps)
c
veratridine
x-sectional area
1
2
3
25%
2.5min
d
0.5
dF/F
2.5min
sodium signal (CoroNa)
f
Fluorescence lifetime
τfast (ps)
Calibrated [Na+] (mM)
5 min
g
Normalized counts
time (ns)
0mM
10mM
30mM
50mM
70mM
90mM
110mM
h
109mM
9mM
150
τfast (ps)
650
i
lifetime [τ] (ps)
τslow
τfast
[Na+]pipette (mM)
j
Area
(% of baseline)
VER
+TTX
low Ca2+
low Na+
NMDA
+APV
k
Na+ (dF/F)
VER
+TTX
NMDA
+APV

Figure 3.1: Neuronal swelling is caused by prolonged increases in intracellular Na^+ and is independent of Ca^{2+}.

(a) CoroNa Green (Na^+ indicator) loaded neurons versus SR101 stained astrocytes (red) in a hippocampal brain slice imaged using two-photon laser scanning microscopy. (b-d) Cortical neurons treated with veratridine (50 μM) show increase in $[Na^+]_i$ followed by swelling (increase in cross sectional area), astrocytes do not swell. (e, f) CoroNa FLIM measurements of $[Na^+]_i$ as neurons swell reveals true time course and magnitude of Na^+ signals that are independent of dye concentration (n=4). (g-i) Calibration of FLIM measurements of neuronal $[Na^+]_i$ with CoroNa. (g) Decay of CoroNa fluorescence changes in salt solutions with varying $[Na^+]$. (h) Dual (simultaneous) whole cell patch clamping of 2 neurons dialyzed with high (109 mM) and low (9 mM) $[Na^+]$ show distinct separation of lifetimes. (i) Calibration of CoroNa lifetimes measured in soma of neurons dialyzed with different $[Na^+]$ shows that the $[Na^+]_i$ can be predicted from τ_{fast}. (j and k) Quantified data shows neuronal swelling is triggered by sodium influx via independent pathways. NMDAR swelling was dependent on Na^+ influx and independent of Ca^{2+}. Control confirms Na^+ signal and swelling caused by veratridine and NMDA was via VGSCs and NMDARs respectively, as they were blocked by antagonists, TTX (1 μM) and d-APV (100 μM). All experiments were done in the presence of 30 mM Cd^{2+}, 20 μM CNQX, 100 μM picrotoxin. Additionally, neurons were pretreated with 100 μM d-APV (NMDAR antagonist) for veratridine experiments and 1 μM TTX (VGSC antagonist) for NMDA experiments to confirm pathways were independent. Scale in (b), 20 μm; scale in (h), 15 μm. VER, veratridine; x-sectional, cross sectional; VGSC, voltage gated sodium channel; SR101, sulforhodamine 101. Control values in panel (j) and panel (k) are also re-plotted in **Fig. 3.5** and **Fig. 3.6** Error bars and shaded region above and below the mean represent SEM.

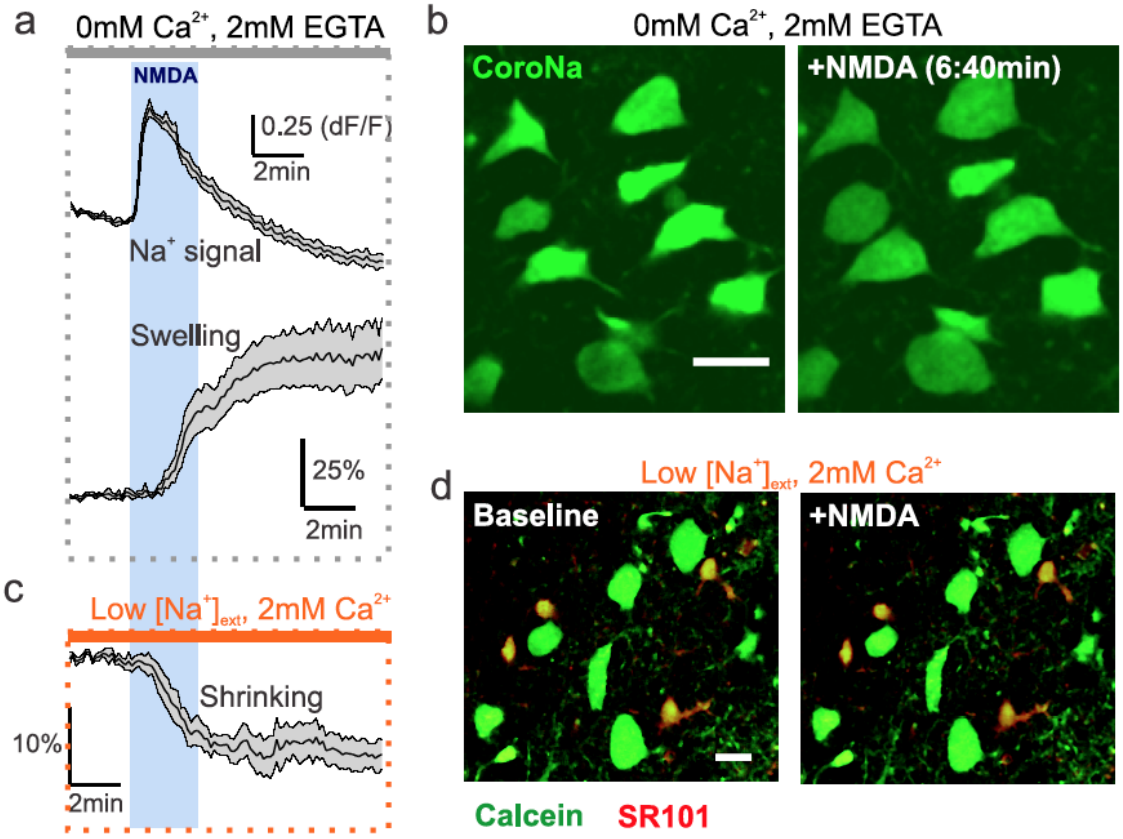

Figure 3.2: NMDAR activation triggers neuronal swelling that requires Na^+ influx, but that is independent of Ca^{2+} influx.

(a and b) Na^+ influx triggers an increase in neuronal volume, measured as the cross sectional area in the absence of extracellular Ca^{2+} (0 mM Ca^{2+}, 2 mM EGTA) (n=5). (c and d) Iso-osmotic replacement of extracellular Na^+ with NMDG (from 152 mM to 26 mM), to reduce Na^+ entry through NMDARs prevents neurons from swelling and causes them to shrink (86.7% of baseline, $p < 0.05$) (n=4). Scale bars, 15 µm (b and d). Shaded area above and below mean represent SEM.

Although an increase in Na^+ preceding swelling was consistently observed, the magnitude and duration of CoroNa fluorescence signals were distorted during cellular swelling due to dye dilution which also reduced fluorescence intensity of the inert dye, Calcein red-AM (**Figure 3.2**). In order to define the true magnitude and time course of the $[Na^+]_i$ increases, we developed a method to record real-time calibrated measurements of $[Na^+]_i$ using two photon fluorescence lifetime imaging (FLIM) which was independent of changes in dye concentrations. When lifetime measurements of CoroNa were first tested in iso-osmotic salt solutions the time constant of decay (τ) increased with increasing $[Na^+]$ (**Figure 3.1g**). However, as the local environment can affect lifetime measurements of dyes (Berezin and Achilefu, 2010) calibrations of CoroNa lifetimes were obtained within the cytoplasm of neurons by whole cell voltage-clamping of neurons and dialysis with different $[Na^+]$ concentrations. CoroNa lifetimes were best fit using a biexponential decay (**Figure 3.3**) with a short lifetime (τ_{fast}) predictive of $[Na^+]_i$ (**Figure 3.1h** and **3.1i**). FLIM of CoroNa loaded neurons revealed that $[Na^+]_i$ increased to approximately 94.46 ± 2.14 mM (calibrated value) throughout veratridine application and gradually recovered after washout (Figure 1E, 1F)

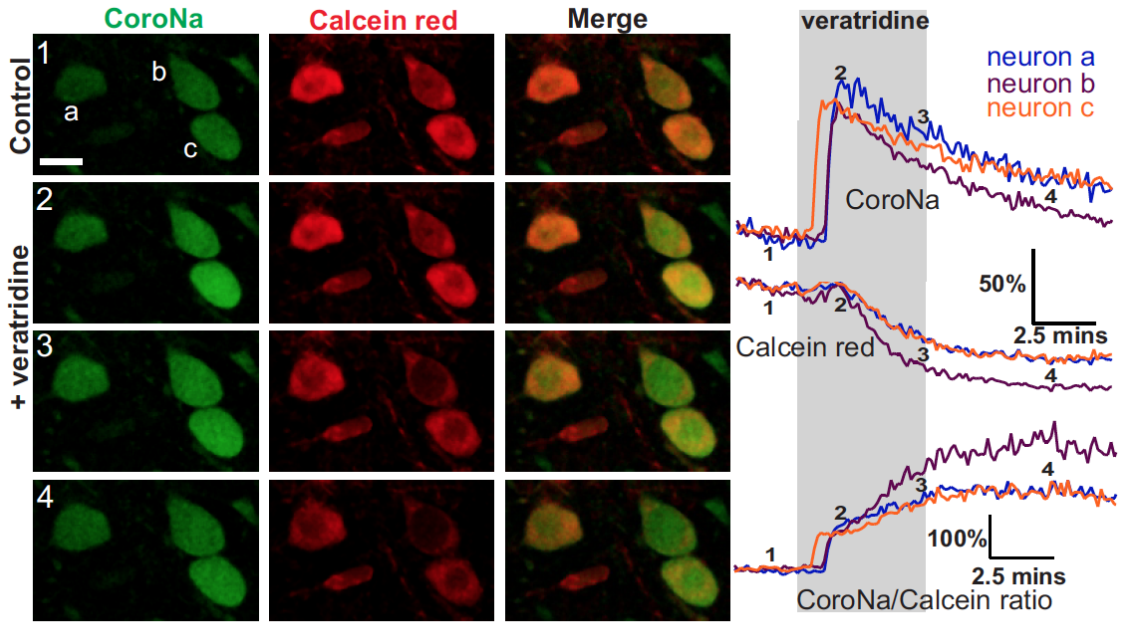

Figure 3.3: Dye dilution results in decreases fluorescence intensity as neurons swell.

Left: example images of neurons loaded with CoroNa and Calcein red that were exposed to veratridine. Right: time course of CoroNa and Calcein Red signals in neurons exposed to veratridine. As neurons begin to swell Calcein Red signal decreases. Scale bar, 10 µm.

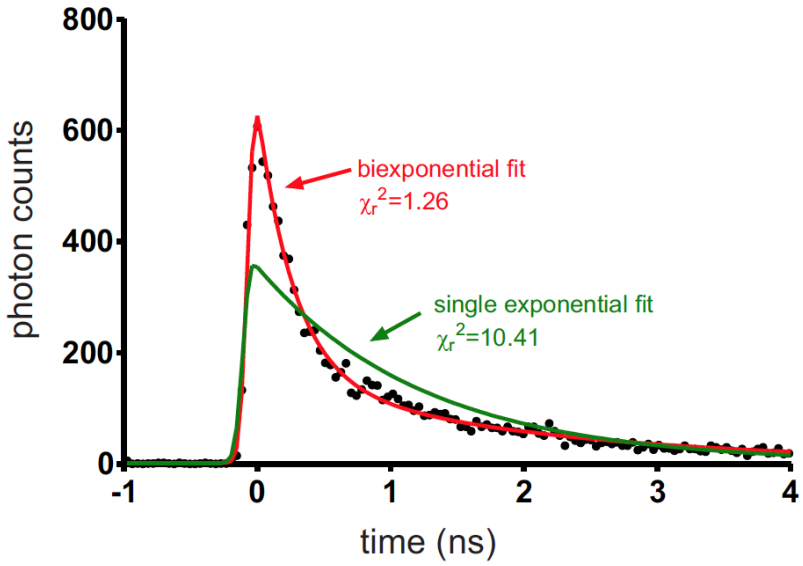

Figure 3.4: Biexponetial decay of CoroNa fluorescence indicates multiple fluorescence components.

Example of single and biexponential fits from a pixel within the cytosol of a cortical neuron loaded with CoroNa-AM. Large deviations in χ^2 from unity (i.e. χ^2 >1.5) typically indicates multiexponential decay resulting from multiple fluorescence components (Berezin and Achilefu, 2010).

3.3.2 Na^+ Influx is Correlated with a Secondary Cl^- Influx that is Required for Neuronal Swelling.

Since cytoplasmic impermeant anions make up the bulk of the intracellular anionic milieu, changes in $[Cl^-]_i$ must be met by an accompanying influx of water, possibly via transporters (Zeuthen, 2010), in attempt to achieve Gibbs-Donnan equilibrium (Glykys et al., 2014). We therefore examined whether prolonged $[Na^+]_i$ increases were associated with a secondary influx of Cl^-, and further whether Cl^- entry was ultimately required for neuronal swelling. Using two-photon FLIM of the Cl^- sensitive dye MQAE (Verkman et al., 1989; Ferrini et al., 2013) we observed that $[Cl^-]_i$ increased in neurons (indicated by a decrease in the fluorescence lifetime) when Na^+ influx was triggered by veratridine application (**Figures 3.5a** and **3.5b**). This Cl^- influx was independent of entry via $GABA_A$Rs as all experiments were performed in the presence of the ligand-gated Cl^- channel antagonist, picrotoxin (100 μM).

Whether neuronal Na^+ and subsequent Cl^- influx were sufficient to increase tissue volume were next investigated by imaging hippocampal/cortical brain slices at low magnification. Application of veratridine triggered dramatic swelling of brain slices that was reduced but still substantial even when the number of Na^+, Ca^{2+} and Cl^- entry pathways were reduced by blockade of glutamate gated AMPARs and NMDARs, voltage gated Ca^{2+} channels (VGCCs), and GABA activated Cl^- channels with a cocktail of blockers (20 μM CNQX, 100 μM d-APV, 30 μM Cd^{2+}, and 100 μM picrotoxin) (**Figures 3.5c, 3.5d**). In contrast, blocking all Cl^- influx pathways by reducing $[Cl^-]_{ext}$ with iso-osmotic replacement of NaCl for Na-gluconate in the extracellular solution dramatically reduced the magnitude of the volume increase of brain slices (**Figure 3.5d**; $p < 0.001$,

ANOVA). These results suggest that even when fast ionotropic glutamate and GABA activated receptors are blocked, increased neuronal $[Na^+]_i$ leads to cytotoxic edema of brain tissue that is dependent on Cl^- influx. We next tested whether reducing the concentration of extracellular Cl^- ($[Cl^-]_{ext}$) also prevented Na^+ induced swelling of individual neurons. Indeed, reducing $[Cl^-]_{ext}$ reduced the swelling of neurons visualized with CoroNa fluorescence (**Figures 3.5e**, **3.5f**; $p < 0.001$, ANOVA), without affecting the $[Na^+]_i$ signal (**Figure 3.5h**; $p > 0.05$, two-tailed student's *t* test). As it has been previously reported that $GABA_AR$ mediated Cl^- influx can contribute to neuronal swelling in cell culture (Hasbani et al., 1998), and to swelling following oxygen glucose deprivation in situ (Allen et al., 2004), the contribution of $GABA_AR$ Cl^- influx to neuronal swelling in our experimental conditions was examined.. Consistent with previous reports, pre-application of the $GABA_AR$ antagonist picrotoxin slightly but significantly reduced the magnitude of neuronal swelling (from 161.7% to 146.9%; **Figure 3.5f**; $p < 0.05$, ANOVA), however, the majority of the volume increase persisted in picrotoxin suggesting that the cause of swelling was dominated by Cl^- influx via an as yet unidentified mechanism. NMDA-induced swelling was also blocked by low $[Cl^-]_{ext}$ (iso-osmotic replacement of NaCl for Na-isethionate) (**Figure 3.5j**; $p < 0.05$, two-tailed student's *t* test). Together, these data indicate that neuronal swelling requires Cl^- influx through a mechanism that is triggered by an increase in $[Na^+]_i$ and that Na^+ entry alone is not sufficient to swell neurons.

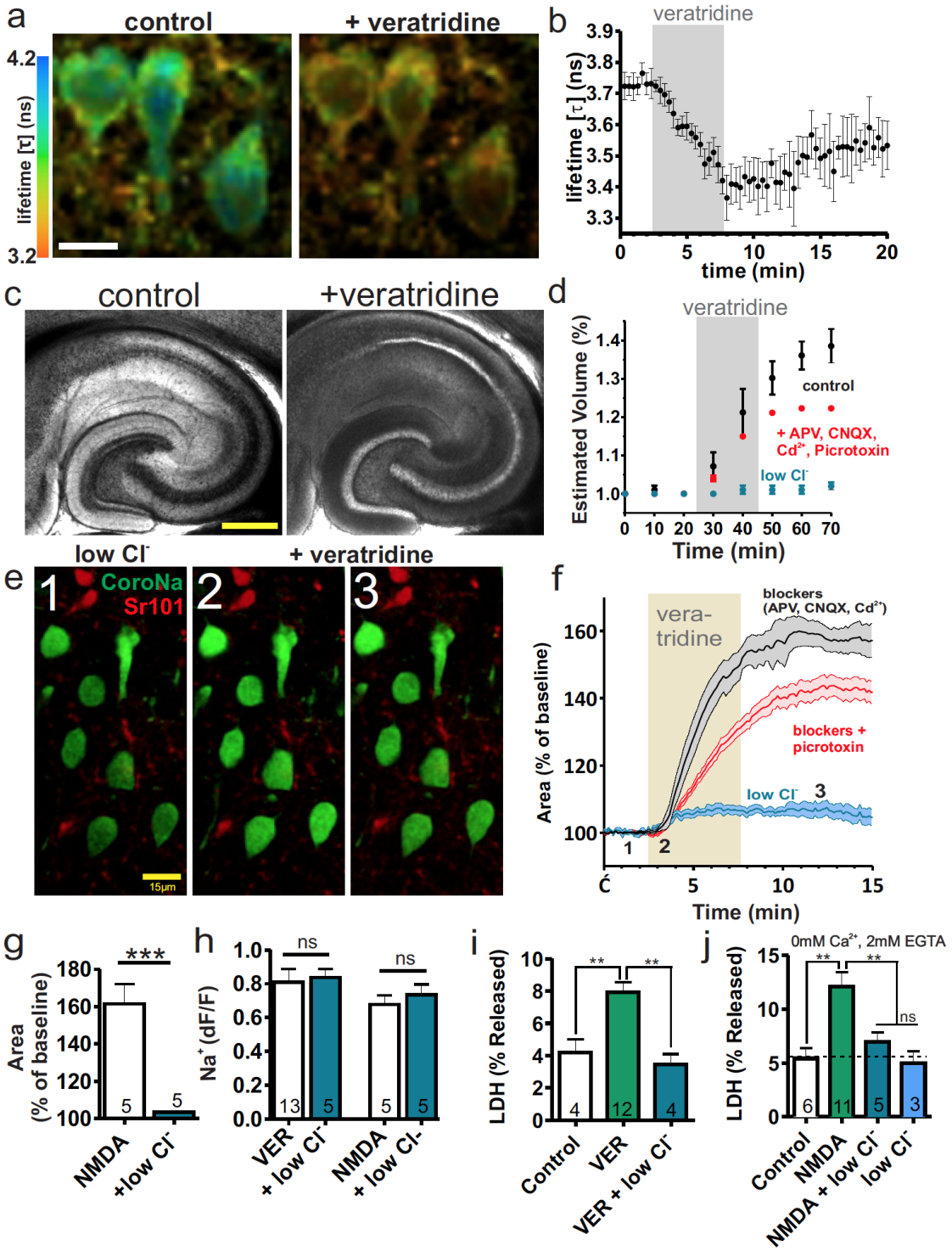
a
control
+ veratridine
4.2
lifetime [τ] (ns)
3.2
b
veratridine
lifetime [τ] (ns)
time (min)
c
control
+veratridine
d
veratridine
Estimated Volume (%)
control
+ APV, CNQX, Cd2+, Picrotoxin
low Cl-
Time (min)
e
low Cl-
+ veratridine
1
CoroNa
Sr101
2
3
15µm
f
vera-tridine
blockers (APV, CNQX, Cd2+)
blockers + picrotoxin
low Cl-
Area (% of baseline)
Time (min)
g
Area (% of baseline)
***
NMDA
+low Cl-
h
Na+ (dF/F)
ns
VER + low Cl-
NMDA + low Cl-
i
LDH (% Released)
Control
VER
VER + low Cl-
j
0mM Ca2+, 2mM EGTA
LDH (% Released)
Control
NMDA
NMDA + low Cl-
low Cl-

Figure 3.5: Na^+ influx is correlated with a secondary Cl^- influx that is required for neuronal swelling and causes cell death.

(a and b) FLIM of Cl^- sensitive dye, MQAE, shows that Cl^- influx is correlated with increases in intracellular [Na^+] (n=5). (c and d) Swelling of neurons causes an increase in brain tissue volume shown by changes in volume of a hippocampal brain slice. (d) Cocktail of fast glutamate receptor, GABA receptor and VGCC blockers slightly reduce tissue swelling ($p<0.01$) but significant Cl^- dependent swelling still occurs ($p < 0.01$) indicating that swelling is dominated by other mechanisms. (d-g) Neuronal swelling is prevented by reducing extracellular Cl^- (10.5 mM) and is only partially inhibited by blocking $GABA_A$Rs. (h) Positive control shows veratridine and NMDAR Na^+ signals were unaffected by low Cl^- solution. (i) Neuronal Na^+ influx via VGSCs causes cell death that is Cl^- dependent as measured by LDH release (iso-osmotic replacement of Cl^- with gluconate). (j) Neuronal Na^+ influx via NMDARs causes cell death that is Cl^- dependent and Ca^{2+} independent (iso-osmotic replacement of Cl^- with isethionate). Scale bars: (a), 10 μm; (c), 1.0 mm; (e), 15 μm. VER, veratridine; VGCC, voltage gated calcium channel; VGSC, voltage gated sodium channel. For experiments in panels (a,b,e and g-j) solutions contained blockers: 30 μM Cd^{2+}, 20 μM CNQX, 100 μM picrotoxin, plus either 100 μM d-APV for veratridine experiments or 1 μM TTX for NMDA experiments. n values in (f); blockers (n=5), +picrotoxin (n=13), low Cl^- (n=5). Error bars and shaded region above and below the mean represent SEM.

3.3.3 Na^+ and Cl^- Dependent Neuronal Swelling Causes Death

Aberrant calcium influx via NMDARs can lead to mitochondrial depolarization and cell death, however, Cl^- removal also reduces ischemia and glutamate evoked early neuronal death in cell culture (Rothman, 1985; Choi, 1987; Goldberg and Choi, 1993), suggesting the existence of two independent pathways ultimately leading to cell death. The impact of the $[Na^+]_i$-triggered Cl^- entry and neuronal swelling on cell viability was further investigated using LDH release as measure of cell death (e.g.(Kajta et al., 2005)). Even in the combined presence of CNQX, picrotoxin and Cd^{2+} to block fast AMPA/KA receptors, GABA-activated Cl^- channels and VGCCs respectively, application (15 min) of either veratridine (50 μM) or NMDA (100 μM, in artificial cerebrospinal fluid (ACSF) containing 0mM Ca^{2+} and 2 mM EGTA) caused a rapid and significant increase in LDH release indicating neurons were dying after 90 min (**Figure 3.5i** and **3.5j**; $p < 0.01$, ANOVA). Both the NMDA-induced and veratridine-induced neuronal death, as indicated by LDH release, were abolished by reducing $[Cl^-]_{ext}$ (**Figures 3.5i** and **3.5j**; $p < 0.01$, ANOVA). This suggests that Na^+-induced Cl^- influx and subsequent swelling results in Ca^{2+}-independent cell death.

3.3.4 Neuronal Swelling and Death Show the Pharmacological Profile of a HCO_3^- / Cl^- Exchanger

There are several candidates for the transmembrane influx of Cl^- in neurons that can be distinguished based on their sensitivity to different antagonists (Jentsch et al., 2002; Alvarez-Leefmans and Delpire, 2009; Verkman and Galietta, 2009) (**Table 3.2**). We hypothesized that by identifying and blocking the source of Cl^- entry that was triggered by Na^+ entry both the Na^+ induced neuronal swelling and corresponding cell death could be prevented. As a first step, pharmacological analyses using the imaging assay of swelling of neurons in brain slices were undertaken in order to screen for the possible involvement of different Cl^- channels and transporters. In separate experiments the following blockers were tested as described in **Table 3.2**; NPPB (200 μM) to block the volume-regulated anion channel (VRAC, VSOR), zinc (300 μM) to block CLC-2, Gd^{3+} (100 μM) to block the Maxi-anion channel, niflumic acid (NFA) (200 μM) to block the Ca^{2+} activated Cl^- conductance (CaCC, bestrophin), carbenoxelone (CBX) (100 μM) to block pannexins/connexins, bumetanide (100 μM) to block cation chloride cotransporters (NKCC1 and KCC2), and DIDS (250 μM) to block Cl^-/HCO_3^- exchangers. All antagonists were both bath applied and present in the puffing pipette used to apply either NMDA or veratridine. Of note, of the various Cl^- channel and transporter blockers examined only DIDS reduced the swelling induced by increased $[Na^+]_i$ (**Figure 3.6a**; $p < 0.05$ compared to all other antagonists, ANOVA). The small volume change in the presence of DIDS was not significantly different from those observed in low Cl^- extracellular solution (**Figure 3.6a**; $p > 0.05$, ANOVA). A substantial $[Na^+]_i$

increase was still observed in DIDS indicating that Na^+ entry was not affected (**Figure 3.6b**). This pattern of block by DIDS but no effect of the numerous other blockers suggested that a Cl^-/HCO_3^- exchanger was the most likely source of Cl^- entry. Although DIDS also blocks VRAC, which has been implicated to play a role in excitotoxic cell death in neuronal cell culture (Inoue and Okada, 2007), under our conditions we observed no protection of either cell volume or cell death in the presence of the potent VRAC blocker, NPPB. DIDS also blocked NMDA-evoked neuronal swelling in a dose-dependent manner (**Figure 3.6c**).

Table 3.2: Pharmacology of antagonists that inhibit chloride channels and chloride transporters

	Antagonist and concentration						
Channel/Transporter	**NPPB (200 μM)**	**NFA (200 μM)**	**Gd^{3+} (100 μM)**	**CBX (100 μM)**	**Zinc (300 μM)**	**Bumetanide (100 μM)**	**DIDS (250 μM)**
VRAC	40-100 μM[1,2]						100-400 μM*[2,3]
CaCC	100 μM[4]	50-100 μM[4,5]					
Maxi-Anion Channel	100 μM[6-8]		30-50 μM[6-8]				100 μM[7]
Pannexins, connexins				100 μM[9-10]			
CLC-2					100 μM[11]		
NKCC1						$K_i \sim 0.1$ uM[12]	
KCC2						$K_i \sim 25\text{-}50$ uM[12]	
SLC4-A3, -A8, -A10							0.1-0.5 mM[13-16]
SLC26A11							0.5-1 mM[17,18]

VRAC, volume regulated anion channel; CaCC, calcium activated chloride channel; NPPB, 5-nitro-2-(3-phenylpropylamino) benzoic acid; NFA, niflumic acid; CBX, carbenoxolone; DIDS, 4,4'-Diisothiocyanato-2,2'-stilbenedisulfonic acid.

***Voltage dependent block**

References: 1.(Inoue and Okada, 2007) 2.(Inoue et al., 2005) 3.(Qiu et al., 2014) 4.(Huang et al., 2012) 5. (White and Aylwin, 1990) 6.(Sabirov et al., 2001) 7. (Sabirov and Okada, 2009) 8. (Fields and Ni, 2010) 9. (Bruzzone et al., 2005) 10. (Thompson et al., 2008) 11. (Staley et al., 1996) 12. (Payne et al., 2003) 13. (Romero et al., 2013) 14.(Svichar et al., 2009) 15.(Grichtchenko et al., 2001) 16.(Parker et al., 2008b) 17.(Xu et al., 2011) 18.(Vincourt et al., 2003)

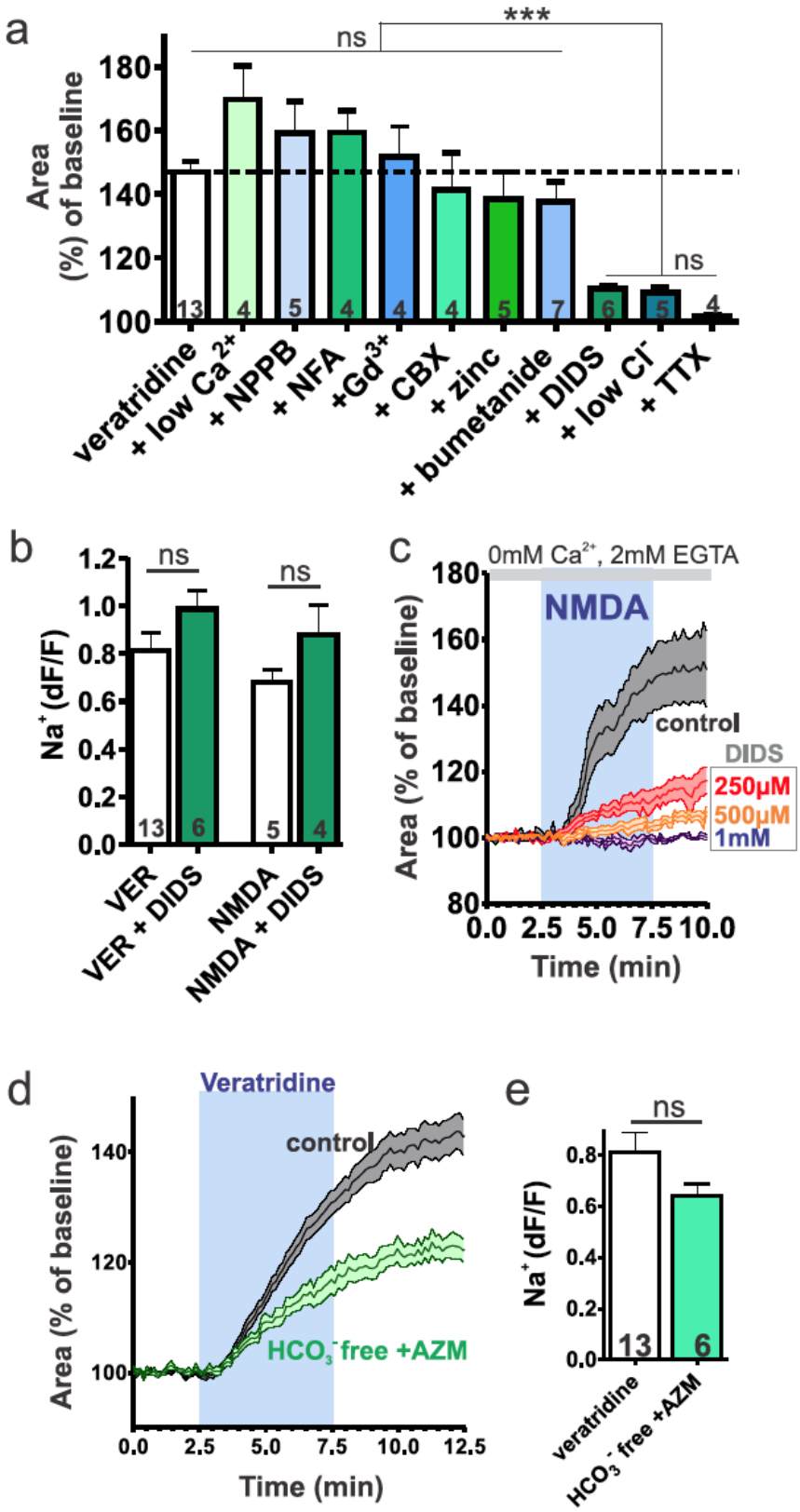
a
ns
***
ns
Area (%) of baseline
180
160
140
120
100
13
4
5
4
4
4
5
7
6
5
4
veratridine
+ low Ca2+
+ NPPB
+ NFA
+Gd3+
+ CBX
+ zinc
+ bumetanide
+ DIDS
+ low Cl-
+ TTX
b
ns
ns
Na+ (dF/F)
1.2
1.0
0.8
0.6
0.4
0.2
0.0
13
6
5
4
VER
VER + DIDS
NMDA
NMDA + DIDS
c
0mM Ca2+, 2mM EGTA
NMDA
control
DIDS
250µM
500µM
1mM
Area (% of baseline)
180
160
140
120
100
80
0.0 2.5 5.0 7.5 10.0
Time (min)
d
Veratridine
control
HCO3- free +AZM
Area (% of baseline)
140
120
100
0.0 2.5 5.0 7.5 10.0 12.5
Time (min)
e
ns
Na+ (dF/F)
0.8
0.6
0.4
0.2
0.0
13
6
veratridine
HCO3- free +AZM

Figure 3.6: Neuronal swelling shows the pharmacological profile of a HCO_3^- / Cl^- exchanger.

(a) Veratridine induced neuronal swelling was blocked by the HCO_3^- /Cl^- exchanger inhibitor, DIDS (250 μM) but not by blockers of several other Cl^- channels or transporters (see Supplementary Table 1). (b) Positive control shows veratridine and NMDA induced Na^+ signal in the presence of DIDS. (c) NMDA induced neuronal swelling was blocked by DIDS in a dose dependent manner; control (n=5), 250 μM (n=4), 500 μM(n=5), 1mM (n=5). (d) Reduction in intracellular HCO_3^-, (HCO_3^- free extracellular solution + 100 μM AZM) reduced the magnitude of neuronal swelling, $p < 0.001$, two-tailed student's *t* test. (e) Positive control shows veratridine induced Na^+ signals in (HCO_3^- free + AZM). All solutions contained blockers: 30 mM Cd^{2+}, 20 μM CNQX, 100 μM picrotoxin, plus either 100 μM d-APV for veratridine experiments or 1 μM TTX for NMDA experiments. VER, veratridine; AZM, acetazolamide. Error bars and shaded region above and below the mean represent SEM.

As it was observed that extracellular Cl^- was required for both neuronal swelling and the subsequent cell death and that DIDS prevented neuronal swelling, we predicted that DIDS would block the Cl^- dependent cell death pathway without affecting the Ca^{2+}-dependent death. DIDS was initially tested for its effectiveness in preventing the swelling induced, Cl^- dependent cell death as measured by LDH efflux in brain slices exposed to veratridine. Indeed, DIDS prevented cell death from veratridine induced Na^+ influx and swelling (**Figure 3.7a**; $p < 0.005$, ANOVA), whereas the VRAC blocker NPPB had no effect. DIDS was further examined on the NMDA Cl^--dependent, Ca^{2+}-independent cell death pathway and on the NMDA Ca^{2+}-dependent cell death pathway. As predicted, DIDS blocked the cell death by NMDA in Ca^{2+} free extracellular solution (**Figure 3.7b**; $p < 0.005$, ANOVA). If however, NMDA was applied in the presence of extracellular Ca^{2+} but reduced extracellular Na^+, cell death still occurred (**Figure 3.7c**; $p < 0.005$, ANOVA) but was not blocked by DIDS (**Figure 3.7c**; $p > 0.05$, ANOVA). These results suggest that two independent cell death pathways co-exist that can be distinguished based on their ionic basis; one that involves swelling, requires Na^+ and Cl^- influx, is Ca^{2+}-independent and is blocked by DIDS, and one that is triggered by Ca^{2+} influx, but that is not blocked by DIDS.

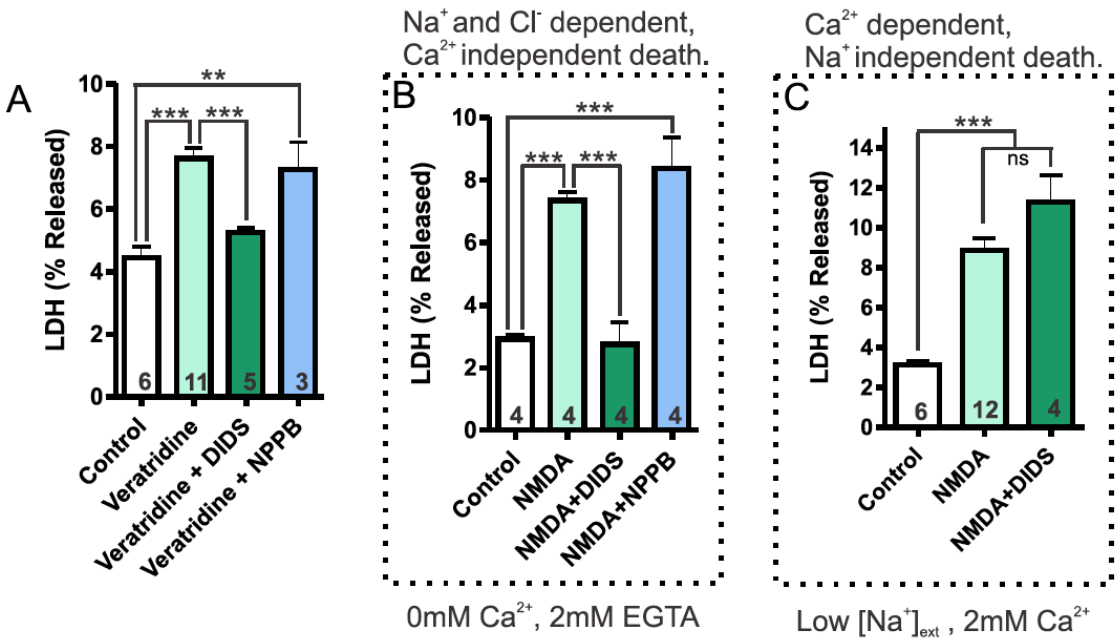

Figure 3.7: DIDS blocks Na^+ and Cl^- dependent, Ca^{2+} independent cell death.

(a) LDH release measurements show Na^+ and Cl^- dependent cell death triggered by veratridine was blocked by the HCO_3^-/Cl^- exchanger antagonist, DIDS but not by the VRAC blocker NPPB. (b) NMDAR Na^+ influx triggers cell death in the absence of extracellular Ca^{2+} that is blocked by DIDS but not NPPB. (c) NMDAR Ca^{2+} influx also triggers cell death that is not blocked by DIDS, indicating separate pathways.

3.3.5 Identification of SLC26A11 as the Predominant Cl^- Influx Pathway Underlying Na^+ Dependent Cytotoxic Neuronal Swelling

Our data indicates that Na^+ entry into neurons is linked to a DIDS-sensitive Cl^- influx pathway that is required for neuronal swelling and mediates cell death. Several DIDS-sensitive candidates are expressed in central nervous system (CNS) neurons of which several act as Cl^-/HCO_3^- exchangers and include the SLC4 family of exchangers that are Cl^-, HCO_3^- dependent (Alvarez-Leefmans and Delpire, 2009; Boron et al., 2009; Romero et al., 2013). Removing extracellular HCO_3^- and adding the carbonic anhydrase inhibitor, acetazolamide, to reduce intracellular HCO_3^- generation resulted in reduced swelling (**Figure 3.6d**; $p < 0.001$, two-tailed student's *t* test) supporting the possibility that one or several of the Cl^-/HCO_3^- exchangers contribute to Cl^- loading and swelling. The DIDS-sensitive Cl^-, HCO_3^- exchangers that are known to be expressed in the cortex and hippocampus are SLC4A3, SLC4A8 and SLC4A10 (Boron et al., 2009; Romero et al., 2013). In addition, SLC26A11 was recently shown to be highly expressed in CNS cortical neurons (Rahmati et al., 2013). SLC26A11 is a member of the sulfate transporter family that in different expression systems has been reported to act variously as a DIDS-sensitive sulfate transporter, a DIDS-sensitive exchanger for Cl^-, SO_4^{2-}, HCO_3^- or H^+-Cl^- or as a Cl^- channel (Vincourt et al., 2003; Xu et al., 2011; Lee et al., 2012a; Rahmati et al., 2013).

Utilizing qRT-PCR, the expression of SLC4 and SLC26 family members was confirmed in both cortical and hippocampal brain tissue (**Figure 3.8**). Based on

their combined pharmacological profile and expression profiles, SLC4-A3,-A8,-A10 and SLC26A11 appeared to be the most promising candidates for the Cl^- entry pathway that causes neuronal swelling. We recently reported the development of an efficient lipid nanoparticle (LNP)-mediated delivery system to introduce siRNAs against specific molecular targets into CNS neurons both *in vivo* and *in vitro* (Rungta et al., 2013) (described in chapter 2). Individual siRNAs targeted against the different SLC candidate genes were encapsulated in LNPs and initially tested for their ability to attenuate expression in both primary neuron cultures and HEK cell expression system (**Figure 3.8**). These *in vitro*-validated siRNA LNPs against the 4 different SLC candidates or a control (luciferase) siRNA were subsequently injected intracranially into the rat somatosensory cortex. After allowing for 5-6 days of recovery, neurons that had taken up DiI labeled LNPs were examined for Na^+ induced Cl^--dependent swelling in cortical slices. Knockdown of SLC4A-3, -8 or -10 either separately (**Figure 3.9**) or together had no effect on the magnitude of veratridine induced neuronal swelling compared to the control luciferase siRNA injected animals (**Figures 3.10a** and **3.10c**; $p > 0.05$, ANOVA). In striking contrast, targeted knockdown of SLC26A11 with two different siRNAs significantly reduced the magnitude of the swelling in neurons as measured by increases in cell size (**Figures 3.10b, d**; $p < 0.05$, ANOVA was performed comparing results from all siRNA groups (luciferase, A3, A8, A10, A3+A8+A10, A11 No.1 and A11 No.2)). These results indicate that the Cl^- influx that is required for neuronal swelling is mediated by SLC26A11.

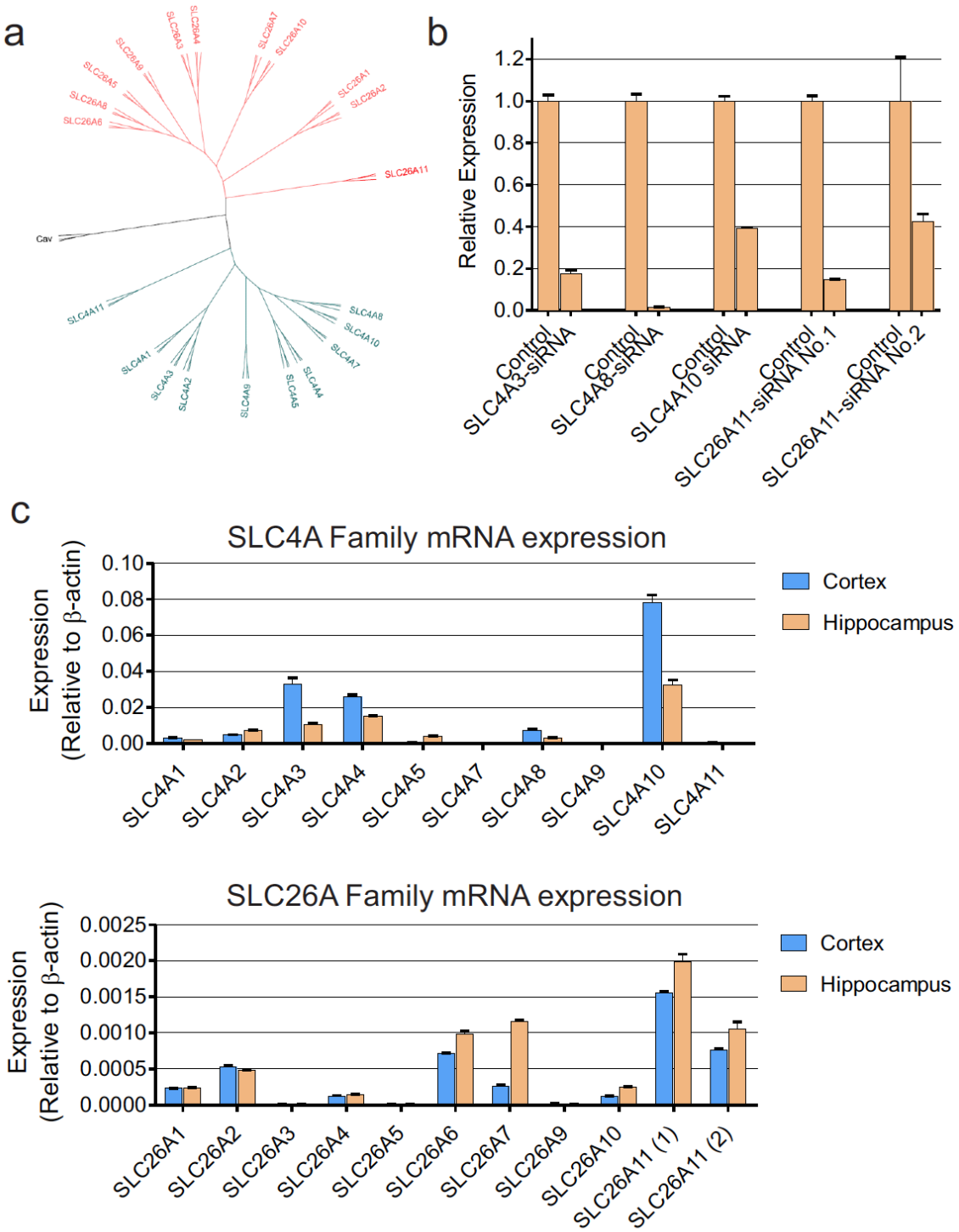
a
SLC26A3
SLC26A4
SLC26A7
SLC26A10
SLC26A9
SLC26A5
SLC26A1
SLC26A2
SLC26A8
SLC26A6
SLC26A11
Cav
SLC4A11
SLC4A8
SLC4A10
SLC4A1
SLC4A7
SLC4A3
SLC4A2
SLC4A9
SLC4A5
SLC4A4
b
Relative Expression
1.2
1.0
0.8
0.6
0.4
0.2
0.0
Control
SLC4A3-siRNA
Control
SLC4A8-siRNA
Control
SLC4A10 siRNA
Control
SLC26A11-siRNA No.1
Control
SLC26A11-siRNA No.2
c
SLC4A Family mRNA expression
Expression
(Relative to β-actin)
0.10
0.08
0.06
0.04
0.02
0.00
SLC4A1
SLC4A2
SLC4A3
SLC4A4
SLC4A5
SLC4A7
SLC4A8
SLC4A9
SLC4A10
SLC4A11
Cortex
Hippocampus
SLC26A Family mRNA expression
Expression
(Relative to β-actin)
0.0025
0.0020
0.0015
0.0010
0.0005
0.0000
SLC26A1
SLC26A2
SLC26A3
SLC26A4
SLC26A5
SLC26A6
SLC26A7
SLC26A9
SLC26A10
SLC26A11 (1)
SLC26A11 (2)
Cortex
Hippocampus

Figure 3.8: SLC26A and SLC4A gene families, siRNA-mediated knockdown and expression profiles.

(a) Protein sequence similarity tree of the SLC26A and SLC4A family members from mouse, rat and humans. (Ca_V = voltage-gated calcium channels $Ca_V1.2$, $Ca_V2.1$ and $Ca_V3.1$ from human). (b) Testing of LNP-packaged modified Dicer siRNA knockdown duplexes (for SLC4A3, SLC4A8, SLC4A10 and SLC26A11) *in vitro*. The data represent quantification using qPCR 72 hrs post-treatment of cultured rat cortical neurons except for unmodified SLC4A10 Dicer siRNA which was tested in HEK293 cells expressing the cloned rSLC4A10 target. Data are normalized to internal rGAPDH mRNA levels. (c) Expression profiles of the SLC4A and SLC26A family members in rat cortex and hippocampus as determined using qPCR. Data are normalized to internal β-actin mRNA levels.

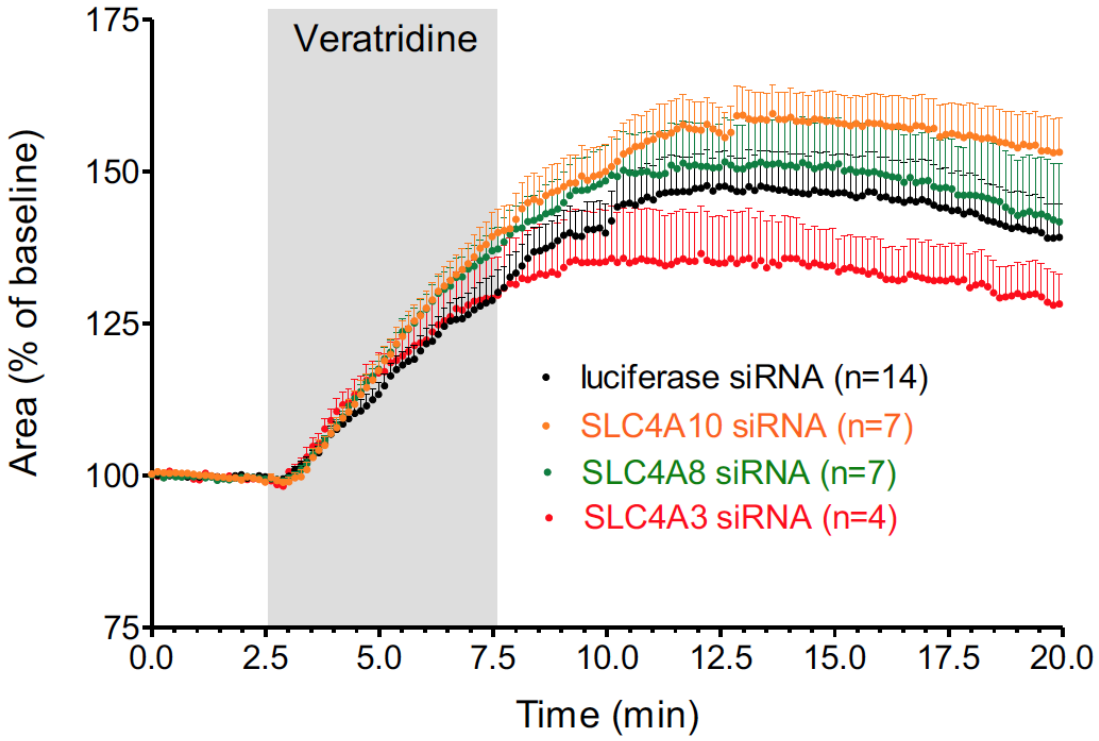

Figure 3.9: siRNA-mediated knockdown of individual SLC4A family members does not alter the magnitude of neuronal swelling.

Transfection of neurons *in vivo* by intracranial injection of LNPs encapsulated with siRNA against SLC4A3, SLC4A8 or SLC4A10 does not significantly decrease neuronal swelling in brain slices following veratridine treatment compared to control (luciferase siRNA transfected neurons). Error bars represent SEM.

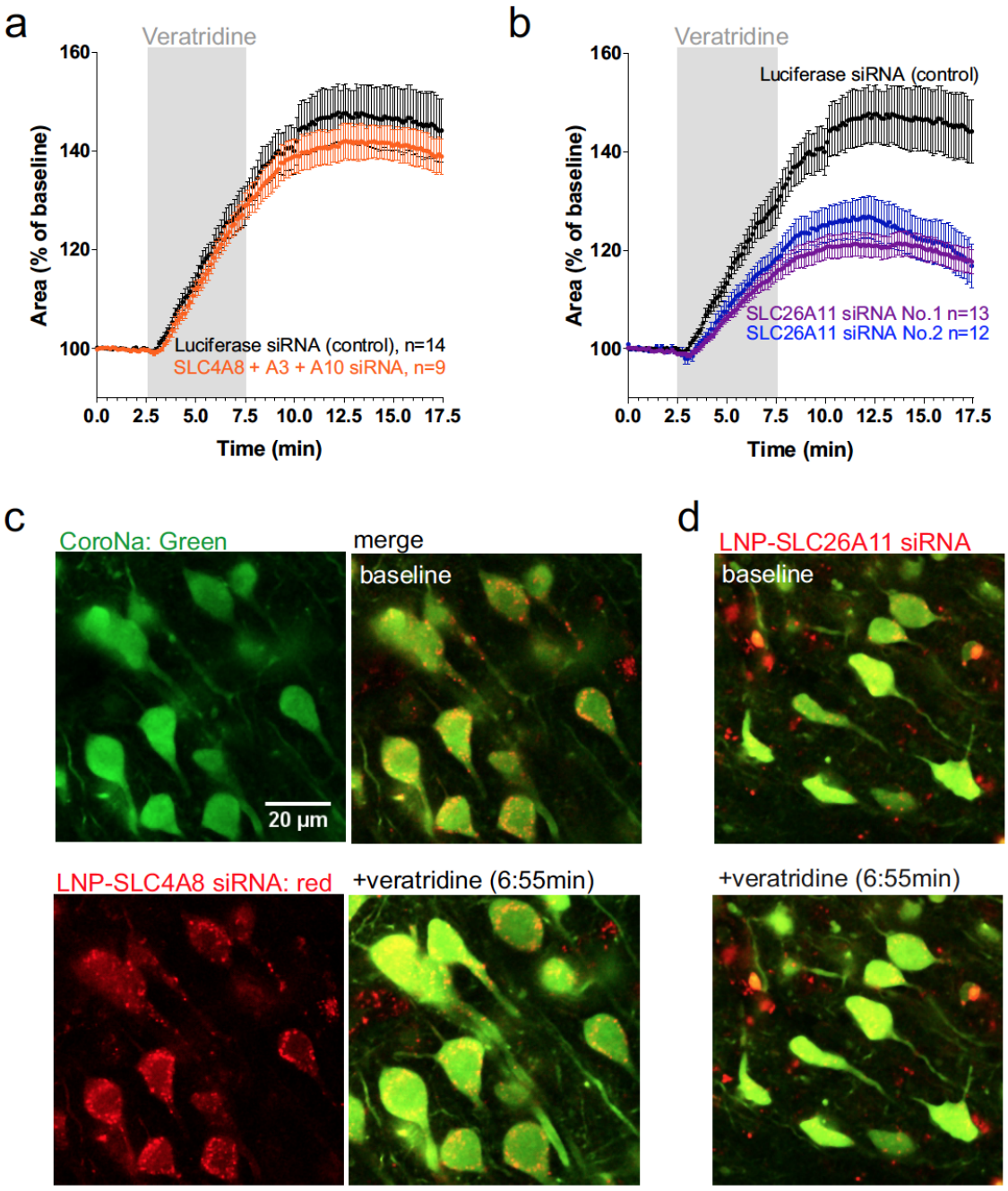
a
Veratridine
Area (% of baseline)
160
140
120
100
0.0 2.5 5.0 7.5 10.0 12.5 15.0 17.5
Time (min)
Luciferase siRNA (control), n=14
SLC4A8 + A3 + A10 siRNA, n=9
b
Veratridine
Luciferase siRNA (control)
SLC26A11 siRNA No.1 n=13
SLC26A11 siRNA No.2 n=12
c
CoroNa: Green
merge
baseline
20 µm
LNP-SLC4A8 siRNA: red
+veratridine (6:55min)
d
LNP-SLC26A11 siRNA
baseline
+veratridine (6:55min)

Figure 3.10: Cl^- influx via SLC26A11 causes cytotoxic neuronal edema following increased $[Na^+]_i$.

(a) *In vivo* knockdown of SLC4A3, A8, A10 with LNP-siRNAs results in no significant difference in the magnitude of neuronal swelling compared to a control (luciferase siRNA) in cortical brain slices imaged 5 days following the injection ($p > 0.05$, ANOVA). (b) Two different siRNA constructs against SLC26A11 result in a significant reduction in the magnitude of veratridine induced neuronal swelling compared to luciferase siRNA ($p < 0.05$, ANOVA). (c and d) Example images of cortical neurons transfected with siRNA using lipid nanoparticle delivery shows SLC26A11 knockdown results in protection from veratridine triggered swelling compared to neurons transfected with SLC4A8 siRNA. DiI staining (red) shows cell uptake of LNP-siRNA. Scale bar in (c) matches scale in (d). Luciferase controls are combined and plotted in both panel (a), (b) and in Figure 3.9. For statistics on magnitude of swelling, ANOVA was performed comparing results from all siRNA groups (luciferase, SLC4A3, -A8, -A10, -A3+A8+A10, SLC26A11 No.1 and No.2). Only SLC26A11 No.1 and No. 2 were significantly different from luciferase (control) siRNA, $p < 0.05$. Error bars represent SEM.

3.4 Discussion

Our results demonstrate that prolonged sodium entry via either of two independent pathways (either VGSCs or NMDARs) converge to activate a Cl^- influx pathway via SLC26A11 that is ultimately required for neuronal swelling and subsequent cell death. When extracellular Cl^- is removed both neuronal swelling and cell death are prevented. Other potential Cl^- channels and exchangers did not appear to contribute significantly under these conditions as their pharmacological inhibitors did not reduce neuronal swelling. Both pharmacological blockade with DIDS and removal of HCO_3^- resulted in reduced neuronal swelling, indicating a Cl^-, HCO_3^- exchanger(s) was likely involved. Utilizing LNP-siRNA-mediated depression of expression of several candidates showed that only reducing SLC26A11, recently described to be highly expressed in CNS neurons, was successful in reducing swelling.

In mature pyramidal neurons of the cortex and hippocampus, resting membrane potential (E_m) is set positive compared to the equilibrium potential for Cl^- (E_{Cl^-}) suggesting that Cl^- is not passively distributed across the plasma membrane (Alvarez-Leefmans and Delpire, 2009). Changing membrane potential also has little effect on intracellular chloride concentrations indicating that there is little Cl^- membrane permeability at rest (Thompson et al., 1988). As such, in order for $[Cl^-]_i$ to rapidly increase in neurons either a chloride transporter has to be activated or a transmembrane Cl^- channel must be opened. Membrane depolarization could also further contribute to Cl^- influx by increasing the driving force for Cl^- entry.

Using an siRNA knockdown approach, we were able to identify the molecular nature of the predominant Cl^- influx pathway that is activated following increases in $[Na^+]_i$ and causes neuronal cytotoxic edema. Our study is the first report of SLC26A11 as a functional Cl^- influx pathway in neurons. A recent study showed that SLC26A11 protein is expressed in neurons throughout the brain and we would predict that similar mechanisms of swelling and neuronal death likely occur. SLC26A11, originally identified as a sulfate transporter has been shown to operate in several modes, including an exchanger for Cl^-, SO_4^{2-}, HCO_3^- or H^+-Cl^- or as a Cl^- channel, depending on the tissue type and the expression system (Vincourt et al., 2003; Xu et al., 2011; Rahmati et al., 2013). The precise mechanism linking Na^+ influx and SLC26A11 mediated Cl^- influx remains to be determined. If SLC26A11 functions as a constitutively active Cl^- channel as proposed (Rahmati et al., 2013), it would be constantly loading the cell with Cl^- at E_m due to the increased driving force for Cl^- entry. Therefore, there must either be a change in the activation state of SLC26A11 or alternatively SLC26A11 may be trafficked to the plasma membrane following increases in Na^+. Electrogenic transport of Cl^- remains a viable possibility, however depolarization of cortical neurons with high K^+ solution (40mM), is not sufficient to cause neuronal swelling unless spreading depression triggers glutamate release which causes Na^+ influx (Zhou et al., 2010; Zhou et al., 2013).

Several questions arise as to the specific conditions and times that SLC26A11 may modulate local and global Cl^- concentration. Aberrant, chloride homeostasis is central to several neurological diseases, and it would therefore be interesting to examine whether SLC26A11 expression or localization changes under such

conditions. Epileptic seizures are commonly observed in patients following ischemia and TBI with these patients responding poorly to anticonvulsants that act on $GABA_A$ receptors (Young et al., 1990), presumably due to increased $[Cl^-]_i$ leading to a depolarizing shift in E_{GABA} (Cohen et al., 2002; Miles et al., 2012). If blocking SLC26A11 reduces the increases in Cl^- that occur during pathologies that are associated with cytotoxic edema, it may be possible to maintain the direction of hyperpolarizing $GABA_AR$ currents, and reduce the generation of post traumatic seizures.

While we find that SLC26A11 represents the predominant Cl^- influx pathway causing neuronal swelling following increased $[Na^+]_i$, pyramidal neurons are endowed with multiple Cl^- influx pathways that may further contribute to Cl^- influx and cause swelling under other conditions. Following excitotoxic insults such as ischemia, the extracellular GABA concentration increases due to a combination of vesicular release and reversal of GABA transporters (Allen et al., 2004), possibly causing Cl^- influx. Our data suggest that although $GABA_ARs$ do in fact contribute to a small portion of neuronal swelling observed in our experiments (Figure 3.5f), the majority of the Cl^- influx is mediated by another mechanism. These results are in agreement with other studies showing a contribution of $GABA_ARs$ to neuronal swelling in cell culture (Hasbani et al., 1998). In brain slices it has also been shown that blocking $GABA_ARs$ leads to a small reduction in the initial rapid increase (<1 min) of the intrinsic optical signal (a marker of cell swelling) following OGD. However, blocking $GABA_ARs$ has no effect on final intrinsic optical signal increase (>2 min) (Allen et al., 2004). Additionally, in this study it was observed that calcium

influx caused $GABA_A$Rs to become completely inactivated within 2 minutes of the anoxic depolarization. These results suggest that although $GABA_A$Rs can contribute to neuronal swelling via a transient chloride influx, the majority of the Cl^- influx observed during ischemia and other excitotoxic insults occurs via a distinct mechanism. In another study, Cl^- imaging in pyramidal neurons with the genetically encoded Cl^- indicator Clomeleon showed no effect of blocking $GABA_A$Rs on the magnitude of the chloride increase during ischemia (Pond et al., 2006), again suggesting that blocking $GABA_A$Rs does not affect the ultimate extent of $[Cl^-]_i$ increase that occurs during ischemia. The authors of this study were unable to identify the mechanism underlying the pathway for Cl- influx that occurred during OGD, however they were able to block a secondary increase in Cl^- that occurred (>1 hour) after re-oxygenation by blocking NKCC1 with bumetanide, although the significance of this late Cl^- influx remains uncertain.

In addition to the Cl^- loading that occurs during excitotoxic insults, Cl^- efflux may also be compromised. As KCC2 directional transport is dependent on the potassium gradient, small changes in extracellular K^+ can have substantial effects on KCC2 mediated Cl^- clearance. Additionally, a recent study demonstrated that glutamate activation of NMDARs leads to phosphorylation and thereby decreased expression of KCC2, leading to decreased recovery of excitotoxic Cl^- loads (Lee et al., 2011). In this study the authors were unable to identify the source of Cl^- influx, but showed that it was independent of NKCC1. If KCC2 mediated Cl^- efflux is indeed compromised following cytotoxic edema, in addition to blocking the influx of Cl^-

perhaps enhancing extrusion of Cl^- (Gagnon et al., 2013) would be additionally beneficial.

The identification to SLC26A11 as a significant Cl^- entry pathway during pathological swelling triggered after Na^+ entry suggests that new strategies could be developed to reduce brain edema. There are numerous different pathways for Na^+ entry that are activated during conditions such as hypoxia, stroke and traumatic brain injury. Our observations that cell death is significantly reduced when overall Cl^- entry is prevented suggests that therapeutic strategies to inhibit SLC26A11 dependent Cl^- entry may have widespread benefit towards treating these different conditions.

Chapter 4: Conclusions

4.1 Summary of Research Findings

4.1.1 Lipid Nanoparticle-siRNA Delivery Mediates Targeted Knockdown of Neuronal Gene Expression *in vitro* and *in vivo*.

In chapter 2, we presented a novel method for transfection of neurons both *in vitro* and *in vivo.* In primary neuronal cultures, we observed transfection rates approaching 100% with no signs of toxicity. By contrast, current non-viral methods exhibit transfection efficiencies of 10% or less and are often accompanied by cell damage (Karra and Dahm, 2010). Therefore, our results suggest that LNPs currently represent the best available method for transfecting neurons in cell culture. We conclude that the highly efficient uptake of LNPs by neurons, is mediated via an endogenous ApoE dependent uptake pathway similar to LNP uptake mechanisms utilized by hepatocytes *in vivo* (Akinc et al., 2010). As astrocytes produce and secrete the majority of the ApoE found in the brain (Pitas et al., 1987), we were able to test the ApoE dependence *in vitro*, by removing neurons from the astrocytes that are normally separated on a feeder layer. Addition of exogenous ApoE proved to facilitate the neuronal uptake of LNPs in a dose dependent manner, with saturation at ApoE concentrations previously reported *in vivo* (Wahrle et al., 2007).

LNP-siRNA systems used in this study had a mean diameter of around 50 nm, allowing them to freely diffuse through the extracellular space of the brain. We

demonstrated that a single intra-cortical LNP-siRNA injection of 2.5 μg siRNA per rat resulted in robust (up to 91%) gene silencing that was sustained for at least 15 days. We proved applicability of LNP-siRNA systems for use in functional genomic studies, by targeted functional loss of a synaptic plasma-membrane protein, NR1. Viral delivery is currently the most effective available method for neuronal transfection *in vivo*, however, disadvantages include time associated with packaging shRNA into high-titer viruses, immunological and safety concerns. LNP-siRNA systems can circumvent these issues, and provide a method to rapidly test various siRNA constructs against the expression of different target proteins. Additionally, LNP-siRNA systems can be used to simultaneously silence multiple genes at once, as is often needed to rule out compensatory and/or complementary pathways (Love et al., 2010). In chapter 3 we demonstrate the usefulness of the LNP-siRNA approach for rapidly evaluating the function of different target proteins. We demonstrated the ability of knocking down different target genes using LNP-siRNA systems *in vivo* either separately or together to determine the molecular identity of a novel neuronal chloride entry pathway that caused cytotoxic neuronal edema and cell death.

4.1.2 Fluorescence Lifetime Imaging of CoroNa Reports Intracellular Na^+ Concentration, Independent of CoroNa Dye Concentration.

Whereas conventional intensity based fluorescence measurements are dependent on the total number of photons emitted, and are therefore reliant on dye concentration, fluorescence lifetime imaging (FLIM) measures the time that the

fluorophore spends in the excited state, and FLIM measurements are therefore independent of dye concentration. This is of particular utility when dye concentrations change such as during cytotoxic edema that occurs during ischemia, spreading depression, traumatic brain injury and epilepsy. Dye dilution from cellular swelling will alter the intensity of the fluorescence signal solely as a result of the decrease in the number of dye molecules within an equivalent volume. Additionally, FLIM provides the capability to calibrate lifetimes with known concentrations of substrate, and report absolute concentrations. Although calibration based measurements can also be performed with ratiometric Na^+ indicators such as sodium-binding benzofuran isophthalate (SBFI), the broad two-photon excitation spectrums of these fluorophores make this approach difficult *in situ*. In chapter 3 we report and characterize a novel method for quantifying intracellular Na^+ using FLIM with the Na^+ indicator CoroNa-Green. Surprisingly, we found that the dye CoroNa-Green selectively loads neurons and not glial cells when bulk loaded in brain slices, making it an excellent indicator for neuronal Na^+. Compared to other sodium indicators (SBFI and Sodium Green), CoroNa-Green exhibits larger fluorescence changes to physiological changes in Na^+ and the AM-form of the dye has been reported by the manufacturer to load cells more efficiently than SBFI or Sodium Green. CoroNa-Green staining of neurons after loading with the AM-form was observed to gradually decrease due to efflux out of neurons. This led to a decrease in intracellular dye concentration that made it difficult to monitor changes in Na^+ over long time periods (e.g. >30 min) (Meier et al., 2006). FLIM is

able to circumvent the error associated with these gradual changes in dye concentration as we observed stable lifetime measurements of CoroNa for > 1 hour.

The FLIM signal from CoroNa excitation was best fit using a biexponential function, with the short lifetime (τ_{fast}) representative of the intracellular Na^+ concentration, whereas the long lifetime (τ_{slow}) did not appear to change with changing Na^+ concentration. The molecular changes that cause τ_{fast} to change with increasing sodium concentration are unknown. In the case of other dyes that increase in fluorescence upon binding substrate such as the Ca^{2+} indicator Oregon-Green-BAPTA-1 (OGB-1), the fluorescence lifetime is predicted by the relative amplitudes of a short lifetime that is given from unbound dye molecules and a longer lifetime from the dye bound to substrate (Wilms et al., 2006; Kuchibhotla et al., 2009), therefore leading to an increase in the average lifetime as the concentration of substrate increases. It is possible that τ_{fast} similarly represents a mixture of bound and unbound CoroNa molecules, with unbound CoroNa exhibiting a very short lifetime close to the instrument response function (IRF) of our imaging system (121ps). *In situ* τ_{fast} showed a linear increase over the concentrations of Na^+ tested (9-109 mM), consistent with observations by (Meier et al., 2006) showing a linear increase in fluorescence intensity with increasing Na^+ concentrations in the physiological range. The inwardly directed Na^+ gradient is a critical factor for the homeostasis of numerous ions and transmitters, and changes in intracellular Na^+ contribute to the cellular damage during various brain pathologies. Currently, imaging of neuronal activity is primarily performed with Ca^{2+} dyes, whereas Na^+ is the major charge carrier during action potentials and excitatory postsynaptic

currents. We conclude that FLIM of CoroNa-Green can be used to quantify changes in intracellular Na^+, and will facilitate the study physiological and pathological Na^+ homeostasis in neurons and possibly other cell types.

4.1.3 Neuronal Swelling is Dependent on Na^+ and Cl^- Influx but Independent of Ca^{2+}

We demonstrated in chapter 3 that prolonged sodium entry via either of two independent pathways (VGSCs or NMDARs) causes neuronal swelling and subsequent cell death. The neuronal swelling ultimately required the influx of Cl^- but was completely independent of Ca^{2+} entry. These results build on previous studies done in the 1980s that identified Na^+ and Cl^- entry as a key requirement for excitotoxic cell death of neurons in cell culture (Rothman, 1985; Choi, 1987). In fact, it was convincingly demonstrated that excitotoxic insults lead to two separate and distinguishable pathways both causing cell death (Choi, 1987). One pathway was characterized by neuronal swelling, occurred early, and was dependent on extracellular Na^+ and Cl^-, but was independent of extracellular Ca^{2+}. The other pathway was marked by gradual neuronal disintegration, occurred late, was dependent on extracellular Ca^{2+}, and could be mimicked by a Ca^{2+} ionophore. The fast Na^+ and Cl^- dependent cell death resembled the morphological phenotype of necrosis, whereas the slower Ca^{2+} dependent cell death resembled apoptosis. Our results show that in brain slices, Na^+ entry into neurons results in swelling and rapid cell death that occurs within 1 hour and that can be completely prevented by removal of extracellular chloride. These results suggest that neuronal swelling and

the subsequent necrotic cell death can indeed be prevented, and that identification and blocking the chloride influx pathway could conceivably be used as a therapeutic treatment against cytotoxic edema and necrotic cell death.

4.1.4 Identification of SLC26A11 as the Predominant Neuronal Cl^- Influx Pathway that Causes Cytotoxic Edema

In order to identify the Cl^- entry pathway that causes neuronal swelling and subsequent cell death we used a two-step approach. First, we performed a pharmacological survey to identify a short list of candidate proteins. Second, we used LNP-siRNA delivery *in vivo* (described in chapter 2) to knockdown different Cl^- influx candidate proteins and tested for their involvement using our swelling assay in brain slices. Our pharmacological screen revealed that the neuronal swelling was completely blocked by a non-specific anion transporter blocker, DIDS, but was insensitive to all other Cl^- channel and transporter blockers tested. This pharmacological profile suggests a Cl^-/HCO_3^- exchanger as the protein responsible for the Cl^- influx that causes neuronal swelling and cell death (Jentsch et al., 2002; Alvarez-Leefmans and Delpire, 2009; Romero et al., 2013) (Table 3.2). Consistent with the pharmacology, additional evidence for the involvement of a Cl^-/HCO_3^- exchanger was provided by the result that the neuronal swelling was significantly reduced when intracellular HCO_3^- was reduced by omitting HCO_3^- from the extracellular solution and blocking carbonic anhydrase (the enzyme that facilitates the production of HCO_3^- from H_20 and CO_2). There are two predominant mammalian gene families that encode HCO_3^-/Cl^- exchangers, the SLC4 and the SLC26 family

(Alper and Sharma, 2013; Romero et al., 2013). A survey of the literature indicates that the electroneutral exchangers SLC4A3, A8 and A10 are expressed in neurons of the hippocampus and cortex, are DIDS sensitive and important contributors to neuronal pH regulation (Jacobs et al., 2008; Svichar et al., 2009; Sinning et al., 2011; Romero et al., 2013). Whereas, SLC4A3 is a Cl^- loader and a HCO_3^- extruder (Svichar et al., 2009), SLC4A8 and A10 function as Na^+ driven exchangers that extrude Cl^- from the cell in exchange for HCO_3^- (Grichtchenko et al., 2001; Damkier et al., 2010). However, given the large increases in Na^+ that trigger neuronal swelling we reasoned that SLC4A8 and SLC4A10 could conceivably reverse and thereby function as Cl^- loaders (Grichtchenko et al., 2001). SLC26A11 was recently shown to be highly expressed in neurons throughout the brain, including pyramidal neurons of the cortex and hippocampus (Rahmati et al., 2013). SLC26A11 has been shown to function as a DIDS sensitive transporter capable of functioning in several different modes; a sulfate transporter, an exchanger for Cl^-, SO_4^{2-}, HCO_3^- or H^+-Cl^- or as a Cl^- channel, depending on the tissue type or the expression system (Vincourt et al., 2003; Xu et al., 2011; Lee et al., 2012a; Rahmati et al., 2013). We therefore confirmed expression, of SLC4A3, A8, A10 and SLC26A11 in rat cortical and hippocampal brain tissue, and then tested for the contribution of these different exchangers using our swelling assay. Unexpectedly, we demonstrated in chapter 3 that the protein encoded by SLC26A11 was responsible for the majority of the Cl^- influx that caused neuronal swelling following increased intracellular Na^+. In contrast, knockdown of SLC4 family Cl^- exchangers either separately or in together had no significant effect on the magnitude of neuronal swelling. The precise

mechanism linking Na^+ influx and SLC26A11 mediated Cl^- influx remains to be determined. If SLC26A11 functions as a constitutively active Cl^- channel as proposed (Rahmati et al., 2013), it would be constantly loading the cell with Cl^- at E_m due to the driving force for Cl^- entry. Therefore, there must either be a change in the activation state of SLC26A11 or alternatively SLC26A11 may be trafficked to the plasma membrane following increases in Na^+. Electrogenic transport of Cl^- remains a viable possibility, however depolarization of cortical neurons with high K^+ solution (40mM), is not sufficient to cause neuronal swelling unless sufficient glutamate release occurs to trigger spreading depression (Zhou et al., 2010; Zhou et al., 2013).

4.2 Limitations and Future Directions.

4.2.1 Enhancement of Lipid Nanoparticle Delivery Systems for Neuronal Transfection

In chapter 2, we demonstrated for the first time successful neuronal transfections using LNP-siRNA systems. We used a DMAP-BLP lipid composition that had been previously optimized for knockdown of target genes in hepatocytes *in vivo* (Belliveau et al., 2012; Jayaraman et al., 2012). Additionally, we used a PEG-DMG type of PEG-lipid with short acyl chains that allow it to dissociate rapidly from LNPs upon dilution (Holland et al., 1996), allowing association of proteins such as ApoE. In chapter 2 we showed that we were able to overcome the distance limitations ~1mm radius of transfection following direct intracortical injections by injecting LNP-siRNA into the lateral cerebral ventricles, however, knockdown was

most effective in brain regions bordering the ventricles, such as the dorsal hippocampus and striatum. It would be expected that a larger radii of distribution could be achieved for LNPs containing a PEG-lipid with longer acyl chains, which dissociate more slowly than the PEG-lipids with shorter acyl chains used here. Enhanced tissue penetration would also be expected for smaller LNPs that can be achieved at higher PEG-lipid levels (Belliveau et al., 2012).

The LNP platform is highly flexible, potentially allowing delivery of other materials to neurons such as drugs, fluorescent dyes and plasmids. However, our initial attempts at expression of exogenous proteins using LNP mediated plasmid delivery to neurons and astrocytes were largely unsuccessful. The lack of success with plasmid delivery may be due to the location of the delivered cargo; LNP systems efficiently deliver their cargo to the cytoplasm, whereas plasmids require translocation to the nucleus. LNP mediated mRNA delivery to neurons would therefore perhaps be a suitable method for expression of exogenous proteins, as has been performed in other cell types (Su et al., 2011). We demonstrated that neurons efficiently take up LNPs, however, uptake by other cell types was not investigated in our study. As other cell types in the brain, such as astrocytes also express lipid receptors, we would expect that glial cells would not be discriminated against in their ability for LNP-siRNA uptake. Evidence for glial uptake is suggested by the high percentage of PTEN knockdown that was observed *in vivo* (up to 91%), as PTEN is a ubiquitously expressed protein. Additionally, although not analyzed in this study, during our in vitro experiments we also observed LNP uptake in the astrocyte feeder layer. A current disadvantage of using LNP mediated knockdown

in the brain, is the inability to perform cell type specific knockdown, as is easily performed with the use of cell type specific promoters when making plasmids. It is possible however, to express exogenous ligands such as antibodies, peptides and small molecule ligands on the LNP surface and enhance uptake by specific cell types (Tam et al., 2013), therefore future development of the LNP platform for use in the brain may facilitate cell type specific transfection in the CNS.

4.2.2 Does SLC26A11 Regulate Neuronal Cl^- Homeostasis?

Our study demonstrates the first report of SLC26A11 as a functional Cl^- influx pathway in neurons. Several questions arise as to under what specific conditions and times SLC26A11 may modulate local and global Cl^- concentration. Aberrant, chloride homeostasis is central to several neurological diseases, and it would therefore be interesting to examine whether SLC26A11 expression or localization changes under such conditions. Epileptic seizures are commonly observed in patients following ischemia and TBI with patients responding poorly to anticonvulsants that act on $GABA_A$A receptors (Young et al., 1990), presumably due to increased $[Cl^-]_i$ leading to a depolarizing shift in E_{GABA}. If blocking SLC26A11 can reduce the increases in Cl^- that occur during pathologies that are associated with cytotoxic edema, it may be possible to maintain the direction of hyperpolarizing $GABA_AR$ currents, and reduce the generation of post traumatic seizures. The cation-chloride cotransporters, NKCC1 and KCC2 are accepted as the primary transporters that govern the shift in E_{Cl} that occurs in development, however a role for HCO_3^-

transporters may also play a role in some neurons (Payne et al., 2003; Gonzalez-Islas et al., 2009; Kim and Trussell, 2009). A developmental time course of SLC26A11 expression should be performed, as it is possible that the contribution of SLC26A11 to Cl^- loading in neurons may change with postnatal development.

4.2.3 What is the Relative Contribution of SLC26A11 Mediated Cl^- Entry to Cytotoxic Edema *in vivo*?

Although the results presented in chapter 3 demonstrate that cytotoxic edema occurs when prolonged increases in intracellular Na^+ causes transmembrane Cl^- entry via SLC26A11 in brain slices, it will be important to test the relative contribution of this mechanism to cytotoxic brain edema *in vivo*. The most accepted animal models of cytotoxic edema are models of ischemic stroke and traumatic brain injury, both of which involve the extensive influx of neuronal Na^+ via various pathways. DIDS completely abolished neuronal swelling in our assay, however, DIDS has many off target effects both in the brain and in the periphery. It will therefore be important to generate selective antagonists against SLC26A11 in the future. Although, we showed that blocking neuronal swelling protects neurons from subsequent rapid cell death in brain slices, it is still possible that these neurons would still die via other slower apoptotic mechanisms. However, it can be argued that regardless of the final fate of these cells, shifting cell death from necrotic to apoptotic cell death would be beneficial as necrosis is associated with the release of inflammatory factors. Reducing inflammation caused by the membrane disruption in necrosis could also reduce the secondary vasogenic edema caused by

inflammation (Donkin and Vink, 2010). In addition to neuronal swelling, astrocyte swelling can also contribute to cytotoxic edema (Kimelberg, 2005; Simard et al., 2006). Astrocytes, swell in response to elevations in extracellular K^+ (Walz, 1987) which occurs following neuronal Na^+ influx. Unlike astrocytes, neurons do not express aquaporin selective water channels, and therefore neuronal volume control has not been studied as extensively. However, this does not mean that neurons cannot transport water. In fact, water transport is a general feature of many transporters, with some transporters exhibiting passive water permeability analogous to that of aquaporins (Zeuthen, 2010). Understanding of both the astrocytic and neuronal swelling mechanisms will most likely be required for optimization of future therapeutics. Future work should test the relative contribution of SLC26A11 mediated Cl^- influx to the magnitude of brain edema and neuronal death in animal models of cytotoxic brain edema *in vivo.*

4.2.4 Do Other Neuronal Cl^- Entry Pathways Contribute to Cytotoxic Edema?

We demonstrated that knockdown of SLC26A11 led to a decrease in the magnitude of the neuronal volume increase by 55% following knockdown of SLC26A11, whereas removal of Cl^- or pharmacological block by DIDS reduced the volume increase by 81% and 78% of control respectively. The resultant volume increase not blocked by SLC26A11 siRNA transfection could either be due to incomplete knockdown of SLC26A11, or alternatively mediated by another Cl^- influx pathway that is also DIDS sensitive.

Following excitotoxic insults such as ischemia, the extracellular GABA concentration increases due to a combination of vesicular release and reversal of GABA transporters (GATs) (Allen et al., 2004), possibly causing Cl^- influx. We demonstrated that although $GABA_A$Rs do in fact contribute to a small portion of neuronal swelling observed in our experiments, the majority of the Cl^- influx was mediated by another mechanism because it was insensitive to picrotoxin. These results are in agreement with other studies showing a contribution of $GABA_A$Rs to neuronal swelling in cell culture (Hasbani et al., 1998). In brain slices it was also shown that blocking $GABA_A$Rs led to a small reduction in the initial rapid increase (<1 min) of the intrinsic optical signal (a marker of cell swelling) following OGD, however, blocking $GABA_A$Rs had no effect on final intrinsic optical signal increase (>2 min)(Allen et al., 2004). Additionally it was observed that calcium influx caused $GABA_A$Rs to become completely inactivated within 2 minutes of the anoxic depolarization. These results suggest that although $GABA_A$Rs can contribute to neuronal swelling via a transient chloride influx, the majority of the Cl^- influx that occurs during ischemia and other excitotoxic insults occurs via other mechanisms. In another study, Cl^- imaging in pyramidal neurons with the genetically encoded Cl^- indicator Clomeleon showed no effect of blocking $GABA_A$Rs on the magnitude of the chloride increase during *in vitro* ischemia (Pond et al., 2006), again suggesting that blocking $GABA_A$Rs does not effect the final extent of $[Cl^-]_i$ increase that occurs in ischemia. The authors of this study were unable to identify the mechanism underlying the pathway for Cl^- influx that occurred during OGD, however they were able to block a small secondary increase in Cl^- that occurred (>1 hour) after re-

oxygenation by blocking NKCC1 with bumetanide, although the significance of this late Cl^- influx in the brain slice remains uncertain. In addition to the Cl^- loading that occurs during excitotoxic insults, Cl^- efflux may also be compromised. As KCC2 directional transport is dependent on the potassium gradient, small changes in extracellular K^+ can have substantial effects on KCC2 mediated Cl^- clearance. A recent study demonstrated that glutamate activation of NMDARs can lead to phosphorylation and thereby decreased expression of KCC2, leading to decreased recovery of excitotoxic Cl^- loads (Lee et al., 2011), however, the authors were again unable to identify the source of Cl^- influx, but showed that it was independent of NKCC1. If KCC2 mediated Cl^- efflux is indeed compromised following cytotoxic edema, in addition to blocking influx of Cl^- perhaps enhancing extrusion of Cl^- (Gagnon et al., 2013) would be additionally beneficial.

4.2.5 Development of Specific Inhibitors Against SLC26A11

The development of specific antagonists against SLC26A11 will facilitate functional studies and potentially lead to therapeutics for the treatment of cytotoxic brain edema. We demonstrated that DIDS completely prevented the neuronal swelling following prolonged Na^+ influx in our study and DIDS has also been shown to be neuroprotective *in vivo* in a rat model of transient ischemic stroke (Inoue et al., 2007). However, DIDS has several other targets in the brain and in the periphery and is therefore not an ideal antagonist. A viable method to screen for antagonists against SLC26A11 is to express the exogenous protein in an expression system and

screen it against a chemical library. Recently the group of Yves De Koninck developed a simple fluorometric assay to measure $[Cl^-]_i$ by expressing the genetically encoded ratiometric Cl^- indicator, clomeleon in a cell line (Gagnon et al., 2013). Ideally, the cell line would not endogenously express SLC26A11, and could therefore be used as a control in the absence of SLC26A11 expression. Additionally, validation for selectivity against SLC26A11 should be confirmed by testing positive hits against cell lines expressing other Cl^-/HCO_3^- transporters such as those of the SLC4 family. It was reported that when expressed in HEK-293 cells, SLC26A11 was constitutively active (Rahmati et al., 2013), suggesting that blocking SLC26A11 should either decrease or increase intracellular Cl^- depending on Cl^- gradient of the cell type, which can be controlled by modulating the extracellular $[Cl^-]$.

4.3 Clinical significance

4.3.1 Lipid Nanoparticle-siRNA Systems to Treat Psychiatric and Neurological Disorders

Clinical studies using LNP-siRNA systems in peripheral tissues have been quite promising, and immunostimulatory effects of LNP-siRNA injections are reported to be infrequent and readily managed, see http://www.alnylam.com/capella/wp-content/uploads/2012/07/Alnylam-ALN-TTR02-PhaseI-Results-120716.pdf. Consistent with these results we found no evidence that LNP-siRNAs themselves caused immunostimulatory effects in brain slices, measured by synthesis of TNF-α triggered by LNPs. In addition, there are

now well-established methods to reduce or eliminate siRNA immunogenicity by adjusting siRNA chemistry (Bramsen and Kjems, 2012).

As LNP-siRNA systems are currently unable to cross the BBB, the therapeutic utility of LNP-siRNA for treatment of neurological disorders would require direct injection into the brain. Although, such treatments are controversial, there are now a number of clinically accepted therapies relying on direct pumping of therapeutics into the CSF (North, 1997; Dash and Cudworth, 1998). A lipid-based formulation of cytarabine has gained clinical acceptance for treatment of brain cancer following direct administration into CSF (Phuphanich et al., 2007). Furthermore, a number of clinical trials are now in progress for treatments of serious neurological diseases that rely on continuous infusion of ASOs into the CSF (Smith et al., 2006; Robinson, 2012).

4.3.2 Treatment of Cytotoxic Brain Edema

Currently all clinical treatment options for cytotoxic brain edema are symptomatic, with the goal of reducing intracranial pressure (ICP), rather than targeting the underlying cellular mechanisms causing the edema (Unterberg et al., 2004; Donkin and Vink, 2010). Although most cases of brain edema are a mixture of both cytotoxic and vasogenic components, brain swelling following traumatic brain injury and ischemia are thought to occur primarily from cytotoxic origin (Marmarou et al., 2006; Rosenblum, 2007). Additionally, even in cases of vasogenic edema, the increases in ICP often lead to constriction of the vasculature and decreased blood

flow that results in the inability to extrude intracellular cations via energy dependent pumps and thus the exacerbation of edema via cytotoxic mechanisms (Liang et al., 2007; Simard et al., 2007). In terms of time of treatment, brain edema normally peaks between 36 and 72 hours following TBI or ischemia a time when most patients have already presented to the hospital (Rabinstein, 2006). Previous clinical trials to prevent cytotoxic edema and/or excitotoxicty have aimed at blocking sources of Na^+ or Ca^{2+} entry into neurons via different pathways such as NMDA glutamate receptors, however, these approaches have been largely unsuccessful (O'Collins et al., 2006). We demonstrate that even when fast glutamate and $GABA_A$ ligand gated channels are blocked, swelling still inevitably occurs as Na^+ entry may ensue via multiple different pathways (e.g. activation of NMDARs, AMPARs, VGSCs, TRPCs, ASICs, pannexin hemichannels, inhibition of Na+/K+ ATPase, etc.), ultimately causing neuronal swelling and cell death. If however, the majority of the chloride entry occurs via a single pathway it may be possible to reduce cytotoxic edema by blocking this pathway. In addition to cytotoxic edema that is life threatening, we demonstrate that the Cl^- mediated neuronal swelling itself leads to cell death in the brain slice. As opposed to apoptotic cell death that is characterized by shrinking, the mechanisms of cell swelling that lead to necrotic cell death are poorly characterized. Recent research suggests that necrotic cell death may also be triggered by distinct molecular pathways, and may be preventable (Zhang et al., 2009; Vandenabeele et al., 2010; Re et al., 2014). The role of SLC26A11 mediated Cl^- influx should be further examined as a potential mechanism underlying neuronal swelling that leads to necrosis.

SLC26A11 should be considered as a potential therapeutic treatment for treating cytotoxic brain edema and excitotoxicity, possibly in combination with other therapeutics.

References:

Aarts M, Iihara K, Wei WL, Xiong ZG, Arundine M, Cerwinski W, MacDonald JF, Tymianski M (2003) A key role for TRPM7 channels in anoxic neuronal death. Cell 115:863-877.

Abascal F, Zardoya R (2012) LRRC8 proteins share a common ancestor with pannexins, and may form hexameric channels involved in cell-cell communication. BioEssays : news and reviews in molecular, cellular and developmental biology 34:551-560.

Abbott NJ (2000) Inflammatory mediators and modulation of blood-brain barrier permeability. Cellular and molecular neurobiology 20:131-147.

Accardi A, Miller C (2004) Secondary active transport mediated by a prokaryotic homologue of ClC Cl- channels. Nature 427:803-807.

Addepalli H, Meena, Peng CG, Wang G, Fan Y, Charisse K, Jayaprakash KN, Rajeev KG, Pandey RK, Lavine G, Zhang L, Jahn-Hofmann K, Hadwiger P, Manoharan M, Maier MA (2010) Modulation of thermal stability can enhance the potency of siRNA. Nucleic Acids Res 38:7320-7331.

Akinc A et al. (2010) Targeted delivery of RNAi therapeutics with endogenous and exogenous ligand-based mechanisms. Molecular therapy : the journal of the American Society of Gene Therapy 18:1357-1364.

Allbritton NL, Verret CR, Wolley RC, Eisen HN (1988) Calcium ion concentrations and DNA fragmentation in target cell destruction by murine cloned cytotoxic T lymphocytes. The Journal of experimental medicine 167:514-527.

Allen NJ, Rossi DJ, Attwell D (2004) Sequential release of GABA by exocytosis and reversed uptake leads to neuronal swelling in simulated ischemia of hippocampal slices. The Journal of neuroscience : the official journal of the Society for Neuroscience 24:3837-3849.

Almaca J, Tian Y, Aldehni F, Ousingsawat J, Kongsuphol P, Rock JR, Harfe BD, Schreiber R, Kunzelmann K (2009) TMEM16 proteins produce volume-regulated chloride currents that are reduced in mice lacking TMEM16A. The Journal of biological chemistry 284:28571-28578.

Alper SL (2009) Molecular physiology and genetics of Na+-independent SLC4 anion exchangers. The Journal of experimental biology 212:1672-1683.

Alper SL, Sharma AK (2013) The SLC26 gene family of anion transporters and channels. Molecular aspects of medicine 34:494-515.

Alvarez-Leefmans FJ, Delpire D (2009) Physiology and Pathology of Chloride Transporters and Channels in the Nervous System. London, UK: Elsevier.

Amiry-Moghaddam M, Ottersen OP (2003) The molecular basis of water transport in the brain. Nature reviews Neuroscience 4:991-1001.

Andrew RD, Labron MW, Boehnke SE, Carnduff L, Kirov SA (2007) Physiological evidence that pyramidal neurons lack functional water channels. Cerebral cortex 17:787-802.

Asahi M, Wang X, Mori T, Sumii T, Jung JC, Moskowitz MA, Fini ME, Lo EH (2001) Effects of matrix metalloproteinase-9 gene knock-out on the proteolysis of blood-brain barrier and white matter components after cerebral ischemia. The Journal of neuroscience : the official journal of the Society for Neuroscience 21:7724-7732.

Back T, Ginsberg MD, Dietrich WD, Watson BD (1996) Induction of spreading depression in the ischemic hemisphere following experimental middle cerebral artery occlusion: effect on infarct morphology. Journal of cerebral blood flow and metabolism : official journal of the International Society of Cerebral Blood Flow and Metabolism 16:202-213.

Barros LF, Hermosilla T, Castro J (2001) Necrotic volume increase and the early physiology of necrosis. Comparative biochemistry and physiology Part A, Molecular & integrative physiology 130:401-409.

Basha G, Novobrantseva TI, Rosin N, Tam YY, Hafez IM, Wong MK, Sugo T, Ruda VM, Qin J, Klebanov B, Ciufolini M, Akinc A, Tam YK, Hope MJ, Cullis PR (2011) Influence of cationic lipid composition on gene silencing properties of lipid nanoparticle formulations of siRNA in antigen-presenting cells. Molecular therapy : the journal of the American Society of Gene Therapy 19:2186-2200.

Belliveau NM, Huft J, Lin PJ, Chen S, Leung AK, Leaver TJ, Wild AW, Lee JB, Taylor RJ, Tam YK, Hansen CL, Cullis PR (2012) Microfluidic Synthesis of Highly Potent Limit-size Lipid Nanoparticles for In Vivo Delivery of siRNA. Mol Ther Nucleic Acids 1:e37.

Ben-Ari Y, Gaiarsa JL, Tyzio R, Khazipov R (2007) GABA: a pioneer transmitter that excites immature neurons and generates primitive oscillations. Physiological reviews 87:1215-1284.

Bereczki D, Liu M, Prado GF, Fekete I (2000) Cochrane report: A systematic review of mannitol therapy for acute ischemic stroke and cerebral parenchymal hemorrhage. Stroke; a journal of cerebral circulation 31:2719-2722.

Berezin MY, Achilefu S (2010) Fluorescence lifetime measurements and biological imaging. Chemical reviews 110:2641-2684.

Binder DK, Yao X, Verkman AS, Manley GT (2006a) Increased seizure duration in mice lacking aquaporin-4 water channels. Acta neurochirurgica Supplement 96:389-392.

Binder DK, Yao X, Zador Z, Sick TJ, Verkman AS, Manley GT (2006b) Increased seizure duration and slowed potassium kinetics in mice lacking aquaporin-4 water channels. Glia 53:631-636.

Blaesse P, Airaksinen MS, Rivera C, Kaila K (2009) Cation-chloride cotransporters and neuronal function. Neuron 61:820-838.

Boistel J, Fatt P (1958) Membrane permeability change during inhibitory transmitter action in crustacean muscle. The Journal of physiology 144:176-191.

Boron WF, Chen L, Parker MD (2009) Modular structure of sodium-coupled bicarbonate transporters. J Exp Biol 212:1697-1706.

Bortner CD, Cidlowski JA (1996) Absence of volume regulatory mechanisms contributes to the rapid activation of apoptosis in thymocytes. Am J Physiol 271:C950-961.

Bortner CD, Cidlowski JA (1998) A necessary role for cell shrinkage in apoptosis. Biochemical pharmacology 56:1549-1559.
Bramsen JB, Kjems J (2012) Development of Therapeutic-Grade Small Interfering RNAs by Chemical Engineering. Front Genet 3:154.
Bruzzone R, Barbe MT, Jakob NJ, Monyer H (2005) Pharmacological properties of homomeric and heteromeric pannexin hemichannels expressed in Xenopus oocytes. Journal of neurochemistry 92:1033-1043.
Bu G (2009) Apolipoprotein E and its receptors in Alzheimer's disease: pathways, pathogenesis and therapy. Nature reviews Neuroscience 10:333-344.
Burette AC, Weinberg RJ, Sassani P, Abuladze N, Kao L, Kurtz I (2012) The sodium-driven chloride/bicarbonate exchanger in presynaptic terminals. The Journal of comparative neurology 520:1481-1492.
Busch E, Gyngell ML, Eis M, Hoehn-Berlage M, Hossmann KA (1996) Potassium-induced cortical spreading depressions during focal cerebral ischemia in rats: contribution to lesion growth assessed by diffusion-weighted NMR and biochemical imaging. Journal of cerebral blood flow and metabolism : official journal of the International Society of Cerebral Blood Flow and Metabolism 16:1090-1099.
Candelario-Jalil E, Yang Y, Rosenberg GA (2009) Diverse roles of matrix metalloproteinases and tissue inhibitors of metalloproteinases in neuroinflammation and cerebral ischemia. Neuroscience 158:983-994.
Carini R, Autelli R, Bellomo G, Albano E (1999) Alterations of cell volume regulation in the development of hepatocyte necrosis. Experimental cell research 248:280-293.
Carini R, Bellomo G, Benedetti A, Fulceri R, Gamberucci A, Parola M, Dianzani MU, Albano E (1995) Alteration of Na+ homeostasis as a critical step in the development of irreversible hepatocyte injury after adenosine triphosphate depletion. Hepatology 21:1089-1098.
Chen LM, Kelly ML, Parker MD, Bouyer P, Gill HS, Felie JM, Davis BA, Boron WF (2008) Expression and localization of Na-driven Cl-HCO(3)(-) exchanger (SLC4A8) in rodent CNS. Neuroscience 153:162-174.
Choe KY, Olson JE, Bourque CW (2012) Taurine release by astrocytes modulates osmosensitive glycine receptor tone and excitability in the adult supraoptic nucleus. The Journal of neuroscience : the official journal of the Society for Neuroscience 32:12518-12527.
Choi DW (1985) Glutamate neurotoxicity in cortical cell culture is calcium dependent. Neuroscience letters 58:293-297.
Choi DW (1987) Ionic dependence of glutamate neurotoxicity. The Journal of neuroscience : the official journal of the Society for Neuroscience 7:369-379.
Choi HA, Badjatia N, Mayer SA (2012a) Hypothermia for acute brain injury--mechanisms and practical aspects. Nature reviews Neurology 8:214-222.
Choi HB, Gordon GR, Zhou N, Tai C, Rungta RL, Martinez J, Milner TA, Ryu JK, McLarnon JG, Tresguerres M, Levin LR, Buck J, Macvicar BA (2012b) Metabolic Communication between Astrocytes and Neurons via Bicarbonate-Responsive Soluble Adenylyl Cyclase. Neuron 75:1094-1104.

Churchwell KB, Wright SH, Emma F, Rosenberg PA, Strange K (1996) NMDA receptor activation inhibits neuronal volume regulation after swelling induced by veratridine-stimulated Na+ influx in rat cortical cultures. The Journal of neuroscience : the official journal of the Society for Neuroscience 16:7447-7457.

Clark S, Jordt SE, Jentsch TJ, Mathie A (1998) Characterization of the hyperpolarization-activated chloride current in dissociated rat sympathetic neurons. The Journal of physiology 506 (Pt 3):665-678.

Clifton GL, Miller ER, Choi SC, Levin HS, McCauley S, Smith KR, Jr., Muizelaar JP, Wagner FC, Jr., Marion DW, Luerssen TG, Chesnut RM, Schwartz M (2001) Lack of effect of induction of hypothermia after acute brain injury. The New England journal of medicine 344:556-563.

Cohen I, Navarro V, Clemenceau S, Baulac M, Miles R (2002) On the origin of interictal activity in human temporal lobe epilepsy in vitro. Science 298:1418-1421.

Coull JA, Boudreau D, Bachand K, Prescott SA, Nault F, Sik A, De Koninck P, De Koninck Y (2003) Trans-synaptic shift in anion gradient in spinal lamina I neurons as a mechanism of neuropathic pain. Nature 424:938-942.

Coull JA, Beggs S, Boudreau D, Boivin D, Tsuda M, Inoue K, Gravel C, Salter MW, De Koninck Y (2005) BDNF from microglia causes the shift in neuronal anion gradient underlying neuropathic pain. Nature 438:1017-1021.

Craig AM, Banker G, Chang W, McGrath ME, Serpinskaya AS (1996) Clustering of gephyrin at GABAergic but not glutamatergic synapses in cultured rat hippocampal neurons. J Neurosci 16:3166-3177.

Crepel V, Panenka W, Kelly ME, MacVicar BA (1998) Mitogen-activated protein and tyrosine kinases in the activation of astrocyte volume-activated chloride current. The Journal of neuroscience : the official journal of the Society for Neuroscience 18:1196-1206.

Damkier HH, Nielsen S, Praetorius J (2007) Molecular expression of SLC4-derived Na+-dependent anion transporters in selected human tissues. American journal of physiology Regulatory, integrative and comparative physiology 293:R2136-2146.

Damkier HH, Aalkjaer C, Praetorius J (2010) Na+-dependent HCO3- import by the slc4a10 gene product involves Cl- export. The Journal of biological chemistry 285:26998-27007.

Darby M, Kuzmiski JB, Panenka W, Feighan D, MacVicar BA (2003) ATP released from astrocytes during swelling activates chloride channels. Journal of neurophysiology 89:1870-1877.

Dash AK, Cudworth GC, 2nd (1998) Therapeutic applications of implantable drug delivery systems. J Pharmacol Toxicol Methods 40:1-12.

Davidson BL, McCray PB, Jr. (2011) Current prospects for RNA interference-based therapies. Nature reviews Genetics 12:329-340.

De Groat WC, Lalley PM, Saum WR (1972) Depolarization of dorsal root ganglia in the cat by GABA and related amino acids: antagonism by picrotoxin and bicuculline. Brain Res 44:273-277.

Dearden NM, Gibson JS, McDowall DG, Gibson RM, Cameron MM (1986) Effect of high-dose dexamethasone on outcome from severe head injury. Journal of neurosurgery 64:81-88.

Dijkhuizen RM, Beekwilder JP, Van der Worp HB, Van der Sprenkel JW, Tulleken KAF, Nicolay K (1999) Correlation between tissue depolarizations and damage in focal ischemic rat brain. Brain Research 840.

Diringer MN, Zazulia AR (2004) Osmotic therapy: fact and fiction. Neurocritical care 1:219-233.

Donkin JJ, Vink R (2010) Mechanisms of cerebral edema in traumatic brain injury: therapeutic developments. Current opinion in neurology 23:293-299.

Doyon N, Prescott SA, Castonguay A, Godin AG, Kroger H, De Koninck Y (2011) Efficacy of synaptic inhibition depends on multiple, dynamically interacting mechanisms implicated in chloride homeostasis. PLoS computational biology 7:e1002149.

Dreier JP (2011) The role of spreading depression, spreading depolarization and spreading ischemia in neurological disease. Nature medicine 17:439-447.

Duan D, Winter C, Cowley S, Hume JR, Horowitz B (1997) Molecular identification of a volume-regulated chloride channel. Nature 390:417-421.

Dzhala V, Valeeva G, Glykys J, Khazipov R, Staley K (2012) Traumatic alterations in GABA signaling disrupt hippocampal network activity in the developing brain. The Journal of neuroscience : the official journal of the Society for Neuroscience 32:4017-4031.

Dzhala VI, Talos DM, Sdrulla DA, Brumback AC, Mathews GC, Benke TA, Delpire E, Jensen FE, Staley KJ (2005) NKCC1 transporter facilitates seizures in the developing brain. Nature medicine 11:1205-1213.

Dzhala VI, Kuchibhotla KV, Glykys JC, Kahle KT, Swiercz WB, Feng G, Kuner T, Augustine GJ, Bacskai BJ, Staley KJ (2010) Progressive NKCC1-dependent neuronal chloride accumulation during neonatal seizures. The Journal of neuroscience : the official journal of the Society for Neuroscience 30:11745-11761.

Eisenberg HM, Frankowski RF, Contant CF, Marshall LF, Walker MD (1988) High-dose barbiturate control of elevated intracranial pressure in patients with severe head injury. Journal of neurosurgery 69:15-23.

Elinder F, Akanda N, Tofighi R, Shimizu S, Tsujimoto Y, Orrenius S, Ceccatelli S (2005) Opening of plasma membrane voltage-dependent anion channels (VDAC) precedes caspase activation in neuronal apoptosis induced by toxic stimuli. Cell death and differentiation 12:1134-1140.

Elmore S (2007) Apoptosis: a review of programmed cell death. Toxicologic pathology 35:495-516.

Ferrini F, Trang T, Mattioli TA, Laffray S, Del'Guidice T, Lorenzo LE, Castonguay A, Doyon N, Zhang W, Godin AG, Mohr D, Beggs S, Vandal K, Beaulieu JM, Cahill CM, Salter MW, De Koninck Y (2013) Morphine hyperalgesia gated through microglia-mediated disruption of neuronal Cl(-) homeostasis. Nature neuroscience 16:183-192.

Fields RD, Ni Y (2010) Nonsynaptic communication through ATP release from volume-activated anion channels in axons. Science signaling 3:ra73.

Fink ME (2012) Osmotherapy for intracranial hypertension: mannitol versus hypertonic saline. Continuum 18:640-654.
Fire A, Xu S, Montgomery MK, Kostas SA, Driver SE, Mello CC (1998) Potent and specific genetic interference by double-stranded RNA in Caenorhabditis elegans. Nature 391:806-811.
Fischmeister R, Hartzell HC (2005) Volume sensitivity of the bestrophin family of chloride channels. The Journal of physiology 562:477-491.
Fishman RA (1975) Brain edema. The New England journal of medicine 293:706-711.
French LA, Galicich JH (1964) The Use of Steroids for Control of Cerebral Edema. Clinical neurosurgery 10:212-223.
Gagnon M, Bergeron MJ, Lavertu G, Castonguay A, Tripathy S, Bonin RP, Perez-Sanchez J, Boudreau D, Wang B, Dumas L, Valade I, Bachand K, Jacob-Wagner M, Tardif C, Kianicka I, Isenring P, Attardo G, Coull JA, De Koninck Y (2013) Chloride extrusion enhancers as novel therapeutics for neurological diseases. Nature medicine 19:1524-1528.
Ginsberg MD, Pulsinelli WA (1994) The ischemic penumbra, injury thresholds, and the therapeutic window for acute stroke. Annals of neurology 36:553-554.
Glykys J, Dzhala V, Egawa K, Balena T, Saponjian Y, Kuchibhotla KV, Bacskai BJ, Kahle KT, Zeuthen T, Staley KJ (2014) Local impermeant anions establish the neuronal chloride concentration. Science 343:670-675.
Goldberg MP, Choi DW (1993) Combined oxygen and glucose deprivation in cortical cell culture: calcium-dependent and calcium-independent mechanisms of neuronal injury. J Neurosci 13:3510-3524.
Gomes JA, Stevens RD, Lewin JJ, 3rd, Mirski MA, Bhardwaj A (2005) Glucocorticoid therapy in neurologic critical care. Critical care medicine 33:1214-1224.
Gonzalez-Islas C, Chub N, Wenner P (2009) NKCC1 and AE3 appear to accumulate chloride in embryonic motoneurons. Journal of neurophysiology 101:507-518.
Grichtchenko, II, Choi I, Zhong X, Bray-Ward P, Russell JM, Boron WF (2001) Cloning, characterization, and chromosomal mapping of a human electroneutral Na(+)-driven Cl-HCO3 exchanger. The Journal of biological chemistry 276:8358-8363.
Grunder S, Thiemann A, Pusch M, Jentsch TJ (1992) Regions involved in the opening of CIC-2 chloride channel by voltage and cell volume. Nature 360:759-762.
Hail N, Jr., Carter BZ, Konopleva M, Andreeff M (2006) Apoptosis effector mechanisms: a requiem performed in different keys. Apoptosis : an international journal on programmed cell death 11:889-904.
Hamann S, Kiilgaard JF, la Cour M, Prause JU, Zeuthen T (2003) Cotransport of H+, lactate, and H2O in porcine retinal pigment epithelial cells. Experimental eye research 76:493-504.
Hamann S, Herrera-Perez JJ, Bundgaard M, Alvarez-Leefmans FJ, Zeuthen T (2005) Water permeability of Na+-K+-2Cl- cotransporters in mammalian epithelial cells. The Journal of physiology 568:123-135.
Hartings JA, Rolli ML, Lu XC, Tortella FC (2003) Delayed secondary phase of peri-infarct depolarizations after focal cerebral ischemia: relation to infarct

growth and neuroprotection. The Journal of neuroscience : the official journal of the Society for Neuroscience 23:11602-11610.
Hartwell RC, Sutton LN (1993) Mannitol, intracranial pressure, and vasogenic edema. Neurosurgery 32:444-450; discussion 450.
Hartzell C, Putzier I, Arreola J (2005) Calcium-activated chloride channels. Annual review of physiology 67:719-758.
Hasbani MJ, Hyrc KL, Faddis BT, Romano C, Goldberg MP (1998) Distinct roles for sodium, chloride, and calcium in excitotoxic dendritic injury and recovery. Experimental neurology 154:241-258.
Heimlich G, Bortner CD, Cidlowski JA (2004) Apoptosis and cell volume regulation: the importance of ions and ion channels. Advances in experimental medicine and biology 559:189-203.
Hentschke M, Wiemann M, Hentschke S, Kurth I, Hermans-Borgmeyer I, Seidenbecher T, Jentsch TJ, Gal A, Hubner CA (2006) Mice with a targeted disruption of the Cl-/HCO3- exchanger AE3 display a reduced seizure threshold. Molecular and cellular biology 26:182-191.
Hille C, Lahn M, Lohmannsroben HG, Dosche C (2009) Two-photon fluorescence lifetime imaging of intracellular chloride in cockroach salivary glands. Photochemical & photobiological sciences : Official journal of the European Photochemistry Association and the European Society for Photobiology 8:319-327.
Hodgkin AL, Horowicz P (1959) The influence of potassium and chloride ions on the membrane potential of single muscle fibres. The Journal of physiology 148:127-160.
Holland JW, Hui C, Cullis PR, Madden TD (1996) Poly(ethylene glycol)--lipid conjugates regulate the calcium-induced fusion of liposomes composed of phosphatidylethanolamine and phosphatidylserine. Biochemistry 35:2618-2624.
Hommel JD, Sears RM, Georgescu D, Simmons DL, DiLeone RJ (2003) Local gene knockdown in the brain using viral-mediated RNA interference. Nature medicine 9:1539-1544.
Homsi S, Federico F, Croci N, Palmier B, Plotkine M, Marchand-Leroux C, Jafarian-Tehrani M (2009) Minocycline effects on cerebral edema: relations with inflammatory and oxidative stress markers following traumatic brain injury in mice. Brain Res 1291:122-132.
Hossmann KA (1994) Viability thresholds and the penumbra of focal ischemia. Annals of neurology 36:557-565.
Hossmann KA (1996) Periinfarct depolarizations. Cerebrovascular and brain metabolism reviews 8:195-208.
Huang CG, Lamitina T, Agre P, Strange K (2007) Functional analysis of the aquaporin gene family in Caenorhabditis elegans. American journal of physiology Cell physiology 292:C1867-1873.
Huang WC, Xiao S, Huang F, Harfe BD, Jan YN, Jan LY (2012) Calcium-activated chloride channels (CaCCs) regulate action potential and synaptic response in hippocampal neurons. Neuron 74:179-192.

Huberfeld G, Wittner L, Clemenceau S, Baulac M, Kaila K, Miles R, Rivera C (2007) Perturbed chloride homeostasis and GABAergic signaling in human temporal lobe epilepsy. The Journal of neuroscience : the official journal of the Society for Neuroscience 27:9866-9873.

Hughes FM, Jr., Bortner CD, Purdy GD, Cidlowski JA (1997) Intracellular K+ suppresses the activation of apoptosis in lymphocytes. The Journal of biological chemistry 272:30567-30576.

Hutchison JS, Ward RE, Lacroix J, Hebert PC, Barnes MA, Bohn DJ, Dirks PB, Doucette S, Fergusson D, Gottesman R, Joffe AR, Kirpalani HM, Meyer PG, Morris KP, Moher D, Singh RN, Skippen PW, Hypothermia Pediatric Head Injury Trial I, the Canadian Critical Care Trials G (2008) Hypothermia therapy after traumatic brain injury in children. The New England journal of medicine 358:2447-2456.

Iliff JJ, Wang M, Liao Y, Plogg BA, Peng W, Gundersen GA, Benveniste H, Vates GE, Deane R, Goldman SA, Nagelhus EA, Nedergaard M (2012) A paravascular pathway facilitates CSF flow through the brain parenchyma and the clearance of interstitial solutes, including amyloid beta. Science translational medicine 4:147ra111.

Inoue H, Okada Y (2007) Roles of volume-sensitive chloride channel in excitotoxic neuronal injury. The Journal of neuroscience : the official journal of the Society for Neuroscience 27:1445-1455.

Inoue H, Mori S, Morishima S, Okada Y (2005) Volume-sensitive chloride channels in mouse cortical neurons: characterization and role in volume regulation. The European journal of neuroscience 21:1648-1658.

Inoue H, Ohtaki H, Nakamachi T, Shioda S, Okada Y (2007) Anion channel blockers attenuate delayed neuronal cell death induced by transient forebrain ischemia. Journal of neuroscience research 85:1427-1435.

Jacobs S, Ruusuvuori E, Sipila ST, Haapanen A, Damkier HH, Kurth I, Hentschke M, Schweizer M, Rudhard Y, Laatikainen LM, Tyynela J, Praetorius J, Voipio J, Hubner CA (2008) Mice with targeted Slc4a10 gene disruption have small brain ventricles and show reduced neuronal excitability. Proceedings of the National Academy of Sciences of the United States of America 105:311-316.

Jayaraman M, Ansell SM, Mui BL, Tam YK, Chen J, Du X, Butler D, Eltepu L, Matsuda S, Narayanannair JK, Rajeev KG, Hafez IM, Akinc A, Maier MA, Tracy MA, Cullis PR, Madden TD, Manoharan M, Hope MJ (2012) Maximizing the Potency of siRNA Lipid Nanoparticles for Hepatic Gene Silencing In Vivo. Angew Chem Int Ed Engl 51:8529-8533.

Jennings ML (1976) Proton fluxes associated with erythrocyte membrane anion exchange. The Journal of membrane biology 28:187-205.

Jentsch TJ, Stein V, Weinreich F, Zdebik AA (2002) Molecular structure and physiological function of chloride channels. Physiol Rev 82:503-568.

Jonas P, Bischofberger J, Sandkuhler J (1998) Corelease of two fast neurotransmitters at a central synapse. Science 281:419-424.

Kaila K, Voipio J (1987) Postsynaptic fall in intracellular pH induced by GABA-activated bicarbonate conductance. Nature 330:163-165.

Kajta M, Trotter A, Lason W, Beyer C (2005) Effect of NMDA on staurosporine-induced activation of caspase-3 and LDH release in mouse neocortical and hippocampal cells. Brain Res Dev Brain Res 160:40-52.
Kaneko H, Nakamura T, Lindemann B (2001) Noninvasive measurement of chloride concentration in rat olfactory receptor cells with use of a fluorescent dye. American journal of physiology Cell physiology 280:C1387-1393.
Kaneko H, Putzier I, Frings S, Kaupp UB, Gensch T (2004) Chloride accumulation in mammalian olfactory sensory neurons. J Neurosci 24:7931-7938.
Karra D, Dahm R (2010) Transfection techniques for neuronal cells. The Journal of neuroscience : the official journal of the Society for Neuroscience 30:6171-6177.
Kaufmann AM, Cardoso ER (1992) Aggravation of vasogenic cerebral edema by multiple-dose mannitol. Journal of neurosurgery 77:584-589.
Kerr JF (1971) Shrinkage necrosis: a distinct mode of cellular death. The Journal of pathology 105:13-20.
Kerr JF, Wyllie AH, Currie AR (1972) Apoptosis: a basic biological phenomenon with wide-ranging implications in tissue kinetics. British journal of cancer 26:239-257.
Kim Y, Trussell LO (2009) Negative shift in the glycine reversal potential mediated by a Ca2+- and pH-dependent mechanism in interneurons. The Journal of neuroscience : the official journal of the Society for Neuroscience 29:11495-11510.
Kimelberg HK (1995) Current concepts of brain edema. Review of laboratory investigations. Journal of neurosurgery 83:1051-1059.
Kimelberg HK (2004) Water homeostasis in the brain: basic concepts. Neuroscience 129:851-860.
Kimelberg HK (2005) Astrocytic swelling in cerebral ischemia as a possible cause of injury and target for therapy. Glia 50:389-397.
Kimelberg HK, Macvicar BA, Sontheimer H (2006) Anion channels in astrocytes: biophysics, pharmacology, and function. Glia 54:747-757.
Klatzo I (1967) Presidental address. Neuropathological aspects of brain edema. Journal of neuropathology and experimental neurology 26:1-14.
Klatzo I (1987) Pathophysiological aspects of brain edema. Acta neuropathologica 72:236-239.
Kordasiewicz HB, Stanek LM, Wancewicz EV, Mazur C, McAlonis MM, Pytel KA, Artates JW, Weiss A, Cheng SH, Shihabuddin LS, Hung G, Bennett CF, Cleveland DW (2012) Sustained Therapeutic Reversal of Huntington's Disease by Transient Repression of Huntingtin Synthesis. Neuron 74:1031-1044.
Kuchibhotla KV, Lattarulo CR, Hyman BT, Bacskai BJ (2009) Synchronous hyperactivity and intercellular calcium waves in astrocytes in Alzheimer mice. Science 323:1211-1215.
Kuffler SW, Edwards C (1958) Mechanism of gamma aminobutyric acid (GABA) action and its relation to synaptic inhibition. Journal of neurophysiology 21:589-610.

Kwon CH, Luikart BW, Powell CM, Zhou J, Matheny SA, Zhang W, Li Y, Baker SJ, Parada LF (2006) Pten regulates neuronal arborization and social interaction in mice. Neuron 50:377-388.

Lauritzen M, Dreier JP, Fabricius M, Hartings JA, Graf R, Strong AJ (2011) Clinical relevance of cortical spreading depression in neurological disorders: migraine, malignant stroke, subarachnoid and intracranial hemorrhage, and traumatic brain injury. Journal of cerebral blood flow and metabolism : official journal of the International Society of Cerebral Blood Flow and Metabolism 31:17-35.

Laviolette SR, Gallegos RA, Henriksen SJ, van der Kooy D (2004) Opiate state controls bi-directional reward signaling via GABAA receptors in the ventral tegmental area. Nature neuroscience 7:160-169.

Leao AAP (1944) Spreading depression of activity in cerebral cortex. Journal of neurophysiology 7:359-390.

Lee HH, Deeb TZ, Walker JA, Davies PA, Moss SJ (2011) NMDA receptor activity downregulates KCC2 resulting in depolarizing GABAA receptor-mediated currents. Nature neuroscience 14:736-743.

Lee HJ, Yang WS, Park HW, Choi HS, Kim SH, Kim JY, Choi JY (2012a) Expression of anion exchangers in cultured human endolymphatic sac epithelia. Otology & neurotology : official publication of the American Otological Society, American Neurotology Society [and] European Academy of Otology and Neurotology 33:1664-1671.

Lee JB, Zhang K, Tam YY, Tam YK, Belliveau NM, Sung VY, Lin PJ, LeBlanc E, Ciufolini MA, Rennie PS, Cullis PR (2012b) Lipid nanoparticle siRNA systems for silencing the androgen receptor in human prostate cancer in vivo. International journal of cancer Journal international du cancer 131:E781-790.

Lee S, Yoon BE, Berglund K, Oh SJ, Park H, Shin HS, Augustine GJ, Lee CJ (2010) Channel-mediated tonic GABA release from glia. Science 330:790-796.

Liang D, Bhatta S, Gerzanich V, Simard JM (2007) Cytotoxic edema: mechanisms of pathological cell swelling. Neurosurgical focus 22:E2.

Liu HT, Sabirov RZ, Okada Y (2008a) Oxygen-glucose deprivation induces ATP release via maxi-anion channels in astrocytes. Purinergic signalling 4:147-154.

Liu HT, Toychiev AH, Takahashi N, Sabirov RZ, Okada Y (2008b) Maxi-anion channel as a candidate pathway for osmosensitive ATP release from mouse astrocytes in primary culture. Cell research 18:558-565.

Loo DD, Wright EM, Zeuthen T (2002) Water pumps. The Journal of physiology 542:53-60.

Loo DD, Hirayama BA, Meinild AK, Chandy G, Zeuthen T, Wright EM (1999) Passive water and ion transport by cotransporters. The Journal of physiology 518 (Pt 1):195-202.

Lorenz C, Pusch M, Jentsch TJ (1996) Heteromultimeric CLC chloride channels with novel properties. Proceedings of the National Academy of Sciences of the United States of America 93:13362-13366.

Love KT, Mahon KP, Levins CG, Whitehead KA, Querbes W, Dorkin JR, Qin J, Cantley W, Qin LL, Racie T, Frank-Kamenetsky M, Yip KN, Alvarez R, Sah DW, de Fougerolles A, Fitzgerald K, Koteliansky V, Akinc A, Langer R, Anderson DG (2010) Lipid-like materials for low-dose, in vivo gene silencing. Proc Natl Acad Sci U S A 107:1864-1869.

Lucas DR, Newhouse JP (1957) The toxic effect of sodium L-glutamate on the inner layers of the retina. AMA archives of ophthalmology 58:193-201.

Ma T, Yang B, Gillespie A, Carlson EJ, Epstein CJ, Verkman AS (1998) Severely impaired urinary concentrating ability in transgenic mice lacking aquaporin-1 water channels. The Journal of biological chemistry 273:4296-4299.

MacAulay N, Zeuthen T, Gether U (2002) Conformational basis for the Li(+)-induced leak current in the rat gamma-aminobutyric acid (GABA) transporter-1. The Journal of physiology 544:447-458.

MacAulay N, Gether U, Klaerke DA, Zeuthen T (2001) Water transport by the human Na+-coupled glutamate cotransporter expressed in Xenopus oocytes. The Journal of physiology 530:367-378.

Maeno E, Ishizaki Y, Kanaseki T, Hazama A, Okada Y (2000) Normotonic cell shrinkage because of disordered volume regulation is an early prerequisite to apoptosis. Proceedings of the National Academy of Sciences of the United States of America 97:9487-9492.

Majno G, Joris I (1995) Apoptosis, oncosis, and necrosis. An overview of cell death. The American journal of pathology 146:3-15.

Mameli M, Bellone C, Brown MT, Luscher C (2011) Cocaine inverts rules for synaptic plasticity of glutamate transmission in the ventral tegmental area. Nat Neurosci 14:414-416.

Manley GT, Binder DK, Papadopoulos MC, Verkman AS (2004) New insights into water transport and edema in the central nervous system from phenotype analysis of aquaporin-4 null mice. Neuroscience 129:983-991.

Manley GT, Fujimura M, Ma T, Noshita N, Filiz F, Bollen AW, Chan P, Verkman AS (2000) Aquaporin-4 deletion in mice reduces brain edema after acute water intoxication and ischemic stroke. Nature medicine 6:159-163.

Marmarou A (2007) A review of progress in understanding the pathophysiology and treatment of brain edema. Neurosurgical focus 22:E1.

Marmarou A, Signoretti S, Fatouros PP, Portella G, Aygok GA, Bullock MR (2006) Predominance of cellular edema in traumatic brain swelling in patients with severe head injuries. Journal of neurosurgery 104:720-730.

Marmarou A, Fatouros PP, Barzo P, Portella G, Yoshihara M, Tsuji O, Yamamoto T, Laine F, Signoretti S, Ward JD, Bullock MR, Young HF (2000) Contribution of edema and cerebral blood volume to traumatic brain swelling in head-injured patients. Journal of neurosurgery 93:183-193.

McManus ML, Soriano SG (1998) Rebound swelling of astroglial cells exposed to hypertonic mannitol. Anesthesiology 88:1586-1591.

Meier SD, Kovalchuk Y, Rose CR (2006) Properties of the new fluorescent Na+ indicator CoroNa Green: comparison with SBFI and confocal Na+ imaging. Journal of neuroscience methods 155:251-259.

Mies G. IT, Hossmann K. A. (1993) Correlation between peri-infract DC shifts and ischaemic neuronal damage in rat. Neuroreport 4:709-711.
Miledi R (1982) A calcium-dependent transient outward current in Xenopus laevis oocytes. Proceedings of the Royal Society of London Series B, Containing papers of a Biological character Royal Society 215:491-497.
Miles R, Blaesse P, Huberfeld G, Wittner L, Kaila K (2012) Chloride homeostasis and GABA signaling in temporal lobe epilepsy. In: Jasper's Basic Mechanisms of the Epilepsies, 4th Edition (Noebels JL, Avoli M, Rogawski MA, Olsen RW, Delgado-Escueta AV, eds). Bethesda (MD).
Mount DB, Romero MF (2004) The SLC26 gene family of multifunctional anion exchangers. Pflugers Archiv : European journal of physiology 447:710-721.
Muizelaar JP, Marmarou A, Ward JD, Kontos HA, Choi SC, Becker DP, Gruemer H, Young HF (1991) Adverse effects of prolonged hyperventilation in patients with severe head injury: a randomized clinical trial. Journal of neurosurgery 75:731-739.
Nagashima T, Shirakuni T, Rapoport SI (1990) A two-dimensional, finite element analysis of vasogenic brain edema. Neurologia medico-chirurgica 30:1-9.
Nagelhus EA, Horio Y, Inanobe A, Fujita A, Haug FM, Nielsen S, Kurachi Y, Ottersen OP (1999) Immunogold evidence suggests that coupling of K+ siphoning and water transport in rat retinal Muller cells is mediated by a coenrichment of Kir4.1 and AQP4 in specific membrane domains. Glia 26:47-54.
Nedergaard M, Hansen AJ (1993) Characterization of cortical depolarizations evoked in focal cerebral ischemia. Journal of cerebral blood flow and metabolism : official journal of the International Society of Cerebral Blood Flow and Metabolism 13:568-574.
Nielsen S, Nagelhus EA, Amiry-Moghaddam M, Bourque C, Agre P, Ottersen OP (1997) Specialized membrane domains for water transport in glial cells: high-resolution immunogold cytochemistry of aquaporin-4 in rat brain. The Journal of neuroscience : the official journal of the Society for Neuroscience 17:171-180.
Nimmerjahn A, Kirchhoff F, Kerr JN, Helmchen F (2004) Sulforhodamine 101 as a specific marker of astroglia in the neocortex in vivo. Nat Methods 1:31-37.
North RB, and Levy, R.M. (1997) Neurosurgical management of pain Springer.New York, New York, USA.:360.
O'Collins VE, Macleod MR, Donnan GA, Horky LL, van der Worp BH, Howells DW (2006) 1,026 experimental treatments in acute stroke. Annals of neurology 59:467-477.
Oiki S, Kubo M, Okada Y (1994) Mg2+ and ATP-dependence of volume-sensitive Cl- channels in human epithelial cells. The Japanese journal of physiology 44 Suppl 2:S77-79.
Ojcius DM, Zychlinsky A, Zheng LM, Young JD (1991) Ionophore-induced apoptosis: role of DNA fragmentation and calcium fluxes. Experimental cell research 197:43-49.
Okada Y, Shimizu T, Maeno E, Tanabe S, Wang X, Takahashi N (2006) Volume-sensitive chloride channels involved in apoptotic volume decrease and cell death. The Journal of membrane biology 209:21-29.

Olney JW (1969) Brain lesions, obesity, and other disturbances in mice treated with monosodium glutamate. Science 164:719-721.
Olney JW (1971) Glutamate-induced neuronal necrosis in the infant mouse hypothalamus. An electron microscopic study. Journal of neuropathology and experimental neurology 30:75-90.
Paczynski RP (1997) Osmotherapy. Basic concepts and controversies. Critical care clinics 13:105-129.
Palma L, Bruni G, Fiaschi AI, Mariottini A (2006) Passage of mannitol into the brain around gliomas: a potential cause of rebound phenomenon. A study on 21 patients. Journal of neurosurgical sciences 50:63-66.
Papadopoulos MC, Verkman AS (2007) Aquaporin-4 and brain edema. Pediatric nephrology 22:778-784.
Papadopoulos MC, Manley GT, Krishna S, Verkman AS (2004a) Aquaporin-4 facilitates reabsorption of excess fluid in vasogenic brain edema. FASEB journal : official publication of the Federation of American Societies for Experimental Biology 18:1291-1293.
Papadopoulos MC, Saadoun S, Binder DK, Manley GT, Krishna S, Verkman AS (2004b) Molecular mechanisms of brain tumor edema. Neuroscience 129:1011-1020.
Park H, Oh SJ, Han KS, Woo DH, Park H, Mannaioni G, Traynelis SF, Lee CJ (2009) Bestrophin-1 encodes for the Ca2+-activated anion channel in hippocampal astrocytes. The Journal of neuroscience : the official journal of the Society for Neuroscience 29:13063-13073.
Parker MD, Bouyer P, Daly CM, Boron WF (2008a) Cloning and characterization of novel human SLC4A8 gene products encoding Na+-driven Cl-/HCO3(-) exchanger variants NDCBE-A, -C, and -D. Physiological genomics 34:265-276.
Parker MD, Musa-Aziz R, Rojas JD, Choi I, Daly CM, Boron WF (2008b) Characterization of human SLC4A10 as an electroneutral Na/HCO3 cotransporter (NBCn2) with Cl- self-exchange activity. The Journal of biological chemistry 283:12777-12788.
Payne JA, Rivera C, Voipio J, Kaila K (2003) Cation-chloride co-transporters in neuronal communication, development and trauma. Trends in neurosciences 26:199-206.
Phillis JW, Song D, O'Regan MH (1997) Inhibition by anion channel blockers of ischemia-evoked release of excitotoxic and other amino acids from rat cerebral cortex. Brain Res 758:9-16.
Phuphanich S, Maria B, Braeckman R, Chamberlain M (2007) A pharmacokinetic study of intra-CSF administered encapsulated cytarabine (DepoCyt) for the treatment of neoplastic meningitis in patients with leukemia, lymphoma, or solid tumors as part of a phase III study. J Neurooncol 81:201-208.
Pitas RE, Boyles JK, Lee SH, Foss D, Mahley RW (1987) Astrocytes synthesize apolipoprotein E and metabolize apolipoprotein E-containing lipoproteins. Biochimica et biophysica acta 917:148-161.
Plesnila N (2007) Decompression craniectomy after traumatic brain injury: recent experimental results. Progress in brain research 161:393-400.

Polderman KH (2008) Induced hypothermia and fever control for prevention and treatment of neurological injuries. Lancet 371:1955-1969.
Pond BB, Berglund K, Kuner T, Feng G, Augustine GJ, Schwartz-Bloom RD (2006) The chloride transporter Na(+)-K(+)-Cl- cotransporter isoform-1 contributes to intracellular chloride increases after in vitro ischemia. The Journal of neuroscience : the official journal of the Society for Neuroscience 26:1396-1406.
Porcelli AM, Ghelli A, Zanna C, Valente P, Ferroni S, Rugolo M (2004) Apoptosis induced by staurosporine in ECV304 cells requires cell shrinkage and upregulation of Cl- conductance. Cell death and differentiation 11:655-662.
Preston GM, Carroll TP, Guggino WB, Agre P (1992) Appearance of water channels in Xenopus oocytes expressing red cell CHIP28 protein. Science 256:385-387.
Pushkin A, Kurtz I (2006) SLC4 base (HCO3 -, CO3 2-) transporters: classification, function, structure, genetic diseases, and knockout models. American journal of physiology Renal physiology 290:F580-599.
Qiu Z, Dubin AE, Mathur J, Tu B, Reddy K, Miraglia LJ, Reinhardt J, Orth AP, Patapoutian A (2014) SWELL1, a Plasma Membrane Protein, Is an Essential Component of Volume-Regulated Anion Channel. Cell 157:447-458.
Qizilbash N, Lewington SL, Lopez-Arrieta JM (2002) Corticosteroids for acute ischaemic stroke. The Cochrane database of systematic reviews:CD000064.
Quagliarello V, Scheld WM (1992) Bacterial meningitis: pathogenesis, pathophysiology, and progress. The New England journal of medicine 327:864-872.
Rabinstein AA (2006) Treatment of cerebral edema. The neurologist 12:59-73.
Rabinstein AA, Mueller-Kronast N, Maramattom BV, Zazulia AR, Bamlet WR, Diringer MN, Wijdicks EF (2006) Factors predicting prognosis after decompressive hemicraniectomy for hemispheric infarction. Neurology 67:891-893.
Rahmati N, Kunzelmann K, Xu J, Barone S, Sirianant L, De Zeeuw CI, Soleimani M (2013) Slc26a11 is prominently expressed in the brain and functions as a chloride channel: expression in Purkinje cells and stimulation of V H(+)-ATPase. Pflugers Arch 465:1583-1597.
Rangroo Thrane V, Thrane AS, Plog BA, Thiyagarajan M, Iliff JJ, Deane R, Nagelhus EA, Nedergaard M (2013) Paravascular microcirculation facilitates rapid lipid transport and astrocyte signaling in the brain. Scientific reports 3:2582.
Rao A, Craig AM (1997) Activity regulates the synaptic localization of the NMDA receptor in hippocampal neurons. Neuron 19:801-812.
Rash JE, Yasumura T, Hudson CS, Agre P, Nielsen S (1998) Direct immunogold labeling of aquaporin-4 in square arrays of astrocyte and ependymocyte plasma membranes in rat brain and spinal cord. Proceedings of the National Academy of Sciences of the United States of America 95:11981-11986.
Raslan A, Bhardwaj A (2007) Medical management of cerebral edema. Neurosurgical focus 22:E12.
Re DB, Le Verche V, Yu C, Amoroso MW, Politi KA, Phani S, Ikiz B, Hoffmann L, Koolen M, Nagata T, Papadimitriou D, Nagy P, Mitsumoto H, Kariya S, Wichterle H, Henderson CE, Przedborski S (2014) Necroptosis Drives Motor

Neuron Death in Models of Both Sporadic and Familial ALS. Neuron 81:1001-1008.
Redzic Z (2011) Molecular biology of the blood-brain and the blood-cerebrospinal fluid barriers: similarities and differences. Fluids and barriers of the CNS 8:3.
Rinke I, Artmann J, Stein V (2010) ClC-2 voltage-gated channels constitute part of the background conductance and assist chloride extrusion. The Journal of neuroscience : the official journal of the Society for Neuroscience 30:4776-4786.
Rivera C, Voipio J, Kaila K (2005) Two developmental switches in GABAergic signalling: the K+-Cl- cotransporter KCC2 and carbonic anhydrase CAVII. The Journal of physiology 562:27-36.
Roberts I et al. (2004) Effect of intravenous corticosteroids on death within 14 days in 10008 adults with clinically significant head injury (MRC CRASH trial): randomised placebo-controlled trial. Lancet 364:1321-1328.
Robinson R (2012) Antisense Therapy for ALS Found Safe, but More Safety Data are Sought. Neurology Today 12:4-5.
Romero MF, Fulton CM, Boron WF (2004) The SLC4 family of HCO 3 - transporters. Pflugers Archiv : European journal of physiology 447:495-509.
Romero MF, Chen AP, Parker MD, Boron WF (2013) The SLC4 family of bicarbonate (HCO(3)(-)) transporters. Molecular aspects of medicine 34:159-182.
Rosenblum WI (2007) Cytotoxic edema: monitoring its magnitude and contribution to brain swelling. Journal of neuropathology and experimental neurology 66:771-778.
Rossi DJ, Oshima T, Attwell D (2000) Glutamate release in severe brain ischaemia is mainly by reversed uptake. Nature 403:316-321.
Rothman SM (1985) The neurotoxicity of excitatory amino acids is produced by passive chloride influx. The Journal of neuroscience : the official journal of the Society for Neuroscience 5:1483-1489.
Rungta RL, Choi HB, Lin PJ, Ko RW, Ashby D, Nair J, Manoharan M, Cullis PR, Macvicar BA (2013) Lipid Nanoparticle Delivery of siRNA to Silence Neuronal Gene Expression in the Brain. Molecular therapy Nucleic acids 2:e136.
Sabirov RZ, Okada Y (2009) The maxi-anion channel: a classical channel playing novel roles through an unidentified molecular entity. The journal of physiological sciences : JPS 59:3-21.
Sabirov RZ, Dutta AK, Okada Y (2001) Volume-dependent ATP-conductive large-conductance anion channel as a pathway for swelling-induced ATP release. The Journal of general physiology 118:251-266.
Sabirov RZ, Prenen J, Droogmans G, Nilius B (2000) Extra- and intracellular proton-binding sites of volume-regulated anion channels. The Journal of membrane biology 177:13-22.
Sabirov RZ, Sheiko T, Liu H, Deng D, Okada Y, Craigen WJ (2006) Genetic demonstration that the plasma membrane maxianion channel and voltage-dependent anion channels are unrelated proteins. The Journal of biological chemistry 281:1897-1904.
Sah P, Nicoll RA (1991) Mechanisms underlying potentiation of synaptic transmission in rat anterior cingulate cortex in vitro. J Physiol 433:615-630.

Schroeder BC, Cheng T, Jan YN, Jan LY (2008) Expression cloning of TMEM16A as a calcium-activated chloride channel subunit. Cell 134:1019-1029.
Schwab S, Spranger M, Schwarz S, Hacke W (1997) Barbiturate coma in severe hemispheric stroke: useful or obsolete? Neurology 48:1608-1613.
Semple SC et al. (2010) Rational design of cationic lipids for siRNA delivery. Nature biotechnology 28:172-176.
Shen BO, Jensen G, Bohnert HJ (1997) Increased Resistance to Oxidative Stress in Transgenic Plants by Targeting Mannitol Biosynthesis to Chloroplasts. Plant Physiology 113:1177-1183.
Shenkin HA, Goluboff B, Haft H (1962) The use of mannitol for the reduction of intracranial pressure in intracranial surgery. Journal of neurosurgery 19:897-901.
Sik A, Smith RL, Freund TF (2000) Distribution of chloride channel-2-immunoreactive neuronal and astrocytic processes in the hippocampus. Neuroscience 101:51-65.
Simard JM, Kent TA, Chen M, Tarasov KV, Gerzanich V (2007) Brain oedema in focal ischaemia: molecular pathophysiology and theoretical implications. Lancet neurology 6:258-268.
Simard JM, Chen M, Tarasov KV, Bhatta S, Ivanova S, Melnitchenko L, Tsymbalyuk N, West GA, Gerzanich V (2006) Newly expressed SUR1-regulated NC(Ca-ATP) channel mediates cerebral edema after ischemic stroke. Nature medicine 12:433-440.
Sinning A, Liebmann L, Kougioumtzes A, Westermann M, Bruehl C, Hubner CA (2011) Synaptic glutamate release is modulated by the Na+ -driven Cl-/HCO(3)(-) exchanger Slc4a8. The Journal of neuroscience : the official journal of the Society for Neuroscience 31:7300-7311.
Smith RA, Miller TM, Yamanaka K, Monia BP, Condon TP, Hung G, Lobsiger CS, Ward CM, McAlonis-Downes M, Wei H, Wancewicz EV, Bennett CF, Cleveland DW (2006) Antisense oligonucleotide therapy for neurodegenerative disease. J Clin Invest 116:2290-2296.
Soleimani M (2013) SLC26 Cl-/HCO3- exchangers in the kidney: roles in health and disease. Kidney international 84:657-666.
Somjen GG (2001) Mechanisms of spreading depression and hypoxic spreading depression-like depolarization. Physiological reviews 81:1065-1096.
Somjen GG (2002) Ion regulation in the brain: implications for pathophysiology. The Neuroscientist : a review journal bringing neurobiology, neurology and psychiatry 8:254-267.
Staley K, Smith R, Schaack J, Wilcox C, Jentsch TJ (1996) Alteration of GABAA receptor function following gene transfer of the CLC-2 chloride channel. Neuron 17:543-551.
Staley KJ, Soldo BL, Proctor WR (1995) Ionic mechanisms of neuronal excitation by inhibitory GABAA receptors. Science 269:977-981.
Stauber T, Weinert S, Jentsch TJ (2012) Cell biology and physiology of CLC chloride channels and transporters. Comprehensive Physiology 2:1701-1744.
Strange K, Emma F, Jackson PS (1996) Cellular and molecular physiology of volume-sensitive anion channels. Am J Physiol 270:C711-730.

Strichartz G, Rando T, Wang GK (1987) An integrated view of the molecular toxinology of sodium channel gating in excitable cells. Annu Rev Neurosci 10:237-267.

Su X, Fricke J, Kavanagh DG, Irvine DJ (2011) In vitro and in vivo mRNA delivery using lipid-enveloped pH-responsive polymer nanoparticles. Molecular pharmaceutics 8:774-787.

Sun HS, Jackson MF, Martin LJ, Jansen K, Teves L, Cui H, Kiyonaka S, Mori Y, Jones M, Forder JP, Golde TE, Orser BA, Macdonald JF, Tymianski M (2009) Suppression of hippocampal TRPM7 protein prevents delayed neuronal death in brain ischemia. Nat Neurosci 12:1300-1307.

Suzuki M (2006) The Drosophila tweety family: molecular candidates for large-conductance Ca2+-activated Cl- channels. Experimental physiology 91:141-147.

Suzuki M, Mizuno A (2004) A novel human Cl(-) channel family related to Drosophila flightless locus. The Journal of biological chemistry 279:22461-22468.

Svichar N, Waheed A, Sly WS, Hennings JC, Hubner CA, Chesler M (2009) Carbonic anhydrases CA4 and CA14 both enhance AE3-mediated Cl--HCO3- exchange in hippocampal neurons. The Journal of neuroscience : the official journal of the Society for Neuroscience 29:3252-3258.

Takano K, Latour LL, Formato JE, Carano RA, Helmer KG, Hasegawa Y, Sotak CH, Fisher M (1996) The role of spreading depression in focal ischemia evaluated by diffusion mapping. Annals of neurology 39:308-318.

Takano T, Tian GF, Peng W, Lou N, Lovatt D, Hansen AJ, Kasischke KA, Nedergaard M (2007) Cortical spreading depression causes and coincides with tissue hypoxia. Nature neuroscience 10:754-762.

Tam YY, Chen S, Cullis PR (2013) Advances in Lipid Nanoparticles for siRNA Delivery. Pharmaceutics 5:498-507.

Taylor A, Butt W, Rosenfeld J, Shann F, Ditchfield M, Lewis E, Klug G, Wallace D, Henning R, Tibballs J (2001) A randomized trial of very early decompressive craniectomy in children with traumatic brain injury and sustained intracranial hypertension. Child's nervous system : ChNS : official journal of the International Society for Pediatric Neurosurgery 17:154-162.

Tejima E, Guo S, Murata Y, Arai K, Lok J, van Leyen K, Rosell A, Wang X, Lo EH (2009) Neuroprotective effects of overexpressing tissue inhibitor of metalloproteinase TIMP-1. Journal of neurotrauma 26:1935-1941.

Thompson RJ, Zhou N, MacVicar BA (2006) Ischemia opens neuronal gap junction hemichannels. Science 312:924-927.

Thompson RJ, Jackson MF, Olah ME, Rungta RL, Hines DJ, Beazely MA, MacDonald JF, MacVicar BA (2008) Activation of pannexin-1 hemichannels augments aberrant bursting in the hippocampus. Science 322:1555-1559.

Thompson SM, Deisz RA, Prince DA (1988) Relative contributions of passive equilibrium and active transport to the distribution of chloride in mammalian cortical neurons. Journal of neurophysiology 60:105-124.

Thorne RG, Nicholson C (2006) In vivo diffusion analysis with quantum dots and dextrans predicts the width of brain extracellular space. Proc Natl Acad Sci U S A 103:5567-5572.
Traynelis SF, Wollmuth LP, McBain CJ, Menniti FS, Vance KM, Ogden KK, Hansen KB, Yuan H, Myers SJ, Dingledine R (2010) Glutamate receptor ion channels: structure, regulation, and function. Pharmacological reviews 62:405-496.
Tsien RY (1981) A non-disruptive technique for loading calcium buffers and indicators into cells. Nature 290:527-528.
Unterberg AW, Stover J, Kress B, Kiening KL (2004) Edema and brain trauma. Neuroscience 129:1021-1029.
Vandenabeele P, Galluzzi L, Vanden Berghe T, Kroemer G (2010) Molecular mechanisms of necroptosis: an ordered cellular explosion. Nature reviews Molecular cell biology 11:700-714.
Vargas-Perez H, Ting AKR, Walton CH, Hansen DM, Razavi R, Clarke L, Bufalino MR, Allison DW, Steffensen SC, van der Kooy D (2009) Ventral tegmental area BDNF induces an opiate-dependent-like reward state in naive rats. Science 324:1732-1734.
Verkman AS, Galietta LJ (2009) Chloride channels as drug targets. Nat Rev Drug Discov 8:153-171.
Verkman AS, Sellers MC, Chao AC, Leung T, Ketcham R (1989) Synthesis and characterization of improved chloride-sensitive fluorescent indicators for biological applications. Analytical biochemistry 178:355-361.
Vincourt JB, Jullien D, Amalric F, Girard JP (2003) Molecular and functional characterization of SLC26A11, a sodium-independent sulfate transporter from high endothelial venules. FASEB journal : official publication of the Federation of American Societies for Experimental Biology 17:890-892.
Voss FK, Ullrich F, Münch J, Lazarow K, Lutter D, Mah N, Andrade-Navarro MA, von Kries JP, Stauber T, Jentsch TJ (2014) Identification of LRRC8 Heteromers as an Essential Component of the Volume-Regulated Anion Channel VRAC. Science.
Wahrle SE, Shah AR, Fagan AM, Smemo S, Kauwe JS, Grupe A, Hinrichs A, Mayo K, Jiang H, Thal LJ, Goate AM, Holtzman DM (2007) Apolipoprotein E levels in cerebrospinal fluid and the effects of ABCA1 polymorphisms. Mol Neurodegener 2:7.
Wakeland W, Goldstein B (2005) A computer model of intracranial pressure dynamics during traumatic brain injury that explicitly models fluid flows and volumes. Acta neurochirurgica Supplement 95:321-326.
Walz W (1987) Swelling and potassium uptake in cultured astrocytes. Canadian journal of physiology and pharmacology 65:1051-1057.
Wang C, Shimizu-Okabe C, Watanabe K, Okabe A, Matsuzaki H, Ogawa T, Mori N, Fukuda A, Sato K (2002) Developmental changes in KCC1, KCC2, and NKCC1 mRNA expressions in the rat brain. Brain research Developmental brain research 139:59-66.
Wang X, Takahashi N, Uramoto H, Okada Y (2005) Chloride channel inhibition prevents ROS-dependent apoptosis induced by ischemia-reperfusion in mouse cardiomyocytes. Cellular physiology and biochemistry : international

journal of experimental cellular physiology, biochemistry, and pharmacology 16:147-154.
Wang X, Jung J, Asahi M, Chwang W, Russo L, Moskowitz MA, Dixon CE, Fini ME, Lo EH (2000) Effects of matrix metalloproteinase-9 gene knock-out on morphological and motor outcomes after traumatic brain injury. The Journal of neuroscience : the official journal of the Society for Neuroscience 20:7037-7042.
Ward JD, Becker DP, Miller JD, Choi SC, Marmarou A, Wood C, Newlon PG, Keenan R (1985) Failure of prophylactic barbiturate coma in the treatment of severe head injury. Journal of neurosurgery 62:383-388.
Washbourne P, Bennett JE, McAllister AK (2002) Rapid recruitment of NMDA receptor transport packets to nascent synapses. Nat Neurosci 5:751-759.
Weed LH, McKibbens PR (1919) Experimental alterations of brain bulk. Am J Physiol 48:512-530.
Weinreich F, Jentsch TJ (2001) Pores formed by single subunits in mixed dimers of different CLC chloride channels. The Journal of biological chemistry 276:2347-2353.
Welsh FA, Marcy VR, Sims RE (1991) NADH fluorescence and regional energy metabolites during focal ischemia and reperfusion of rat brain. Journal of cerebral blood flow and metabolism : official journal of the International Society of Cerebral Blood Flow and Metabolism 11:459-465.
White MM, Aylwin M (1990) Niflumic and flufenamic acids are potent reversible blockers of Ca2(+)-activated Cl- channels in Xenopus oocytes. Molecular pharmacology 37:720-724.
Wick W, Kuker W (2004) Brain edema in neurooncology: radiological assessment and management. Onkologie 27:261-266.
Wilms CD, Schmidt H, Eilers J (2006) Quantitative two-photon Ca2+ imaging via fluorescence lifetime analysis. Cell calcium 40:73-79.
Wu W, Liu P, Li J (2012) Necroptosis: an emerging form of programmed cell death. Critical reviews in oncology/hematology 82:249-258.
Xie L, Kang H, Xu Q, Chen MJ, Liao Y, Thiyagarajan M, O'Donnell J, Christensen DJ, Nicholson C, Iliff JJ, Takano T, Deane R, Nedergaard M (2013) Sleep drives metabolite clearance from the adult brain. Science 342:373-377.
Xu J, Barone S, Li H, Holiday S, Zahedi K, Soleimani M (2011) Slc26a11, a chloride transporter, localizes with the vacuolar H(+)-ATPase of A-intercalated cells of the kidney. Kidney international 80:926-937.
Yenari MA, Han HS (2012) Neuroprotective mechanisms of hypothermia in brain ischaemia. Nature reviews Neuroscience 13:267-278.
Young GB, Gilbert JJ, Zochodne DW (1990) The significance of myoclonic status epilepticus in postanoxic coma. Neurology 40:1843-1848.
Yu SP, Choi DW (2000) Ions, cell volume, and apoptosis. Proceedings of the National Academy of Sciences of the United States of America 97:9360-9362.
Yu SP, Yeh CH, Sensi SL, Gwag BJ, Canzoniero LM, Farhangrazi ZS, Ying HS, Tian M, Dugan LL, Choi DW (1997) Mediation of neuronal apoptosis by enhancement of outward potassium current. Science 278:114-117.

Zalachoras I, Evers MM, van Roon-Mom WM, Aartsma-Rus AM, Meijer OC (2011) Antisense-mediated RNA targeting: versatile and expedient genetic manipulation in the brain. Frontiers in molecular neuroscience 4:10.

Zeng XN, Xie LL, Liang R, Sun XL, Fan Y, Hu G (2012) AQP4 knockout aggravates ischemia/reperfusion injury in mice. CNS neuroscience & therapeutics 18:388-394.

Zeuthen T (2010) Water-transporting proteins. The Journal of membrane biology 234:57-73.

Zeuthen T, Zeuthen E (2007) The mechanism of water transport in Na+-coupled glucose transporters expressed in Xenopus oocytes. Biophysical journal 93:1413-1416; discussion 1417-1419.

Zeuthen T, Macaulay N (2012) Cotransport of water by Na(+)-K(+)-2Cl(-) cotransporters expressed in Xenopus oocytes: NKCC1 versus NKCC2. The Journal of physiology 590:1139-1154.

Zhang DW, Shao J, Lin J, Zhang N, Lu BJ, Lin SC, Dong MQ, Han J (2009) RIP3, an energy metabolism regulator that switches TNF-induced cell death from apoptosis to necrosis. Science 325:332-336.

Zhang H, Cao HJ, Kimelberg HK, Zhou M (2011) Volume regulated anion channel currents of rat hippocampal neurons and their contribution to oxygen-and-glucose deprivation induced neuronal death. PloS one 6:e16803.

Zhang Y, Zhang H, Feustel PJ, Kimelberg HK (2008) DCPIB, a specific inhibitor of volume regulated anion channels (VRACs), reduces infarct size in MCAo and the release of glutamate in the ischemic cortical penumbra. Experimental neurology 210:514-520.

Zhou N, Gordon GR, Feighan D, MacVicar BA (2010) Transient swelling, acidification, and mitochondrial depolarization occurs in neurons but not astrocytes during spreading depression. Cerebral cortex 20:2614-2624.

Zhou N, Rungta RL, Malik A, Han H, Wu DC, MacVicar BA (2013) Regenerative glutamate release by presynaptic NMDA receptors contributes to spreading depression. Journal of cerebral blood flow and metabolism : official journal of the International Society of Cerebral Blood Flow and Metabolism 33:1582-1594.

Zimmermann TS et al. (2006) RNAi-mediated gene silencing in non-human primates. Nature 441:111-114.